RAINFALL-RUNOFF PROCESSES IN TROPICAL URBAN ENVIRONMENTS

ALI MESHGI

NATIONAL UNIVERSITY OF SINGAPORE

2015

RAINFALL-RUNOFF PROCESSES IN TROPICAL URBAN ENVIRONMENTS

ALI MESHGI

(MSc, Shiraz University)

A THESIS SUBMITTED

FOR THE DEGREE OF DOCTOR OF PHILOSOPHY

DEPARTMENT OF CIVIL AND ENVIRONMENTAL ENGINEERING

NATIONAL UNIVERSITY OF SINGAPORE

2015

DECLARATION

I hereby declare that this thesis is my original work and it has been written by me its entirety.

I have duly acknowledged all the sources of information which have been used in the thesis.

This thesis has also not been submitted for any degree in any university previously.

ALI MESHGI

15 January 2015

This thesis is dedicated to my lovely wife

Shila who has supported me by all

means during my PhD study.

ACKNOWLEDGMENTS

I would like to express my gratitude to all those who have helped me to complete my PhD studies at NUS. I am deeply grateful to my supervisors, Assoc. Prof Vladan Babovic from Department of Civil and Environmental Engineering, National University of Singapore and Assist. Prof May Chui from Department of Civil Engineering, The University of Hong Kong, whose knowledge, experience, encouragement, support, and suggestions helped me throughout the course of my graduate studies. I also would like to express my gratitude to Dr. Petra Schmitter, whose constant guidance, support, and suggestions during my PhD study were significantly helpful. I also wish to thank Singapore Delft Water Alliance (SDWA) for giving me the scholarship and financial support for my PhD study.

I also would like to express my sincere thanks to Dr. Abhay Anand for his warm supports throughout the duration of my research. I also would like to thank Ms. Noor Azizah Bte Aziz and Mr. Bergenwall Bjorn Allan Joakim for their assistance in field study and laboratory testing.

I would like to thank my PhD colleagues, Abhay, Alam, Albert, Jayashree, Kalyan, Nishtha and Serene for their kind supports. I also thank all of my colleagues in SDWA and NUSDeltares Sally, Joost, SK, Jingjie, Jair, Aurelie, Gerard, Umid, Sheela, Desmond, Wang Xuan, Stephane, Ivy, Saedah and many others for their warm supports and kind encouragement.

Lastly, I also gratefully thank my lovely wife, parents, sister and my son for their love, warm supports and constant encouragement.

Table of Contents

Summary

Increasing global urbanization has severely altered the hydrological cycle resulting in the decrease of pervious areas, infiltration and therefore the lateral sub-surface component during rainfall events. Consequently this lead to increasing peak discharges in the urban drainage infrastructure. This call for a better understanding of rainfall-runoff processes in urbanized areas especially with regards to the contributions of specific land use types towards surface and sub-surface flow. However, this knowledge in tropical urban environments is limited. Therefore, the main objective of this research is to better understand the hydrological rainfall-runoff processes in an urban tropical system through a deeper insight into hydrograph flow components and runoff response of specific land use types. This study used genetic programming to establish a physically interpretable modular model consisting of two sub-models to simulate the two hydrograph flow components of baseflow and quickflow. Furthermore it used the modular model to predict the events as well as time series of both flow components and optimization techniques to estimate the contributions of various land use types (i.e. impervious, steep grassland, grassland on mild slope, mixed grasses and trees and relatively natural vegetation) towards baseflow and quickflow in tropical urban systems. A tropical urban catchment in Singapore was chosen to setup a monitoring network for this study. This catchment contains the main land uses (e.g. impervious, grassland, relatively natural vegetation) as well as the main soil types (e.g. loamy sand, clay loam, silt clay, sandy loam) of Singapore. Therefore, understanding the triggers behind rainfall-runoff processes as well as their behaviour at this catchment yields valuable information for tropical urbanized cities such as Singapore.

The results demonstrated the successful prediction of streamflow as well as hydrograph flow components using the modular model developed in this study. The relationship between the input variables in the model (i.e. meteorological data and catchment initial conditions) and its overall structure can be explained in terms of catchment hydrological processes. Therefore, the model is a partial greying of what is often a black-box approach in catchment modelling and has strong extrapolation

capability. The modular model was further modified into a generalized structure and was validated on a large vegetation-dominated basin located in the US.

The events as well as time series predictions of both flow components from the modular model were then used to estimate the effect of various land uses towards hydrograph flow components through robust optimization techniques in Singapore Catchment. The results showed that the sub-catchment containing the highest portion of impervious surfaces (40% of the total area) contributed the least towards the baseflow (6.3%) while the sub-catchment covered by 87% of relatively natural vegetation contributed the most (34.9%). The results also indicated that the average runoff coefficient of different types of land use decreased according to: impervious (0.8), grass on steep slope (0.56), grass on mild slope (0.48), mixed grasses and trees (0.42) and relatively natural vegetation (0.12). The results also suggested that runoff coefficients differ significantly among land uses for all rainfall events.

The outcomes of this study are new methodologies which can yield better insights into the rainfall-runoff processes and helps for better understanding of runoff generation mechanisms in tropical urban environments. This understanding contains valuable information with regards to a physical understanding of rainfall-runoff behaviour when designing appropriate water management infrastructure in tropical megacities. This understanding would also be essential for water resources management and the sustainable development of water resources particularly where communities are dependent on water sources that are more vulnerable to inter-annual fluctuations in precipitation.

List of Tables

List of Figures

List of Nomenclature

Chapter 4

Q	Discharge
C_e	Discharge coefficient
g	gravitational acceleration
θ	Angle of V-notch
h	Water depth
C_{e1}	Discharge coefficient for a V-notch weir
h_1	Water depth above V-notch
C_{e2}	Discharge coefficient for the overlapping portion of the V-notch and Rectangular weirs
h_2	Depth of the V-notch portion
C_{e3}	Discharge coefficient for a Rectangular weir
L	Combined length of the horizontal sections
b_e	The effective weir crest width
h_e	The effective height above weir crest
H	Energy head
b_c	Bottom width of trapezoid shape
z_c	The horizontal component of the side slopes of the trapezoid
y_c	Critical depth in the flume throat
θ	The volumetric water content
S	Sink term
x_i	The spatial coordinates
K_{ij}^A	Components of a dimensionless anisotropy tensor
h	Pressure head
K	Unsaturated hydraulic conductivity
K_s	Saturated hydraulic conductivity
K_r	Relative hydraulic conductivity
t	Time
S_e	The effective fluid saturation
θ_r	Residual water content
θ_s	Saturated water content
l	Pore-connectivity parameter
α	Empirical shape parameter
η	Empirical shape parameter

$q_j^*(t_i)$	Specific measurement at time
β	The vector of optimized parameters
$q_j(t_i, \beta)$	Corresponding model predictions for parameter vector β
v_j	Weights associated with a particular measurement set j
w_{ij}	Weights associated with a particular measurement i within set j
Φ	Objective function
m	Sets of measurements
n_j	Number of measurements in a particular set

Chapter 5

ET_0	Reference evapotranspiration
R_n	Net radiation
Δ	Rate of increase with temperature of the saturation vapour pressure of water at air temperature
G	Soil heat flux
T	Mean daily temperature
U_2	Wind speed at 2m height
e_s	Saturation vapour pressure
e_a	Actual vapour pressure
γ	Psychrometric constant
R	Daily precipitation
Δh_p	Normalized daily average of pressure head
ET_{av}	Annual daily average of evapotranspiration
R_{av}	Annual daily average of precipitation
α	Coefficient in the soil water retention function
n	Exponent in the soil water retention function
l	Pore-connectivity parameter
K_s	Saturated hydraulic conductivity
$Q_{B(\min)}$	Minimum daily baseflow volume
$Q_{B(\max)}$	Maximum daily baseflow volume
A	Surface area of catchment
$h_{(t)}$	Daily averaged pressure head
h_{min}	Minimum daily averaged pressure head
f_k	Filtered quick response at k^{th} sampling instant
y_k	Original streamflow
b_k	Filtered baseflow
β	Filter parameter
w	Case-specific average fraction of the quick flow volumes over the total flow volumes
x_i	Observed value
y_i	Estimated value

$\bar{x}$	Average values of observed
$\bar{y}$	Average values of estimated
σ_x	Standard deviations of x
σ_y	Standard deviations of y
$Q_{B(t)}$	Daily baseflow volume
k	The lag time between the rainfall events and groundwater table responses
B_0	Fitting parameter
B	Fitting parameter

Chapter 6

$Q_{Total(t)}$	Streamflow
$Q_{Baseflow(t)}$	Baseflow
$Q_{\text{Quickflow}(t)}$	Quickflow
$P_{(t-L)}$	Rainfall intensity with L minutes Lag time
Ri_{ave}	Average rainfall intensity of a rainfall event
Ri_{max}	Maximum rainfall intensity of the rainfall event
P_{Total}	Total rainfall depth
EV_D	Event duration
ET	Daily evapotranspiration
CET	Cumulative evapotranspiration before the beginning of the event
D	Dry period before the beginning of the event
Δh_p	Normalized daily average of pressure head
A_P	Paved area of the catchment
A_{Un-P}	Un-paved area of the catchment
A	Total area of the catchment
$P_{(t-L)}$	Rainfall intensity with L minutes of lag time
a	Dimensionless coefficient
c	Dimensionless coefficient
e_n	Precipitation coefficient
b_n	Precipitation coefficient
g_n	Precipitation coefficient
d_n	Precipitation coefficient

Chapter 7

N	Number of events
Q1	The first quartile
Q2	The third quartile
C_T	weighted average runoff coefficient
C_{IMP}	Runoff coefficient of total impervious
C_{GM}	Runoff coefficient of grass on mild slope

C_{GS}	Runoff coefficient of grass on steep slope
C_{MGT}	Runoff coefficient of mixed grasses and trees
C_{RNV}	Runoff coefficient of relatively natural vegetation
Q_{R}	Total run off volume
P	Total precipitation depth

CHAPTER 1 INTRODUCTION

1.1 Backgrounds and Motivations

One of the most important questions in hydrology is how much streamflow occurs in a river or channel in response to a given rainfall event. Answering this question first requires separating rainfall inputs into components which infiltrate and those that flow over the earth's surface and directly enter channels. Infiltrated water can move laterally in the subsurface pathways until it reaches a channel, in which case it is called interflow. Infiltrated water can also percolate to groundwater flow, which may form a relatively steady contribution to streamflow which is called baseflow. In addition, the portion of rainfall which flows over the earth's surface and enters directly into streams is surface runoff. Therefore, streamflow is commonly conceptualized as being composed of baseflow and quickflow (i.e. direct runoff) components. The baseflow component represents the relatively steady contribution to streamflow from groundwater flow, while the quickflow represents the additional streamflow contributed by surface flows (i.e. rapid runoff) and shallow subsurface flows (delayed runoff) (Beven, 2012). Schematic

illustration of the processes involved in the runoff generation is also shown in Figure 1.1.

Understanding and modelling of rainfall-runoff process, especially in an urban system, is essential for water policy and environmental management and enhances the understanding of rainfall-runoff behaviour when designing appropriate water management infrastructure within a basin. To enhance this understanding in an urban environment, factors which may affect rainfall-runoff processes need to be identified. In addition, an appropriate approach should be adopted to model the rainfall-runoff relationship.

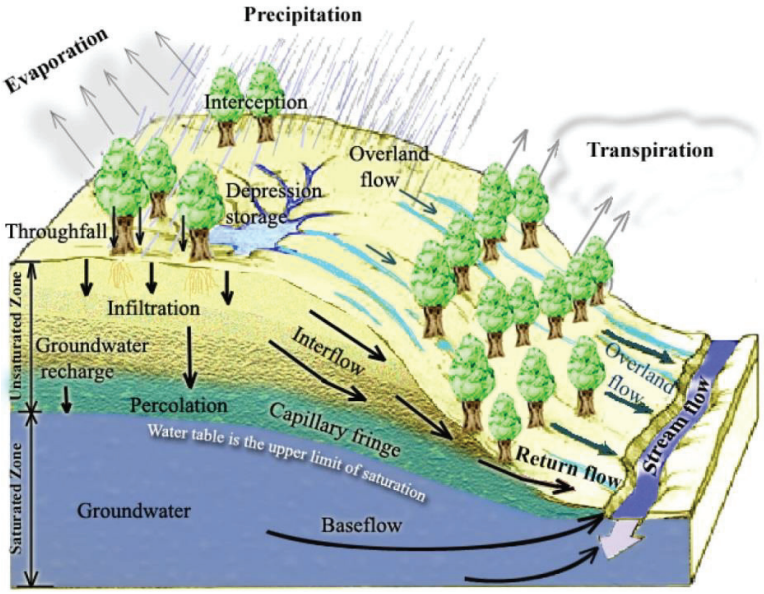

Figure 1.1: Schematic illustration of the processes involved in the runoff generation(Tarboton, 2003)

Increasing urbanization has severely altered the rainfall-runoff processes in many places worldwide, accelerating runoff due to a decrease of pervious areas and therefore reducing infiltration capacities (Marshall and Shortle, 2005). There is now an incentive to restore and enhance infiltration, which would delay and reduce flash floods. Therefore, to better understand rainfall-runoff processes in urbanized areas, it requires an accurate assessment of infiltration rates and soil hydraulic properties of the top soil which is often compacted in an urban environment.

On the other hand, in order to account for a fast drainage of the surface runoff, an intensive drainage network is built to prevent flash floods during heavy storm events (Marshall and Shortle, 2005). However, as cities are dynamically expanding, the continuous increase of impervious surfaces and the accompanied excess runoff often exceeds the present channel capacity resulting in local flash floods. To reduce the impact of surface runoff, water sensitive urban infrastructure (e.g. green roofs, porous pavement, bioretention ponds, swales) retaining rainfall and enhancing infiltration rates in urban cities are being promoted (Burns et al., 2012; Chang, 2010). Water Sensitive Urban Design (WSUD) is an engineering design approach which aims to minimize hydrological and water quality impact of urban development by integrating land use planning with urban water management (Singh and Kandasamy, 2009). The implementation of such technologies requests for a detailed understanding of runoff contributions from each specific land use in order to

plan the location of these local source control measures. Therefore, a better understanding is needed regarding rainfall-runoff processes in urbanized areas, including an accurate assessment of contributions from different land uses towards quickflow as well as baseflow. This understanding would be essential for integrated management and sustainable development of water resources particularly in tropical megacities which are dependent on water sources that are more vulnerable to inter-annual fluctuations in precipitation.

Land use and land cover affect the hydrological processes primarily through changes in hydrological processes such as infiltration, rainfall interception, and evapotranspiration (DeFries and Eshleman, 2004; Potter, 1991; Tran and O'Neill, 2013) which may have significant effects on rainfall-runoff processes and catchment water yields (Roa-García et al., 2011). The various contributions from different land uses towards rainfall-runoff processes have attracted worldwide attention, especially in temperate urban regions (e.g. Burns et al., 2005; Diaz-Palacios-Sisternes et al., 2014; Loperfido et al., 2014; Miller et al., 2014). Comparing runoff generation from different land uses enables us to understand the rainfall-runoff response influenced by particular catchment components and processes and their contribution towards the overall catchment. This understanding contains valuable information with regards to a physical based understanding of rainfall-runoff behaviour when designing appropriate water management infrastructure in tropical megacities. However, it is interesting to note that a review of the literature shows that to

date, no detailed investigation has been done to assess the impact of different land use types on rainfall-runoff processes for tropical urban cities.

On the other hand, quantifying these effects is one of the most challenging issues in hydrology (Stonestrom et al., 2009). With the advances in technology and the increasing need for integrated environmental management, distributed hydrological models, offer an appropriate approach to quantify the land use effects on hydrological responses in watershed scale. Physically-based models usually incorporate simplified forms of physical laws and are generally non-linear, time-varying and deterministic, with parameters that are representative of watershed characteristics. Although these models enhance our physical understanding towards the spatio-temporal variation of hydrological processes and respective water balance components, they require intensive data sets and are highly computational demanding (Dye and Croke, 2003). Moreover, in urban tropical regions, erratic rainfall patterns as well as multiple sequential rainfall events in a relatively short period require special attention as it contributes towards the complexity of rainfall-runoff processes and the conveyance of storm water through concrete lined channels in urban cities. In fact, the behaviour of rainfall-runoff process and moreover sub-surface flow in urban systems experience a high degree of non-linearity and heterogeneity. Therefore, caution is needed when using urban hydrological models that are often designed for temperate climates where rainfall-runoff concepts are simplified as a linear system.

Over the past decades, machine learning tools such as Artificial Neural Network (ANN) and Genetic Programming (GP) have been used to develop rainfall-runoff models (e.g. Babovic, 2005; Babovic and Keijzer, 2006; Jeong and Kim, 2005; Kisi et al., 2013; Sudheer et al., 2002; Talei and Chua, 2012). GP offers advantages over other data driven techniques since it is able to generate a function with understandable structure. However, most data driven models are one unit models with adequate input variables that cover all system processes in one input/output structure (Abrahart and See, 1999; Bowden et al., 2005). Such models combine all the various flow components losing valuable information on their specific contributions which experts need when designing local mitigation measures (Corzo and Solomatine, 2007). In addition, covering all the rainfall-runoff processes in one unit without taking into account the different physically interpretable sub-processes may lead to low accuracy in extrapolation. One way of retaining as much information as possible is to build separate models for each of the different physically interpretable flow components leading to a modular approach (Figure 1.2). As explained before, streamflow is commonly conceptualized to include baseflow and quickflow components. As such, a modular model for the simulation of streamflow time series consisting of separate modular units for baseflow and quickflow (Figure 1.3) would be suitable in quantifying both flow components in a more flexible manner. The idea of a modular model has been used in the modelling tools that use the linear reservoir approach (e.g. Unit hydrograph

methods) by splitting streamflow into baseflow and quickflow components. However, these models may fail to represent the nonlinear dynamics in the rainfall-runoff process (Rajurkar et al., 2002). Therefore, one may use GP for developing a physically interpretable modular model of these processes which is more universally applicable, especially for tropical regions. This modular model could also be used to quantify the effect of land use type on rainfall-runoff processes as well as hydrograph flow components.

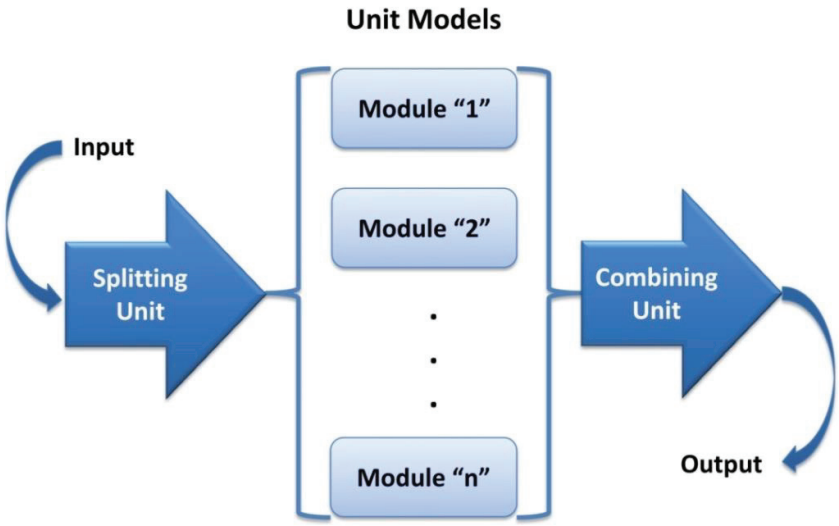

Figure 1.2: General structure of a modular model

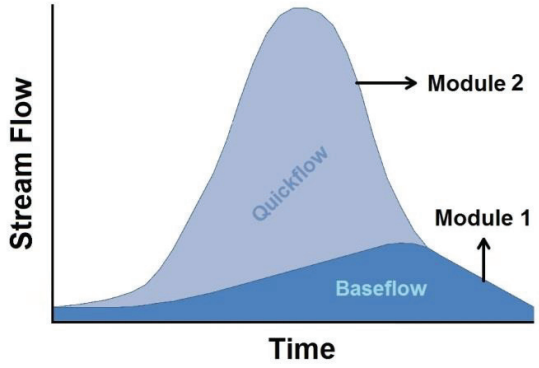

Figure 1.3: Unit models for simulating streamflow in a modular model

1.2 Objectives

The main objective of this thesis was to enhance our understanding on rainfall-runoff processes in an urban tropical system by shedding insights on hydrograph flow component separation and runoff response of specific land use types. Therefore, this study,

i. developed a modular physically interpretable model consisting of two sub-models (i.e. baseflow and quickflow) to simulate streamflow time series and hydrograph flow components
ii. and then enhanced our understanding on various contributions from different land uses towards hydrograph flow components.

In addition, human activities in an urban area may lead to soil compaction and subsequently reducing saturated soil hydraulic conductivity and infiltration capacity which could increase surface runoff during a rainfall

event. Therefore, to better understand rainfall-runoff processes in urbanized areas, this thesis also assessed the impact of urbanization on soil hydraulic properties and infiltration rate.

In addition, the following research questions are addressed in a tropical urbanized system:

- Is GP capable for developing a physically interpretable modular model to simulate the hydrograph flow components?
- What are the contributions of the various land use types towards quickflow?
- How does the baseflow contribution change among sub-catchments with different land uses?
- How do runoff generation processes vary among the different types of rainfall events?
- What are the effects of antecedent catchment conditions on runoff response?

The results of present study contain valuable information with regards to a physical based understanding of rainfall-runoff behaviour when designing appropriate water management infrastructure in tropical megacities. This understanding would be essential for water resources management and the sustainable development of water resources particularly where communities are dependent on water sources that are more vulnerable to inter-annual

fluctuations in precipitation. This knowledge also enables a better understanding of land-cover change effecting on runoff generation in tropical urban systems.

1.3 Outline

In this thesis, a general literature review on the assessment of infiltration rates and soil hydraulic properties, baseflow separation techniques, rainfall-runoff modeling and land use effects on rainfall-runoff processes are provided in Chapter 2. A description of the study sites as well as monitoring program is described in Chapter 3. Chapter 4 of this study is focused on processing and analysis of experimental data from monitoring program. Chapter 5 uses a data driven modelling approach namely GP to derive a novel simple-to-use empirical equation to estimate baseflow time series so that minimal data is required and physical information is preserved. Chapter 6 develops a modular model for the simulation of streamflow time series, consisting of two sub-models (i.e. baseflow and quickflow). A new guideline with regards to the quantification of land-use specific contributions to quickflow component is presented in Chapter 7 which also includes the effect of land use types on the contribution of baseflow to the total discharge. The effect of rainfall events and antecedent catchment condition on runoff generation processes as well as effect of land use types on the runoff coefficient is also discussed in Chapter 7.

Lastly, conclusions and recommendations for future research work are summarized in Chapter 8.

CHAPTER 2 LITERATURE REVIEW

2.1 Introduction

This thesis focused on rainfall-runoff processes in tropical urban environments. The following sections provide further review on studies relating to the objectives of this research mentioned in Chapter 1 to identify the gaps in current state of catchment modeling and also knowledge about the rainfall-runoff processes in tropical urban environments.

2.2 Baseflow Separation Techniques

Baseflow is commonly defined as the groundwater contribution to streamflow which can be affected by watershed characteristics of geomorphology, soil, and land use, as well as climate change (Price, 2011). Various studies have pointed out the significance of baseflow estimation for water policy and environmental management as it enhances the understanding of surface-groundwater interactions and related contaminant transport (Gilfedder et al., 2009; Li et al., 2013b; Smakhtin, 2001). In addition, one of the most important question in urban area is how much streamflow occurs in a river or channel in response to a given rainfall event. Answering this question first requires separating baseflow (i.e. groundwater contribution to streamflow) from total discharge in a river or channel. Therefore, developing

reliable methods to estimate baseflow has been a subject of research over the past decades (Gonzales et al., 2009). However, baseflow identification and quantification still remains cumbersome and highly depends on the availability of monitoring networks and the choice of models. Baseflow cannot be identified easily based on direct field measurements (Li et al., 2013b). Therefore, indirect methods comprising graphical methods (Linsley et al., 1982), recursive digital filters (RDFs) (Arnold and Allen, 1999; Nathan and McMahon, 1990), rating curve methods (Kliner and Knezek, 1974; Sellinger, 1996), tracer based hydrograph separation techniques (McGlynn and McDonnell, 2003), conceptual models such as IHACRES model (Jakeman and Hornberger, 1993) and numerical models (Partington et al., 2011) are commonly employed to quantify baseflow.

Various graphical baseflow separation methods have been developed by assuming baseflow to be equal to streamflow between distinct and consecutive rainfall events (e.g. Linsley et al., 1982). According to Linsley et al (1982) this method is not appropriate for long continuous streamflow records. Furthermore, this approach assumes that the baseflow response is significantly slower than the surface runoff. However, as shown in many case studies in mountainous areas, this assumption is not always valid (McDonnell et al., 2001; Uhlenbrook and Hoeg, 2003).

Tracer based hydrograph separation is another widely used baseflow separation method (Barthold et al., 2010; Brown et al., 1999; Christophersen

and Hooper, 1992; Christophersen et al., 1990; Hooper, 2003; Jones et al., 2006). However, as pointed out by Jones et al. (2006), quantification of pre-event water's contribution to streamflow may lead to huge overestimation due to the importance of dispersivity used in simulating tracer transport.

RDFs are signal processing techniques that remove the high-frequency quick flow signal from a streamflow time series in order to obtain the low-frequency baseflow signal. Numerous RDFs exist for baseflow separation such as one-parameter algorithm (Chapman and Maxwell, 1996), two-parameter algorithm (Chapman, 1999; Eckhardt, 2005) and three-parameter algorithm (Chapman, 1999). As the true values of the baseflow index parameter in these methods are unknown, one cannot conclude which method is best (Eckhardt, 2008). These approaches are often computationally efficient and also overcome the limitations associated with graphical based methods when applied to long continuous streamflow records. Therefore, RDFs are currently the most widely adopted method for baseflow separation. However, these are statistically derived equations that do not directly incorporate physically-meaningful information.

The rating curve method uses the intrinsic relationship between groundwater and stream water levels. According to Kliner and Knezek (1974), baseflow can be estimated by fitting a curve through the available discharge vs. groundwater table time series plot. On the other hand, Sellinger (1996) assumed that the entire streamflow during fair weather periods was composed

of baseflow and then proposed to fit a parabolic equation only to the data corresponding to the recession limbs of the hydrograph after the surface runoff is over. However, according to Gonzales et al. (2009), an exponential function was more suitable than a parabolic equation for their study area. The equation also included an intercept term to account for a constant discharge coming from the deeper aquifer. Fitting parameters in this method can be estimated with the least squares method using observed streamflow and groundwater table data which have to be optimized separately for each event.

Application of physically based numerical modelling for baseflow quantification has been recently explored by Partington et al. (2011). In this method, flow solutions obtained from numerical models are processed by a hydraulic mixing-cell method to quantify hydrograph flow components. This method overcomes many of the limitations of other methods mentioned above. However, to date it has only been tested for a hypothetical catchment. Furthermore, such models are complex, requiring significant computational time and large amounts of data which may not always be available.

Artificial Intelligence (AI) tools such as Genetic Algorithms (GA) have been used widely in hydrology (e.g. Anctil et al., 2006; Babovic, 2005; Kim and Kim, 2008; Sedki et al., 2009). Genetic Programming (GP), a specialization of Genetic Algorithms (GA), has been also employed over the past decades to simplify complex hydrological problems such as the development of rainfall-runoff models based on meteorological data (Babovic

and Keijzer, 2006), predicting natural channel flood routing (Sivapragasam et al., 2008), estimating saturated hydraulic conductivity (Parasuraman et al., 2007), evapotranspiration (Izadifar and Elshorbagy, 2010) and groundwater levels (Fallah-Mehdipour et al., 2013). However, to date, no equation has been derived using GP for determining baseflow based on physical catchment parameters.

2.3 Rainfall-Runoff Modelling

Accurate estimation of streamflow is crucial for planning, design and management of water resources within a basin and has been a subject of research for decades. There are multiple Rainfall-Runoff (R-R) models available that can be applied to simulate streamflow; each one characterized by a different level of complexity, limitations and data requirement (Sorooshian, 2008). These methods can be categorized into two main groups: physically-based models and system theoretic models.

2.3.1 Physically-based models

Physically based models range from conceptual lumped to distributed models. These models usually incorporate simplified forms of physical laws and are generally non-linear, time-varying and deterministic; with parameters that are representative of watershed characteristics. Although these models

enhance our understanding towards the physics of hydrological processes, they require significant computational time that restricts their use to small intensively instrumented catchment (Beven, 2012; Dye and Croke, 2003).

Conceptual lumped rainfall-runoff models consider an integrated description of parameters representing an average value over the entire catchment. These models have been used widely in hydrology over the past decades (e.g. Crawford and Linsley, 1966; Cormary and Guilbot, 1969; Duan et al., 1992; Bergstrom, 1995; Donigan et al., 1995; Havnø et al., 1995). Storm Water Management Model (SWMM) (Huber, 1981), Hydrologic Engineering Center of US Army Corps of Engineers (HEC HMS) (Feldman, 2000), and SOBEK model (Deltares, 2009) are some examples for lumped rainfall runoff model. On the other hand, distributed models can account for spatial variations in input parameters and state variables within the catchment. Therefore, physically based distributed models have the advantage of simulating complex hydrologic systems and utilizing distributed field hydrologic data as compared to lump models. Mike-SHE (DHI, 2003) is one example for physically based distributed models. A lot of efforts have been made over the past decades to improve distributed hydrological models (Beven, 2012). However little or no attention has been paid to modelling the hydrograph response of water within a catchment (McDonnell et al., 2014; Semenova and Beven, 2015).

Recent advances in the development of both lumped and distributed physically based models have led to a number of model evaluation studies. A

detailed discussion of such studies can be found in Refsgaard and Knudsen (1996), and Perrin et al. (2001). A review of these studies shows that the performance accuracy of the two modeling approaches may vary widely. According to Refsgaard and Knudsen (1996), the superiority of complex distributed physically based models over simpler lumped models has not been clearly supported by actual and sufficient performance evaluation tests. In fact, factors such as model structure and the modeler's skill can have greater impact than the type of the model used (Reed et al., 2004).

2.3.2 System theoretic models

Computational costs, parameter requirements and limitations in using physically based models in real hydrological applications have led to the development of simpler models called system theoretic models. These models establish a relationship between input and output functions without the need for a detailed consideration of the physical processes. Linear system theoretic models cannot represent non-linear catchment behavior, and thus drive the application of nonlinear techniques such as Artificial Neural Network (ANN) (e.g. Jeong and Kim, 2005; Kisi et al., 2013; Sudheer et al., 2002; Talei and Chua, 2012) and Artificial Intelligence (AI) (e.g. Babovic, 2005; Babovic and Keijzer, 2002; Babovic and Keijzer, 2006). These kinds of models are

computationally efficient and their results are comparable with those obtained from physically-based models.

The review of studies carried out on adaptability in ANN reveals that these efforts suffer from being a black-box model where little (or no) information of the physics to be extracted (Todini, 2007). Therefore, ANN cannot be used to generate a model which can be generalized for other catchments.

Artificial Intelligence (AI) tools such as Genetic Programming (GP) has been employed over the past decades for R-R modeling (e.g. Babovic, 2005; Babovic and Keijzer, 2006; Kisi et al., 2013; Whigham and Crapper, 2001). GP may offer advantages over other data driven techniques such as ANN since it is more likely to generate a function with understandable structure and therefore has been applied in different studies to generate R-R modeling. However, those available formulations only incorporate rainfall and/or streamflow and consequently are local and cannot be generalized and adopted in other catchments with different physical characteristics. Most data driven models are one unit models with input/output structure and adequate input variables that covers all the processes in a system (Abrahart and See, 1999; Bowden et al., 2005). However, such models do not contain the knowledge that experts may have about the studied system which may lead to low accuracy in extrapolation (Corzo and Solomatine, 2007).

As stated above, data driven techniques such as GP are computationally efficient as compared to physically based models and their results are

comparable with those obtained from physically-based models. However, most data driven models do not provide any information about the physical process in the catchment and also little or no attention has been paid to incorporate hydrological knowledge into these models. This calls for further progress in this type of catchment modeling. One way of incorporating hydrological knowledge into these models is to uncover and build separate models for each of the different physically interpretable sub-processes, which is called a modular approach.

A modular approach has been employed over the past decades to split a hydrological process into smaller sub-processes in order to improve the model's performance such as monthly discharge prediction (Zhang and Govindaraju, 2000), river flow modeling (Hu et al., 2001), flood-forecasting (Solomatine and Xue, 2004) and rainfall time series prediction (Wu and Chau, 2013). For example, Hu et al. (2001) divided the flow range into three regions including high, medium and low regions and employed separate ANN models to predict the river flow. Their results demonstrated that the range-dependent network performed significantly better than the conventional global ANN. As a modular approach has been successful in improving a number of complex hydrological predictions, it may also enhance streamflow simulation. Therefore, one may use GP for developing a modular model of these processes which is more universally applicable and contains information about the physical process in the catchment.

2.4 The Effects of Land Use on Rainfall-Runoff Processes

Land use and land cover affect the hydrological processes primarily through changes in hydrological factors such as infiltration, rainfall interception, and evapotranspiration (DeFries and Eshleman, 2004; Potter, 1991; Tran and O'Neill, 2013) which may have significant effects on rainfall-runoff processes and catchment water yields (Roa-García et al., 2011). The various contributions from different land uses towards rainfall-runoff processes have attracted worldwide attention, especially in temperate urban regions (e.g. Burns et al., 2005; Diaz-Palacios-Sisternes et al., 2014; Loperfido et al., 2014; Miller et al., 2014). The Results of their studies showed that land use types do seem to exert a major control on runoff coefficients, indicating that there is a strong positive correlation between the amount of quickflow and increasing urbanization (e.g. Sun et al., 2013). Their results also show that changing of land use types from pervious to impervious surfaces has a significant impact on surface runoff. Nevertheless the knowledge about the exact contributions of different land use types is still limited and at the catchments scale still waits to be defined. The results of some studies also indicated that increasing urbanization (i.e. impervious surface) might be resulted in significant loss of groundwater flow (i.e. baseflow) in streams due to the reduced infiltration (Chang, 2007; Kottegoda and Natale, 1994; Leopold

and Geological, 1968; Rose and Peters, 2001; Simmons and Reynolds, 1982). Their results indicated a negative relationship between the amount of impervious surfaces and baseflow contributions into streamflow (i.e. decreasing baseflow contributions with increasing impervious surfaces). According to these studies, in general, changing of land use types from pervious to impervious surfaces (e.g. roads, roofs, sidewalks, parking lots) associated with urban development reduces infiltration, thus increasing storm runoff while reducing baseflow. This could consequently increase peak discharges in urban drainage infrastructure. The effect of land use types on hydrological processes in a humid tropical forest region has also been investigated by a number of researchers (e.g. Muñoz-Villers and McDonnell, 2013; Roa-García et al., 2011; Salemi et al., 2013). However, it is interesting to note that a review of the literature shows that to date, no detailed investigation has been done to assess the impact of different land use types on hydrological processes for an urban tropical system. Therefore, the contributions of land use towards hydrograph flow components in tropical urban environments need to be investigated.

On the other hand, quantifying these effects is one of the most challenging issues in hydrology (Stonestrom et al., 2009). Paired-catchment studies have been widely applied in many studies as a means of determining the land use contributions towards runoff generation (e.g. Brown et al., 2005; Holko and Kostka, 2008; Malmer, 1992). In this approach, two catchments with similar

characteristics such as slope, soils, area, climate and vegetation are selected where one catchment is used for treatment and the other remains as a control (Brown et al., 2005). However, due to space constrains and land use policies imposed by governments, paired-catchment studies cannot be applied in some urban areas. Therefore, paired- catchment studies in urban areas are less common in the literature. With the advances in technology and the increasing need for integrated environmental management, the distributed hydrological models, offer an appropriate approach to quantify the land-use effects on hydrological responses in watershed scale (Chu et al., 2010; Haverkamp et al., 2005; Li et al., 2013a; Li et al., 2013c; VanShaar et al., 2002; Yang et al., 2013). Although these models enhance our understanding towards the physics of hydrological processes and allow describing the spatial distribution and temporal variability of water balance components, they require significant computational time and large amounts of data (Dye and Croke, 2003). Moreover, in urban tropical regions, erratic rainfall patterns as well as multiple sequential rainfall events in a relatively short period require special attention as it contributes towards the complexity of rainfall-runoff processes and the conveyance of storm water through concrete lined channels in urban cities. In fact, the behavior of rainfall-runoff process and moreover sub-surface flow in urban systems experience a high degree of non-linearity and heterogeneity. Therefore, caution is needed when using urban hydrological models that are

often designed for temperate climates where rainfall-runoff concepts are simplified as a linear system.

2.5 Assessment of Soil Hydraulic Properties and Infiltration Rate

Human activities in an urban area may lead to soil compaction and subsequently reducing saturated soil hydraulic conductivity and infiltration capacity which could increase surface runoff during a rainfall event. Therefore, to better understand rainfall-runoff processes in urbanized areas, it requires an accurate assessment of soil hydraulic properties and infiltration rate.

Developing reliable methods to determine soil hydraulic properties has been a subject of research over the past decades (Šimůnek and van genuchten, 1996a). Many laboratory and field methods are available to estimate the hydraulic conductivity as a function of pressure head or water content (Dane et al., 2002). The long column method (Corey, 2002), the crust method (Bouma *et al.*, 1983) and the transient procedures (Bruce and Klute, 1956) are some popular laboratory methods which measure the hydraulic parameters using the direct inversion of Darcy's law. The instantaneous profile method, the various unit-gradient type approaches, the sorptivity methods associated with ponded infiltration and the crust method based on steady water flow (Yeh and Šimůnek, 2002) are also some field methods to estimate the soil hydraulic

properties. Field methods in general are more realistic and accurate than laboratory ones because of the larger volume of soil involved, the continuity in the soil profile versus depth and the soils are also minimal disturbed (Vachaud and Dane, 2002).

Double ring or tension infiltrometers are also commonly employed in the field to measure infiltration rates (Fodor *et al.*, 2011; Kechavarzi *et al.*, 2009; Perroux and White, 1988; Timlin *et al.*, 1994; van Tol *et al.*, 2012). Minimal disturbance of soil surface, short testing time and little water requirements (Ankeny *et al.*, 1991) are some advantages of tension infiltrometers, when compared to double rings. Tension infiltrometer data from unconfined and steady-state conditions can be analyzed by Wooding's analytical approach (Wooding, 1968). However, limitations associated with this approach (e.g., uncertainty regarding the time required for steady-state conditions) have motivated researchers to find alternative solutions (Vandervaere *et al.*, 2000). Therefore, Šimůnek and van Genuchten (1996) proposed an inverse modeling approach to estimate the soil hydraulic parameter from tension infiltrometer data. In this inverse modeling approach, based on the Richards' equation (Richards, 1931) and the cumulative infiltration data from tension infiltrometer, the hydraulic properties can be estimated using optimization techniques which minimize the difference between the observed and the simulated values (Šimůnek and van genuchten, 1996a; Šimůnek and van genuchten, 1997). HYDRUS software package (Šimůnek et al., 2006) which is

a Windows based modeling environment for water flow and solute and heat transport in variably saturated porous media can be applied to estimate the soil hydraulic properties using an inverse modeling approach.

Estimating soil hydraulic parameters from tension infiltrometer data on horizontal land surfaces using an inverse modeling approach with HYDRUS-2D have been performed by a number of researchers (Kechavarzi et al., 2009; Ramos et al., 2006; Šimůnek and van genuchten, 1996a; Šimůnek et al., 1999; Ventrella et al., 2005). The equipment has also been used to determine saturated and near-saturated hydraulic properties on sloped surfaces. For example, a study on the influence of slope aspects and slope gradients has been presented by Casanova et al. (2000). Their results showed that the estimated hydraulic conductivities increased with increasing slope angles. In another study, the use of tension and double ring infiltrometers for determining hydraulic properties of silt loam in sloping landscapes have been investigated (Bodhinayake, 2004) . Their results indicated that there were no significant differences in the estimated hydraulic properties for slopes between 0 to 20% using both numerical and experimental methods. Raoof and Pilpayeh (2011) also estimated unsaturated hydraulic properties for loamy soil in sloping areas by numerical inversion using HYDRUS and concluded that estimated hydraulic conductivity decreases with increasing land slope. To sum up, there have been several studies investigating the impact of land slope on the hydraulic properties estimated using tension infiltrometer, each on a

particular soil type. However, there has not been research on investigating and comparing the impact across different soil types and at various slope angles, and the effect of applying a 2D approximation to the fully 3D process.

Estimation of hydraulic properties could also be very sensitive to the measurements of initial and final water content (Ramos, 2006) and error in the measurements of initial and final water content may lead to over- or under-estimation of the hydraulic conductivity (Šimůnek and van Genuchten, 1996b). According to Casanova et al (2000) the estimated hydraulic conductivities are larger in south-facing slopes than north-facing ones because the south-facing slope received more direct sun than north-facing one and thus contained less initial water content. These results confirmed that estimated hydraulic conductivity could also be affected by initial water content. It is interesting to note that a review of the literature shows that no detailed investigation has been done to examine the impact of initial water content on the hydraulic conductivity estimated from tension infiltrometer.

2.6 Discussion

The review of studies mentioned in Section 2.2 reveals that GP has been successful in solving a number of complex hydrological problems and therefore it can potentially be used to estimate baseflow. Compared to numerical hydrological models, GP models require significantly less

computation time and input data for calibration. Moreover, estimating baseflow using discharge data is widely available (e.g., RDFs), however, to date, no equation has been derived using GP for determining baseflow based on physical catchment parameters and groundwater table fluctuations. Deriving an equation based on easy to measure groundwater table fluctuations enables baseflow predictions in catchments where discharge monitoring is absent. This method could also contribute to multi-proxy estimations of baseflow where both streamflow and groundwater water table measurements are available. In addition, the simple equations approximated by GP can be implemented in a modular model for streamflow simulations.

The review of studies carried out on Section 2.3 reveals that Machine learning tools such as ANN and GP have been widely used for rainfall-runoff modeling as they need less computational time as compared to other methods such as physically-based models. ANN is a black-box model where little or no information of the physics can be extracted. Therefore, GP may offer advantages over ANN since it is able to generate a function with understandable structure and therefore it has been applied in different studies to generate a rainfall-runoff function. However, these attempts suffer from the following drawback: developing one unit models with adequate input variables that cover all system processes in one input/output structure; therefore, these models lose valuable information on their specific contributions which experts need when designing local mitigation measures.

In addition, proposed formulations only contain rainfall and/or streamflow data and consequently they are local and cannot be generalized and adopted in other catchments which have different physical characteristics. Moreover, covering all the rainfall-runoff processes in one unit without taking into account the different physically interpretable sub-processes may lead to low accuracy in extrapolation. On the other hand, a modular approach could be employed to split a hydrological process into smaller sub-processes in order to improve the model's performance and incorporating hydrological knowledge that experts may have about the system. As streamflow is commonly conceptualized to include baseflow and quickflow components, modular units in a modular model for the simulation of streamflow time series would be suitable in identifying baseflow and quickflow components. These identified components incorporate underlying sub-processes. The idea of a modular model has been also used in the linear reservoir approach by splitting streamflow into baseflow and quickflow components. However, these simpler models may fail to represent the nonlinear dynamics in the rainfall-runoff process. On the other hand, the linearity assumption is not needed when using GP. Therefore, one may use GP for developing a physically based non-linear modular model of these processes which is more universally applicable.

As can be seen in the afore-mentioned studies highlighted in Section 2.4, efforts have been made to understand the land use specific contributions towards rainfall-runoff processes, especially in temperate urban regions.

However, this knowledge in tropical urban environments is still limited. On the other hand, quantifying land use contributions towards rainfall-runoff processes remain among the most challenging issues in hydrology. Therefore, contributions of specific land uses towards rainfall-runoff processes in tropical urban environments need to be investigated using an appropriate approach. This understanding is essential for integrated water resources management and the sustainable development of water resources particularly in tropical megacities. In addition, this understanding contains valuable information with regards to a physical based understanding of rainfall-runoff behaviour when designing appropriate water management infrastructure in tropical urban environments.

As it can be inferred from the studies reviewed in Section 2.5, researchers have successfully applied HYDRUS-2D to estimate the hydraulic parameters on horizontal surfaces from numerical inversion of tension infiltrometer data with an axisymmetrical two dimensional domain. In fact, when the tension infiltrometer is placed on a horizontal surface, the three-dimensional infiltration process can be simplified to an axisymmetrical two-dimensional (i.e., depth and radius) process. However, when the tension infiltrometer is placed on a slope, it is no longer an axisymmetrical 2D problem. As HYDRUS-3D does not offer an inverse option and there is not yet any software package developed to specifically analyze the tension infiltrometer data based on 3D inverse modeling, it is tempting to assume that the 3D

problem can be solved as a 2D problem with the flat surface using either HYDRUS-2D or the DISC computer software (free open source) (Šimůnek and van genuchten, 2000). However, there is not yet a conclusion regarding the effect of applying a 2D approximation to estimate hydraulic conductivity from tension infiltrometer data collected from different land slopes of various soil types. Therefore, the maximum allowable slope at which accurate hydraulic estimations can be deduced for each soil type using 2D approximation should be investigated. The impact of initial water content on the hydraulic conductivity estimated from tension infiltrometer should also be investigated. In addition, the initial water content that gives the most accurate estimations of soil hydraulic conductivity from a tension infiltrometer has to be determined for different soil types.

CHAPTER 3 DESCRIPTION OF THE STUDY SITES, MONITORING PROGRAMME AND FIELD STUDIES

3.1 Introduction

As stated in Chapter 2, the main objective of this thesis was to enhance our understanding on rainfall-runoff processes in an urban tropical system by shedding insights on hydrograph flow component separation and runoff response of specific land uses. This required extensive climatic, physiographic, hydrologic and land use data for a tropical urban catchment. Therefore, a tropical catchment in Singapore was chosen to setup a monitoring network. The measured and collected data in this catchment were processed and analyzed in Chapter 4 and then used in Chapters 5 and 6 to derive a physically interpretable modular model to estimate baseflow and quickflow. It was also employed in Chapter 7 to examine the influence of land use in runoff generation in the tropical urban context.

3.2 Kent Ridge Catchment, Singapore

A small catchment (8.5 ha) namely Kent Ridge Catchment located in the southern part of Singapore was chosen to setup an intensive monitoring network (Figure 3.1). This catchment contains all the main land use types of

Singapore and hence being considered representative from a hydrological point of view. A small catchment was chosen for this study since it was more economically and technically feasible to install a dense monitoring equipment network in a small area, reducing the data uncertainty and inaccuracy in the spatial distribution of precipitation and delineation of land uses. The elevation varies from a 14.04 m to 75.84 m above sea level and the overall topography of the catchment is characterized by steep slopes. The pattern of rainfall varies over the year due to the two monsoons: the northeast (mid-November to early March) and the southwest monsoon (mid-June to September). Moderate to heavily rainfall events to intense thunderstorm activity are typically observed in the monsoon period while long shower events interrupted by thunderstorms occur in the inter-monsoon period.

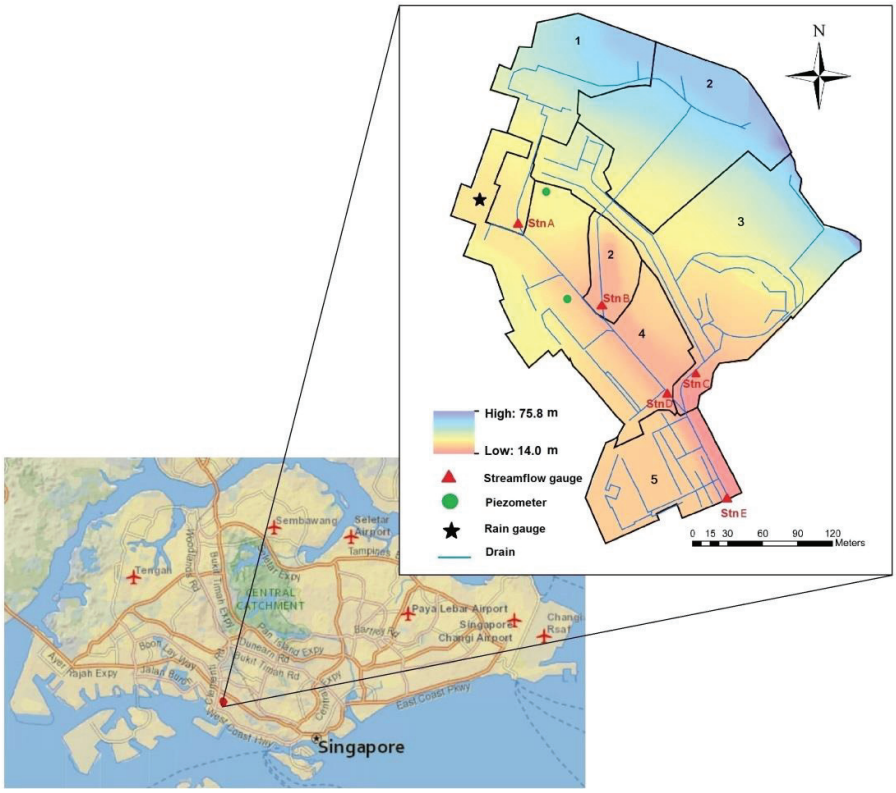

Figure 3.1 Location of Kent Ridge Catchment, Singapore, and its respective topography, monitoring stations, sub-catchments and drainage infrastructure

According to the weather station maintained by the NUS Department of Geography located nearby the study catchment, the mean annual precipitation from 2004 until 2013 is 2500 mm and the mean daily temperature varies between a minimum of 23.9°C and maximum of 32.3°C. The mean annual relative humidity is 84.2%, while the mean annual wind velocity is 15km/hour. The whole catchment was divided into 6 sub-catchments (Figure

3.1). The sub-catchments were identified based on the Digital Elevation Map (DEM) as well as their drainage location on the network.

A land use map of the catchment (Figure 3.2) was created combining the information from Google Earth, NUS campus map and field observations. The identified land use types, typically for Singapore, included impervious surfaces (i.e. roof top, road, and paved car parks), grasses on (Figure 3.3a) and steep slopes (Figure 3.3b), mixed grasses and trees (Figure 3.3c) and relatively natural vegetation (Figure 3.3d) which are relatively representative for Singapore. Therefore, understanding the behavior and the mechanism of rainfall-runoff processes at Kent Ridge catchment would yield valuable information for tropical urbanized cities such as Singapore.

Twenty-five soil samples were also collected from different parts of the catchment in order to create a soil map for the Kent Ridge catchment (See Section 4.4).

Figure 3.2: Land use map of Kent Ridge Catchment, Singapore

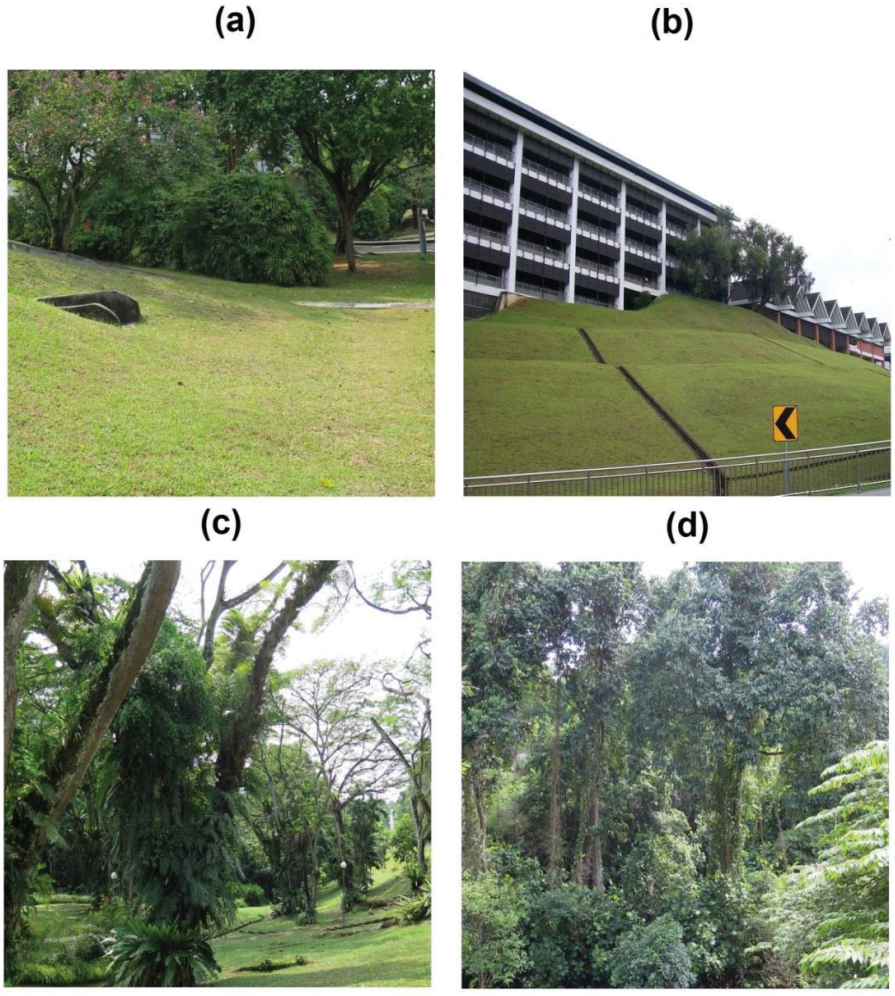

Figure 3.3: Land use types of Kent Ridge Catchment including a) grass on mild slope, b) grass on steep slope, c) mixed grasses and trees and d) relatively natural vegetation

3.2.1 Monitoring Program

3.2.1.1 Rainfall, discharge and groundwater table measurements

One rainfall monitoring station was installed within the Kent Ridge catchment (Figure 3.1) and operated from September 2011 to August 2012 and January to June 2013 at one-minute intervals with an accuracy of 0.2 mm. The ideal location for installing a rain gauge would be a flat area with no tall obstructions in the near vicinity. Therefore, the rain gauge has been installed on one of the roof tops of Kent Ridge Catchment. With the aims of setting up a dense flow monitoring program, five sub-catchments have been first identified based on catchment topography. Streamflow gauges have then been installed at the outlet of each sub-catchment. Sub-catchment 1 and 2 drain into Stations A and B, respectively, while Station C measured discharges from sub-catchment 3. Stations A and B together with the discharge draining from sub-catchment 4 are recorded by Station D. The outlet (Station E) receives the flows from the upstream Stations C and D as well as those from sub-catchment 5. Water level measurement stations (Figure 3.1) recorded at the same temporal resolution during the same period as the rain gauge. Types of control structure for discharge monitoring stations are shown in Figure 3.4. Measured water levels were converted into discharge using appropriate stage-discharge relationships (See Section 4.2). Drainage areas of the five discharge monitoring locations are presented in Table 3.1. In addition, land uses relative distribution for the monitoring stations are listed in Table 3.2. To record

groundwater table elevations one pressure transducer operated concurrently from January 2012 to June 2013 at 15-minute intervals (Figure 3.1). To measure these fluctuations relative to the variations in atmospheric pressure, another pressure transducer was installed but suspended in the air.

Figure 3.4: Types of control structure for streamflow monitoring stations within Kent Ridge Catchment, Singapore

Table 3.1: Drainage areas of the discharge monitoring stations within the Kent Ridge Catchment with their control structure type

Station	IDs of the contributing sub-catchment areas (Figure 1)	Control structure type	Total drainage area (m^2)
A	1	V Notch weir	13576
B	2,3	Composite weir	18721
C	4	Rectangular weir	21862
D	1,2,3,4,5	Flume	53904
E	1,2,3,4,5,6	Flume	85000

Table 3.2: Relative distribution of land uses for each of sub-catchments within the Kent Ridge Catchment

Station	Impervious surfaces (%)	Grass on Steep Slope (%)	Grass on Mild Slope (%)	Mixed grasses and trees (%)	Relatively natural vegetation (%)
A	40	0	15	9	36
B	5	0	7	1	87
C	24	0	27	1	48
D	20	4	13	17	47
E	25	6	16	11	42

3.2.2 Tension infiltrometer measurements

As stated in Section 2.5, better understanding of rainfall-runoff processes in urbanized areas also requires an accurate assessment of infiltration rate and soil hydraulic properties of the top soil which is often compacted in an urban area. The estimation of soil hydraulic properties from field methods such as tension infiltrometers are usually considered more accurate than laboratory methods due to the more capacity of soil involved and continuity in the soil

profile vs. depth in the ground. Tension infiltrometers allow water to infiltrate into the soils at various specified pressure heads. The resulting infiltration rates can then be analyzed for soil hydraulic properties by inverse numerical methods.

As infiltration process is highly influenced by soil texture and land uses, six locations with different land uses and soil textures was selected for tension infiltrometer measurements as shown in Figure 4.4. All the measurements were performed at three slope angles (i.e., 0, 10 and 20 degrees). To set up the experiment (Figure 3.5), grass was first removed from a circular area of the soil surface for the placement of the infiltrometer disc. A thin layer of fine sand was poured over that circular area to ensure a good contact between the soil and the nylon mesh of the infiltrometer disc.

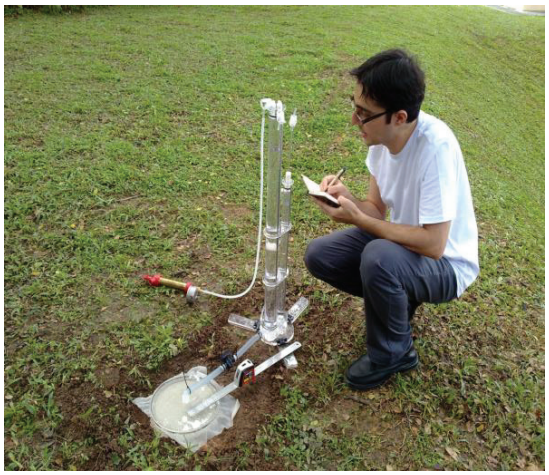

Figure 3.5: Measuring of tension infiltrometer data

The sand layer was moistened 30 seconds before the start of the measurement to prevent air from entering the disk. Two soil samples, one with sand layer moistening and the other without, were taken under the sand layer for water content measurement to confirm that the sand layer moistening does not affect the initial water content of the tension infiltrometer experiment. All the experiments were conducted with consecutive supply pressure heads of -15, -10, -6, -3 and -1cm that were respectively adjusted at 40, 75, 90, 110 and 130 minutes of experiment time. For tests on slopes, natural slopes were chosen to avoid disturbing the top soil. To create the same pressure heads at the center of the disc and the outlet of bubble tower on a slope, the water reservoir as well as bubble tower were elevated using a wooden bench. The pressure heads inside the disk infiltrometer are not uniform on slopes. Maintaining a pressure head at the center of the disk to be at the specified value would give an average pressure head inside the disk at the specified value. To determine the initial and final water content of the soils, disturbed gravimetric samples were taken. To avoid disturbing the soil for infiltrometer measurement, soil sample was taken 30cm away from the disk for initial water content; however, the final water content was determined from the soil directly under the disk at the end of experiment. The samples were sent to the lab to measure their masses before and after oven-drying for 24 hours at 105 degrees Celsius (i.e. known as wet mass and dry mass). The water mass was calculated

as the difference between the wet and dry masses. This initial and final water content were then used as inputs for the inverse modeling.

HYDRUS-2D was then employed to estimate the hydraulic parameters from numerical inversion of tension infiltrometer data (See Section 4.5)

3.3 Beaver River Basin, US

The empirical equations derived in Chapter 5 and 6 of the present thesis were based on the data collected from a tropical urban catchment (i.e. Kent Ridge Catchment, Singapore). To test the potential for more widespread applications in catchments with different climate and physical features, the performance of the generalized empirical equations was evaluated using an independent dataset located in the US. The US catchment (i.e. Beaver River Basin) is vegetation-dominated basin (Figure 3.6), with a third-order stream located in southern Rhode Island. It has an area of 23 km2, which is more than 270 times larger than Singapore catchment. The land uses are mainly parks, forest, non-urban development and water bodies which are very different compared to those in Singapore catchment. In fact, Beaver River Basin is a rural watershed with approximately 2.4% impervious area (Figure 3.7). In addition, Beaver River Basin has a temperate climate while the Singapore catchment has a tropical climate.

This basin is a sub-watershed of the, Pawcatuck-Wood Sub-basin, in the New England Region. The elevation ranges from a 34 m to 171 m above sea level and the slopes vary from flat to a maximum of 14.7% with the majority of the watershed exhibiting a slope between 0 to 3%.. The soils in this watershed are generally drained, having loamy sand or sandy loam textures which have moderately low runoff potential. The mean annual precipitation of this area is about 1350 mm.

Hourly streamflow and groundwater table data were downloaded from U.S. Geological Survey (USGS) website (http://www.usgs.gov) while hourly rainfall data (2008-2013) was downloaded from National Oceanic and Atmospheric Administration (NOAA) website (http://www.noaa.gov).

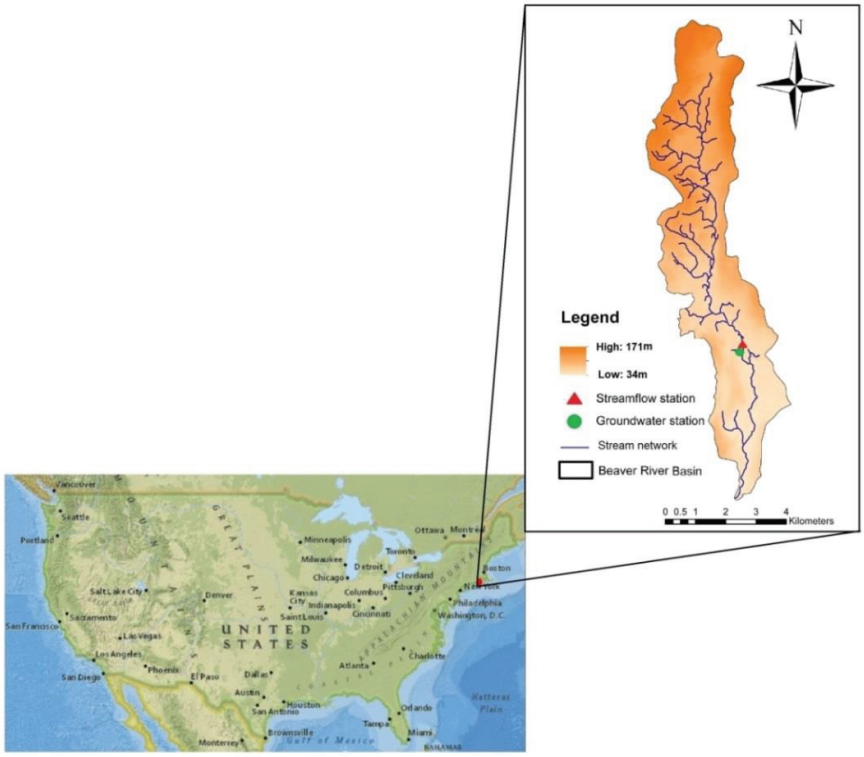

Figure 3.6: Location of Beaver River Basin, Rhode Island, US (National Geographic, 2012) with DEM (Rhode Island Digital Atlas, 2014), monitoring stations and stream network

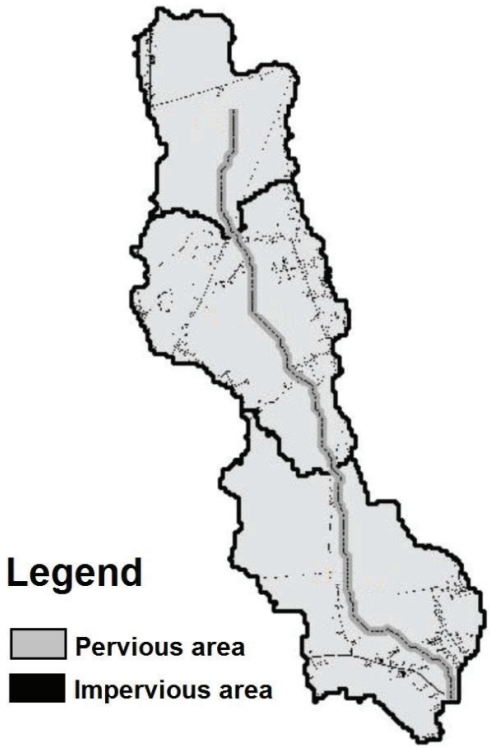

Figure 3.7: Pervious and impervious areas in the Beaver River basin

CHAPTER 4 PROCESSING AND ANALYSIS OF EXPERIMENTAL DATA

4.1 Introduction

The main scope of this chapter was to process and analyze the measured and collected data in Chapter 4. Measured water levels in Chapter 3 were first converted into discharge using standard stage-discharge relationships for the control structures (Bos, 1989). Discharge data as well measured rainfall and groundwater data in Chapter 3 were then processed to identify the anomalies using the Aquarius software. Processed data were then used in Chapter 5 and 6 to derive a physically interpretable modular model to estimate baseflow and quickflow and also employed in Chapter 7 to examine the influence of land use in runoff generation in the tropical urban context. In addition, soil samples collected from different parts of the catchment in Chapter 3 were analysed using the sieve method as well as a soil particle size analyser to create a soil map for the Kent Ridge Catchment, Singapore. Moreover, the field tension infiltrometer data (Chapter 3) was used to estimate the soil hydraulic properties based on inverse modeling and optimization techniques using HYDRUS-2D. The estimated soil hydraulic parameters were used as initial estimates for the surface layer of soil defined in HYDRUS-2D in Chapter 5.

4.2 Stage–Discharge Relationships in Discharge Monitoring Stations

As mentioned in Section 3.2.1.1, measured water levels were converted into discharge using appropriate stage-discharge relationships. This section presents the stage–discharge relationships in streamflow monitoring stations.

a) Station-A (V-notch weir):

The basic stage-discharge equation for a V-notch weir is (Bos, 1989):

$$Q = \frac{8}{15} C_e \sqrt{2g} \tan\left(\frac{\theta}{2}\right) h^{2.5} \quad 4.1$$

where:

- Q is discharge (m^3/s)
- Ce is discharge coefficient
- g is gravitational acceleration (m/s^2)
- θ is angel of the V-notch
- h is water depth above V-notch (m)

Stage–discharge relationship in Station-A was first calculated using Equation 4.1 and then plotted in Figure 4.1.

b) Station-B (Composite weir):

The basic stage-discharge equation for a Composite weir is (Bos, 1989):

$$Q = \frac{8}{15} C_{e1} \sqrt{2g} \tan\left(\frac{\theta}{2}\right) {h_1}^{2.5} - \frac{8}{15} C_{e2} \sqrt{2g} \tan\left(\frac{\theta}{2}\right) (h_1 - h_2)^{2.5}$$

$$+ \frac{2}{3} C_{e3} L \sqrt{2g} (h_1 - h_2)^{1.5} \quad 4.2$$

where:

- Q is discharge (m^3/s)
- C_{e1} is discharge coefficient for a V-notch weir
- θ is angel of the V-notch
- h_1 is water depth above V-notch (m)
- C_{e2} is discharge coefficient for the overlapping portion of the V-notch and Rectangular weirs
- h_2 is depth of the V-notch portion (m)
- C_{e3} is discharge coefficient for a Rectangular weir
- L is combined length of the horizontal sections
- g is gravitational acceleration (9.8 m/s^2)

Stage–discharge relationship in Station-B was first calculated using Equation 4.2 and then plotted in Figure 4.1.

c) Station-C (Rectangular weir):

The basic stage-discharge equation for a rectangular weir is (Bos, 1989):

$$Q = \frac{2}{3} C_e b_e \sqrt{2g} {h_e}^{1.5} \qquad 4.3$$

where:

- Q is discharge (m^3/s)
- C_e is discharge coefficient
- b_e is the effective weir crest width
- g is gravitational acceleration (9.8 m/s^2)
- h_e is the effective height above weir crest (m)

Stage–discharge relationship in Station-C was first calculated using Equation 4.3 and then plotted in Figure 4.1.

d) Station-D and -E (Flume):

The basic stage-discharge equation for a trapezoidal flume can be written as follows (Bos, 1989):

$$Q = C_e[b_c y_c + z_c {y_c}^2] \times [2g(H - y_c]^{0.5} \quad 4.4$$

where:

- Q is discharge (m^3/s)
- H is energy head which is a function of $h_l + \frac{V^2}{2g}$, where h_l is head above the flume (m) and V is average velocity in the cross section (m^2/s)
- C_e is discharge coefficient which is a function of H/L ratio, where L is length of flume throat
- b_c is bottom width of trapezoid shape (m)
- z_c is the horizontal component of the side slopes of the trapezoid
- y_c is critical depth in the flume throat (m)

Stage–discharge relationship in Station-D and -E were first calculated from Equation 4.4 and then plotted in Figure 4.1.

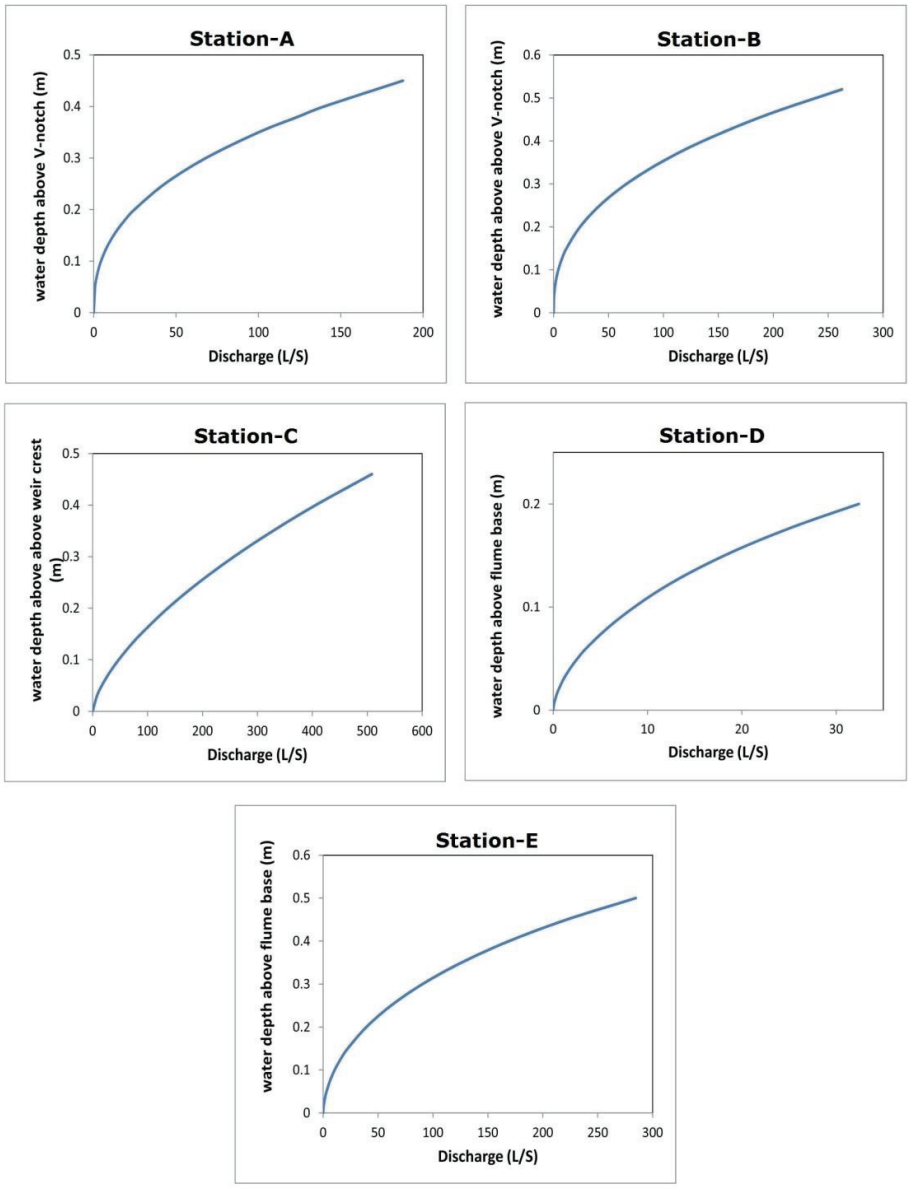

Figure 4.1: Stage-discharge rating curves in discharge monitoring stations within the Kent Ridge Catchment

4.3 Discharge, Rainfall and Groundwater Data Processing

Identification of recorded inconsistencies and other anomalies in discharge, rainfall and groundwater data and data cleaning (e.g. outliers removal, missing data interpolation) were performed using the Aquarius software (Aquatic Informatics Inc., 2009).

For data processing the following modules in the Aquarius software were applied: data input, visualization and reporting, data preprocessing, correction and data output. In the first stage, the quick view object was used to detect inconsistencies and other anomalies in the data by comparing the data from different monitoring stations. In the second stage, model based correction object was used to train the model to fill data gaps as well as to correct inconsistencies and other anomalies in the data.

The quality of discharge data at each station was first assessed using Aquarius software and then 150 events were selected for clustering analysis (See CHAPTER 7) and quantifying land use contributions towards quickflow (See CHAPTER 7). A summary of statistical feature of the discharge monitoring data is presented in Table 4.1.

Table 4.1 : Statistical feature of the discharge monitoring data for the selected events

Station	N	Mean (m^3)	StDev (m^3)	Minimum (m^3)	Q1 (m^3)	Median (m^3)	Q3 (m^3)	Maximum (m^3)
A	150	105.1	160.3	3.7	11.7	33	123	695.9
B	150	56.72	88.58	1.8	6.06	17.01	64.99	487.3
C	150	123.7	176.1	4.3	22.1	51.2	152.4	914.8
D	150	313.3	463.1	13.5	42.1	108.5	375.1	2357
E	150	464.7	686.5	19.9	55.6	171.2	572.2	3602.9

N: Number of events
Q1: The first quartile
Q3: The third quartile

With regards to the groundwater table time series, the groundwater level depth (WL) was calculated as follows:

$$WL = BD - CL + P_{Diver} - P_{Baro} \qquad 4.5$$

where, WL is the groundwater level (m), BD is the borehole depth (m), CL is the cable length (m), P_{Baro} is the atmospheric pressure (m) and P_{Diver} is the pressure exerted by the water column (WC) and the atmospheric pressure (m).

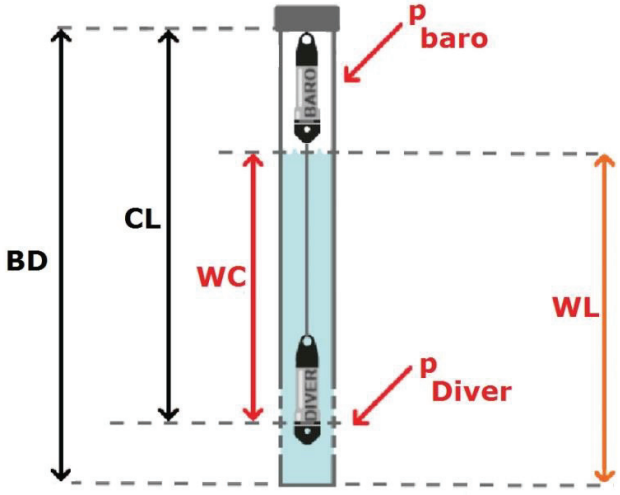

Figure 4.2: An example of a monitoring well

A summary of statistical feature of the groundwater level monitoring data is presented in Table 4.2.

Table 4.2 : Statistical feature of the groundwater level monitoring data

Station	Mean (m)	StDev (m)	Minimum (m)	Median (m)	Maximum (m)
BH1	4.4	0.4	3.6	4.4	5.4
BH2	8.8	0.3	8.1	8.8	9.6

4.4 Soil Particle Size Analysis

Twenty-five soil samples collected from different parts of the catchment were analysed using the sieve method as well as a soil particle size analyser (MaterSizer). The results were then verified with those in a soil report available for this area (Ryobi Geotechnique PTE LTD, 2005). Finally, a soil map was developed using ARCGIS 10 based on the USDA classification (Figure 4.3) and polygon of influence method as shown in Figure 4.4. 55% of the catchment is loamy sand soil while only 9% and 2.7% was sandy loam and silt loam, respectively. Clay loam is the second major soil texture comprising 33.3%.

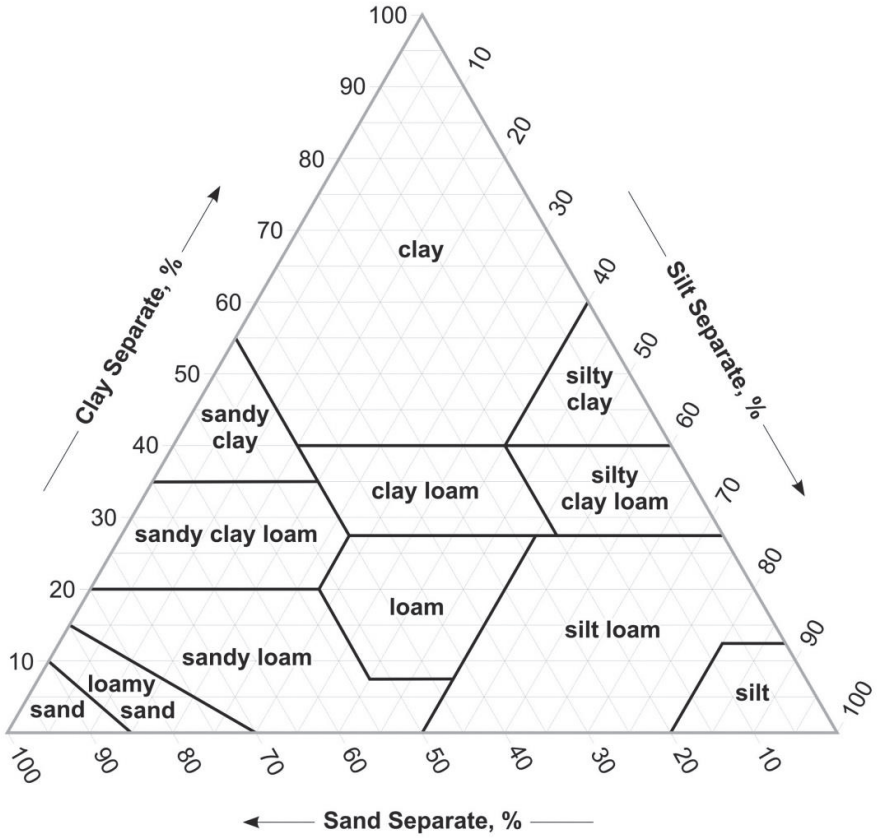

Figure 4.3: Standard USDA soil texture triangle

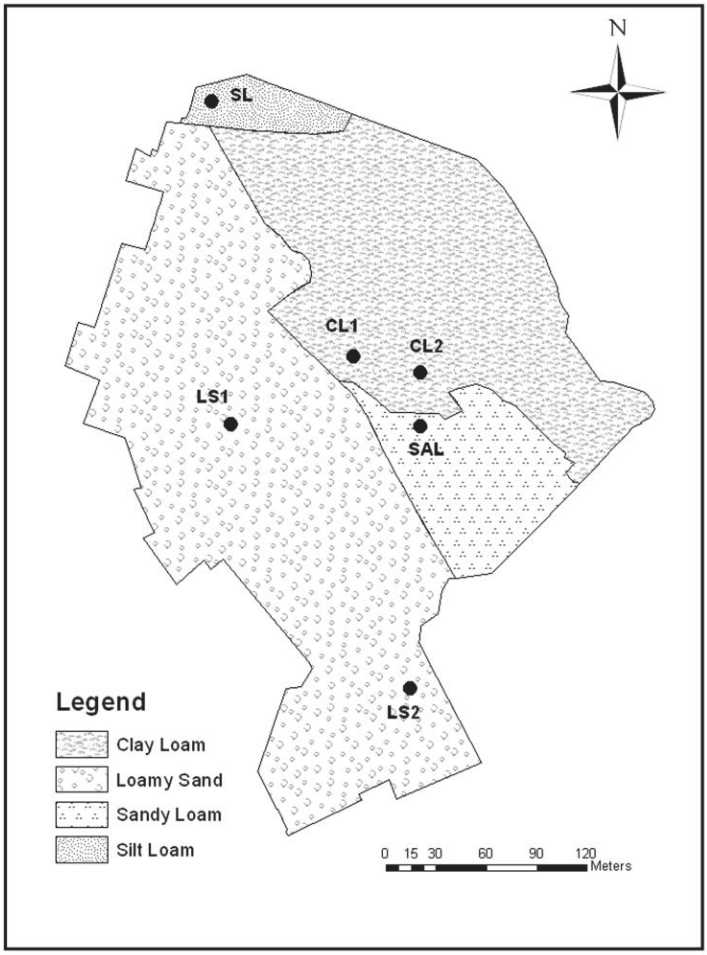

Figure 4.4: Soil map of Kent Ridge Catchment, Singapore, with the locations of tension infiltrometer experiments

4.5 Analyzing Tension Infiltrometer Data

4.5.1 Inverse Modeling

The field tension infiltrometer data was used to estimate the soil hydraulic properties based on inverse modeling and optimization techniques using HYDRUS-2D. The inverse modeling approach, that is already built within HYDRUS-2D, is based on the following function (Šimůnek and van genuchten, 1996a):

$$\phi(\beta, q_m) = \sum_{j=1}^{m} \left\{ v_j \sum_{i=1}^{n_j} w_{ij} \left[q_j^*(t_i) - q_j(t_i, \beta) \right]^2 \right\} \qquad (4.6)$$

where m represents the different sets of measurements (e.g., infiltration data, the final water content); n_j is the number of measurements in a particular set, $q_j^*(t_i)$ is the specific measurement at time t_i for the jth measurement set, β is the vector of optimized parameters (e.g., θ_r , θ_s , α, η, k_s, and l), $q_j(t_i, \beta)$ represents the corresponding model predictions for parameter vector β; v_j and w_{ij} are weights associated with a particular measurement set j or a measurement i within set j, respectively. Minimization of the objective function Φ is accomplished by using the Levenberg-Marquardt nonlinear minimization method (Marquardt, 1963). It should be noted that HYDRUS-2D assumes a flat surface and neglects any effects of slope in its estimations of hydraulic conductivity.

4.5.2 Estimating Soil hydraulic properties

Figure 4.5 shows the experimental and fitted cumulative infiltration curves versus time at consecutive supply pressure heads of -15,-10,-6 ,-3 and -1. The small breaks in the infiltration curve were caused by brief interruptions to change the tension head and to adjust the tension for a new time interval. As can be seen, excellent agreement between the measured and fitted cumulative field infiltration curves were obtained when the soil hydraulic parameters for the van Genuchten's model were optimized.

Figure 4.6 shows the water retention curves obtained through numerical inversion of the field-measured tension disk infiltrometer data. The results indicate that water content estimated by numerical inversion in particular was very close to the final water content measured at the end of the infiltration tests. Many researchers have also shown that there is a close fit between these values with those simulated by inverse model (Simunek, Wendroth et al. 1999; Ventrella, Losavio et al. 2005; Ramos, Goncalves et al. 2006; Verbist, Cornelis et al. 2009). The soil hydraulic parameters determined by model are given in Table 4.4.

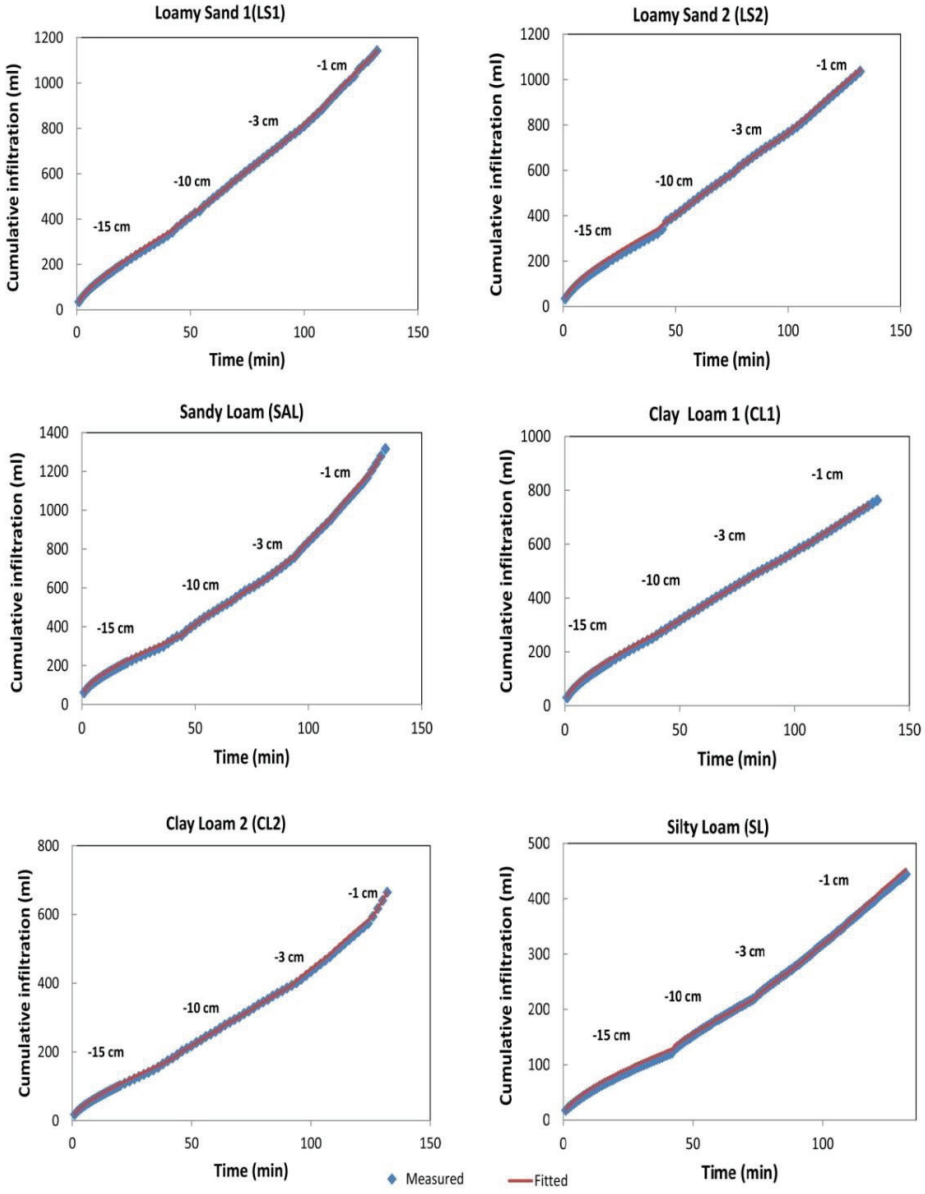

Figure 4.5: Measured and optimized cumulative infiltration curves for a tension disc infiltrometer experiment

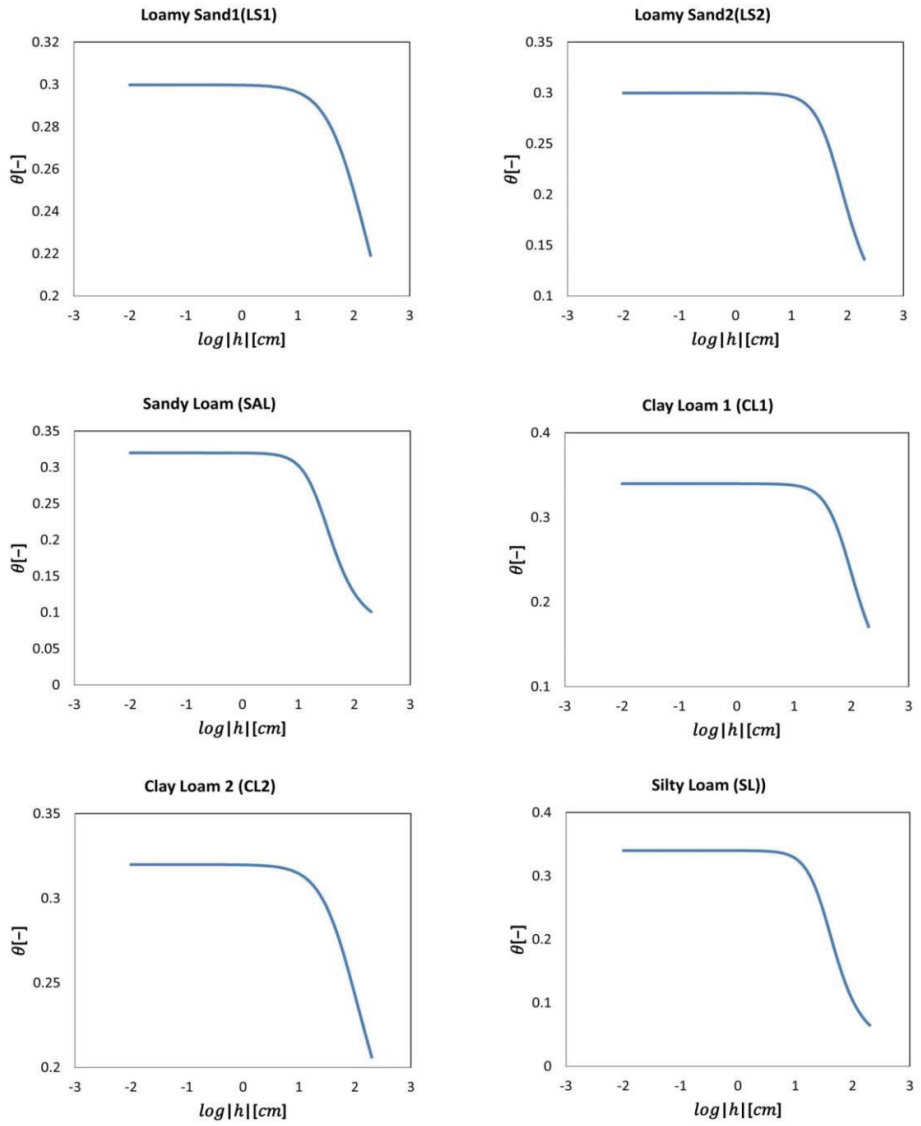

Figure 4.6: Water retention curve obtained through numerical inversion of the field-measured tension disk infiltrometer data

The results showed that less infiltration rate was observed for loamy sand 2 when compared to loamy sand 1. The main reason behind this result is probably due to different land-uses. In fact, loamy sand 1 area is covered by trees and grass while loamy sand 2 area is just covered by grass. As trees have an extended root zone which significantly increases infiltration rates, loamy sand 1 has a higher infiltration rate.

The results also showed that the saturated hydraulic conductivity for loamy sand and sandy loam soil is significantly lower than the generally reported rate for this soil type. In fact, human activities, resulting in soil compaction and subsequently reducing soil porosity and infiltration capacity, in recreational grass areas, play an important role in generating surface runoff (Dadkhah and Gifford, 1980). However the estimated soil hydraulic conductivity for non-urban areas (i.e. relatively natural vegetation) corresponded to the soil hydraulic conductivity related to the soil texture.

4.5.3 Further investigation on analyzing tension infiltrometer data[1]

Tension infiltrometers are primarily designed to be deployed on horizontal land surfaces and their applications have been studied widely using an inverse numerical tool HYDRUS-2D. However, as urban landscapes are often non-

[1] Reprinted from Hydrological Processes, 28, Meshgi et al., Analysing tension infiltrometer data from sloped surface using two-dimensional approximation,744-752, http://onlinelibrary.wiley.com/doi/10.1002/hyp.9621/abstract , Copyright (2012), with permission from John Wiley and Sons.

horizontal, infiltration through tension infiltrometers on sloped surfaces is no longer an axisymmetrical two-dimensional (2D) process but a fully three-dimensional (3D) one. In addition, to date, there is not software package available to specifically analyse the tension infiltrometer data based on 3D inverse modelling. Therefore, the effect of simplifying the 3D problem to a 2D one on the hydraulic conductivity estimated using tension infiltrometer data needs to be examined.

This section focused on the accuracy and constraints related to infiltration measurements by infiltrometers at steep terrains and the simulation of these infiltration processes in a two dimensional domain (HYDRUS-2D) were then assessed. For this purpose, tension infiltrometer data on different slopes and soil types has been obtained from Kent Ridge Catchment, Singapore (See Section 3.2.2). In addition, tension infiltrometer data of six soil types on different slopes and with different initial water content was simulated using HYDRUS-3D. Combining field measurements, forward and inverse modeling, the influence of applying a 2D approximation on hydraulic property estimations using tension infiltrometer data was examined.

4.5.3.1 Forward Modelling

To overcome the limitations in the field work mentioned in Section 3.2.2, a numerical model HYDRUS 3D (Šejna, 2007) was employed to simulate the application of a tension infiltrometer disk on a wider range of slopes, soil

types and initial water contents. The simulated results (i.e., cumulative infiltration rates) thus form a more complete set of tension infiltrometer data for further analysis. The governing flow equation can be described by the modified Richards' equation which is solved numerically using HYDRUS 3D (Šejna, 2007):

$$\frac{\partial \theta}{\partial t} = \frac{\partial}{\partial x_i}\left[K\left(K_{ij}^{A}\frac{\partial h}{\partial x_i} + K_{iz}^{A}\right)\right] - S \qquad (4.7)$$

where θ is the volumetric water content ($\mathrm{L^3L^{-3}}$), S is a sink term ($\mathrm{T^{-1}}$), x_i are the spatial coordinates (L), K_{ij}^{A} are components of a dimensionless anisotropy tensor K^A (The diagonal entries of $\mathrm{K_{ij}^{A}}$ equal one and the off-diagonal entries zero for an isotropic medium), h is the pressure head (L), t is time (T) and K is the unsaturated hydraulic conductivity ($\mathrm{LT^{-1}}$) given by :

$$\mathrm{K(h,x,y,z) = K_s(x,y,z)K_r(x,y,z)} \qquad (4.8)$$

where $\mathrm{K_s(LT^{-1})}$ and $\mathrm{K_r(-)}$ are the saturated and relative hydraulic conductivity, respectively.

This forward modeling further requires the following relationships for the effective fluid saturation and the hydraulic conductivity (van genuchten, 1980):

$$S_e(h) = \frac{\theta(h) - \theta_r}{\theta_s - \theta_r} = \frac{1}{(1 + |\alpha h|^{\eta})^{1-\frac{1}{\eta}}} \qquad (4.9)$$

$$K(h) = K_s \frac{\left[(1 + |\alpha h|^{\eta})^{1-\frac{1}{\eta}} - |\alpha h|^{\eta-1}\right]^2}{(1 + |\alpha h|^{\eta})^{(1-\frac{1}{\eta})(l+2)}} \qquad (4.10)$$

where S_e is the effective fluid saturation (-), K_s is the saturated hydraulic conductivity (LT^{-1}), θ_r and θ_s denote the residual and saturated water content (L^3L^{-3}), respectively; l is the pore-connectivity parameter (-), and α (L^{-1}) and η (-) are empirical shape parameters.

First, soil hydraulic parameters of the van Genuchten functions ($\theta_r, \theta_s, \alpha, \eta, l$, K_s) for the six soil textural classes of the USDA were chosen according to Carsel and Parrish (1988) (Table 4.3). Tension infiltrometer data at small incremental changes of slope for six soil types was then simulated. Modeling domain and boundary conditions at 20-degree slope is shown in Figure 4.7.

Table 4.3: Soil hydraulic parameters of the van Genuchten functions (van genuchten, 1980) for six soil textural classes of the USDA chosen according to Carsel and Parrish (1988)

Soil Texture	$\boldsymbol{\theta_r}$ $(\boldsymbol{L^3L^{-3}})$	$\boldsymbol{\theta_s}$ $(\boldsymbol{L^3L^{-3}})$	$\boldsymbol{\alpha}$ $(\boldsymbol{cm^{-1}})$	$\boldsymbol{\eta}$ $(-)$	$\boldsymbol{K_s}$ $(\boldsymbol{cm\ min^{-1}})$
Sand	0.045	0.43	0.145	2.68	0.495
Loamy Sand	0.057	0.41	0.124	2.28	0.243
Sandy Loam	0.065	0.41	0.075	1.89	0.074
Loam	0.078	0.43	0.036	1.56	0.017
Silt Loam	0.067	0.45	0.02	1.41	0.008
Clay	0.068	0.38	0.008	1.09	0.003

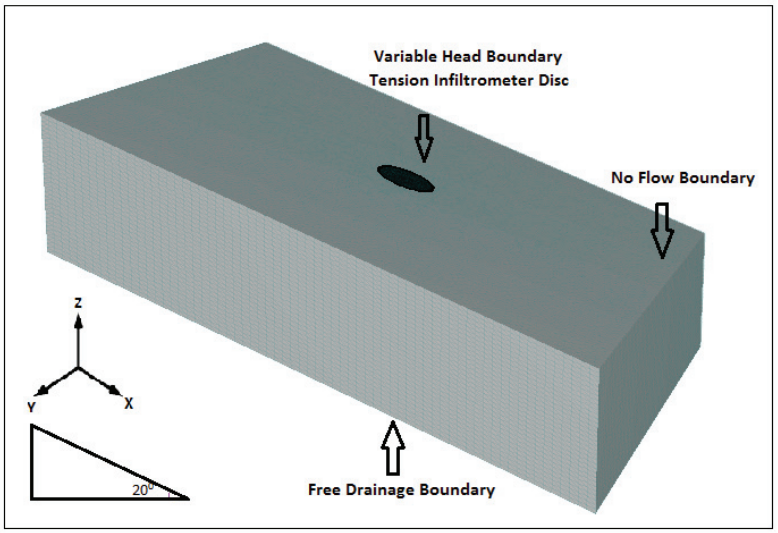

Figure 4.7**:** Modeling domain and boundary conditions at 20-degree land slope in HYDRUS 3D

All the simulations were conducted with the same consecutive supply pressure heads and duration time as in the field study. The radius of the disc tension infiltrometer was assumed to be 10cm, and the initial water content was assumed to be 20% which is about the average water content in the field. Soil hydraulic parameters of the van Genuchten functions (van genuchten, 1980) for the six soil textural classes of the USDA were chosen according to Carsel and Parrish (1988). Using the same conditions, tension infiltrometer data was also simulated at different initial water content (i.e., 10, 20 and 30%) for the six soil types to investigate the effect of initial water content. Finally, tension

infiltrometer data was also simulated on horizontal surfaces but with different initial water content for the different soil types.

4.5.3.2 Statistical Test

The hydraulic conductivities from different sources were analyzed using statistical tools available in the SPSS software version 18 developed by International Business Machines (IBM) corporation to determine whether they are significantly different from each other. As the hydraulic conductivity values do not come from normal distribution, the nonparametric statistics test namely Kolmogorov–Smirnov (KS) test which is sensitive to the shape of the cumulative distribution functions of the two samples is the most suitable test for this research. Two hydraulic conductivity values are considered as significantly different from each other when the absolute difference between them exceeds the calculated Kolmogorov–Smirnov's critical value at 0.05 significant level.

The KS test was applied to the different estimated hydraulic conductivities obtained:

(1) from field experiments to determine whether those from 10-degree and 20-degree slopes are significantly different from those on the horizontal surface for the different soil types,

(2) from the simulations for the different soil types on 10-, 20-, 30- and 40- degree slopes to determine whether they are significantly different from those on the horizontal surface,

(3) from the simulations on various slopes to determine the maximum allowable slope at which accurate hydraulic estimations can be deduced for each soil type using 2D approximation,

(4) from the simulations with different initial water content and also at different slope angles to investigate the effect of initial water content on the maximum allowable slope for employing 2D approximation to estimate hydraulic conductivity from tension infiltrometer data,

and finally from the simulations on the horizontal surface with different initial water content to determine the water content that gives the most accurate estimations for different soil types. The estimated hydraulic parameters using the inverse approach at different initial water content were compared with the actual (or true) values input into the forward models to see whether they are significantly different.

4.5.3.3 Effect of Land Slope on the Estimation of Soil Hydraulic Conductivity

a Analysis based on the field experiments

Estimated hydraulic parameters based on the field experiments for all the soil types are given in Table 4.4. The unsaturated hydraulic conductivity curves of the loamy sand 1 and silty loam soils are shown in Figure 4.8 as examples as they give the highest and lowest infiltration rates. The KS test results suggested that there are no significant differences between the hydraulic conductivities estimated using data from 10-degree slope and horizontal surface on all the soil types except clay loam 1. However, the differences in those from 20-degree slope and the horizontal surface of loamy sand 1 and sandy loam soil were significant. The results therefore showed that the 2D approximation can be applied on soils that are less hydraulic conductive, namely loamy sand 2, silt loam and clay loam 1 and 2 up to 20-degree slopes. In other words, the impact of 2D approximation to estimate the hydraulic conductivity on sloped surfaces was more significant on soils with higher hydraulic conductivity.

For clay loam 1, the estimated hydraulic conductivity on 10-degree slope was found to be significantly different from those on horizontal surface. However, those from 20 degree slope were not found to be significantly different.

Table 4.4: Soil hydraulic parameters in the Kent Ridge Catchment, Singapore, estimated from numerical inversion using field measurements

Soil Texture	*Slope (Degree)*	θ_s $(cm^3 cm^{-3})$	α (cm^{-1})	η $(-)$	K_s $(cm\ min^{-1})$	l $(-)$
	0	0.30	0.01	1.40	0.012	-0.14
Loamy Sand 1	10	0.30	0.01	1.38	0.014	-0.16
	20	0.30	0.01	1.34	0.016	-0.14
	0	0.30	0.02	2.02	0.005	-0.17
Loamy Sand 2	10	0.30	0.02	2.06	0.005	-0.17
	20	0.30	0.02	2.08	0.005	-0.60
	0	0.34	0.03	2.24	0.003	0.72
Silt Loam	10	0.34	0.03	2.23	0.003	0.50
	20	0.34	0.03	2.24	0.003	0.50
	0	0.32	0.04	2.12	0.012	0.08
Sandy Loam	10	0.32	0.04	2.14	0.012	0.62
	20	0.32	0.04	2.20	0.012	0.26
	0	0.34	0.01	2.11	0.002	-0.14
Clay Loam 1	10	0.34	0.01	1.78	0.003	-0.12
	20	0.34	0.01	2.12	0.002	-0.06
	0	0.32	0.02	1.52	0.007	-0.92
Clay Loam 2	10	0.32	0.02	1.53	0.007	-1.42
	20	0.32	0.02	1.56	0.007	-0.24

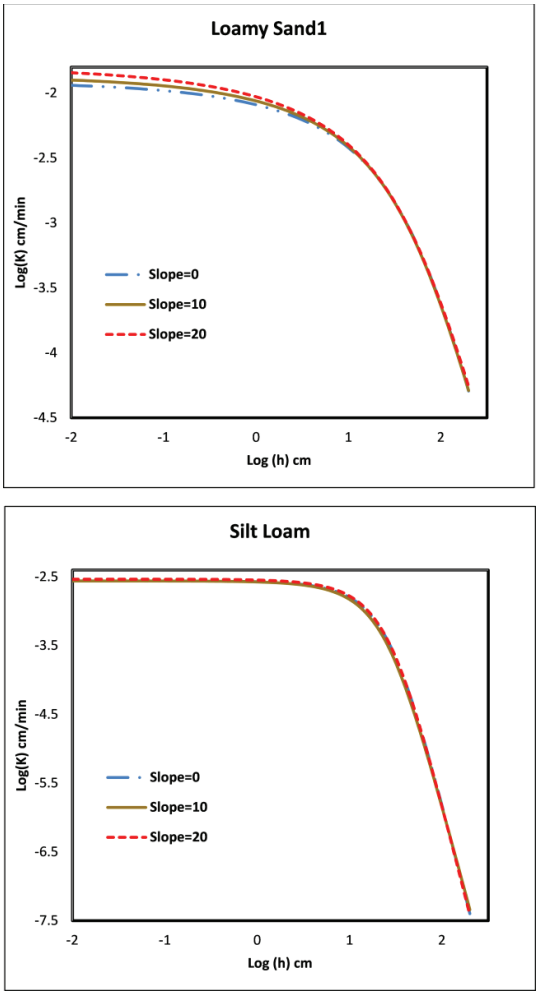

Figure 4.8: Estimated hydraulic conductivities of loamy sand 1 and silt loam at different slopes by inversing field experimental data

The results should be probably due to two major reasons. First, the differences in the initial water content, which were 24, 18 and 24% for 0-,10- and 20-degree slope respectively. More discussions on the impact of initial water content can be found in section 3.2. Second, as soil is intrinsically heterogeneous, it is impossible to repeat the experiment on exactly the same soil profile but with different slope angles. In addition, the effect of 20-degree slope on 2D approximation of loamy sand 1 was significant but not for loamy sand 2. The main reason behind this result is again due to heterogeneity (i.e., different land-uses and soil compaction conditions) because less infiltration rate was observed for loamy sand 2.

The estimated hydraulic parameters as listed in Table 4.4 were also input into HYDRUS 3D to model the infiltration process. The cumulative infiltration curves from field experiments and from simulations yield excellent agreement. This confirms that HYDRUS 3D can be used to forward model tension infiltrometer data for the studies on a wider range of slopes and initial water content.

b Analysis based on forward simulations

The differences in the simulated cumulative infiltration on two soil types (i.e., loamy sand and silt loam as examples) at various slopes are shown in Figure 4.9. Based on the results of the inverse modeling, the effect of the 2D

approximation on the estimated hydraulic conductivities of loamy sand and silt loam soil types is also shown in Figure 4.10.

The KS test showed that there were no significant differences between the hydraulic conductivities estimated using the data from 10-degree slope and the horizontal surface for all soil types except sandy soil. In contrast, hydraulic conductivities estimated from tension infiltrometer data of all soil types simulated on slope more than 30 degrees were significantly different from the ones obtained on the horizontal surface. In addition, silt loam and clay soil estimations were less sensitive to slope when compared to others. Water content under the tension infiltrometer disk for loamy sand and silt loam at the end of the simulation at a 20-degree land slope is shown in Figure 4.11. The water content profile for the soil with higher infiltration rate, i.e., loamy sand, was more asymmetric, implying a stronger effect of gravity and a higher sensitivity to slope.

The maximum land slope at which the estimated hydraulic conductivity was not significantly different from those at horizontal surface is listed in Table 4.5 for different soil types. The results indicate that the higher the infiltration rate, the gentler the slope infiltrometer has to be deployed on and vice versa. The maximum allowable slope for employing the 2D approximation to estimate hydraulic conductivity from tension infiltrometer data on clayey and sandy soil are 25 and less than 3 degree, respectively.

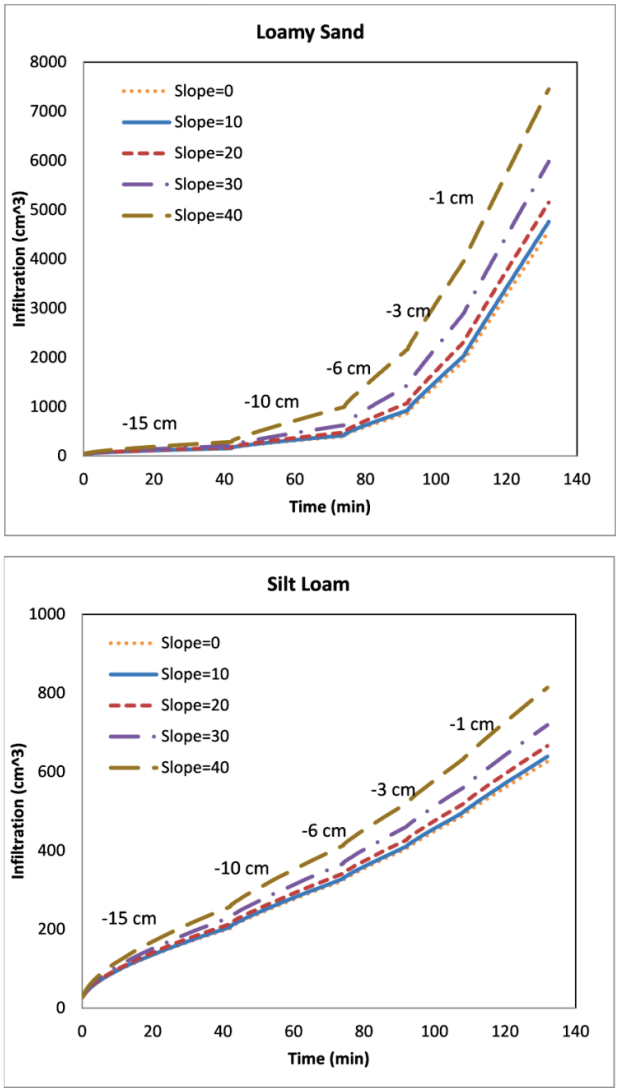

Figure 4.9: Cumulative infiltration into loamy sand and silt loam at various slopes obtained from HYDRUS 3D simulations with same initial pressure head (-100 cm)

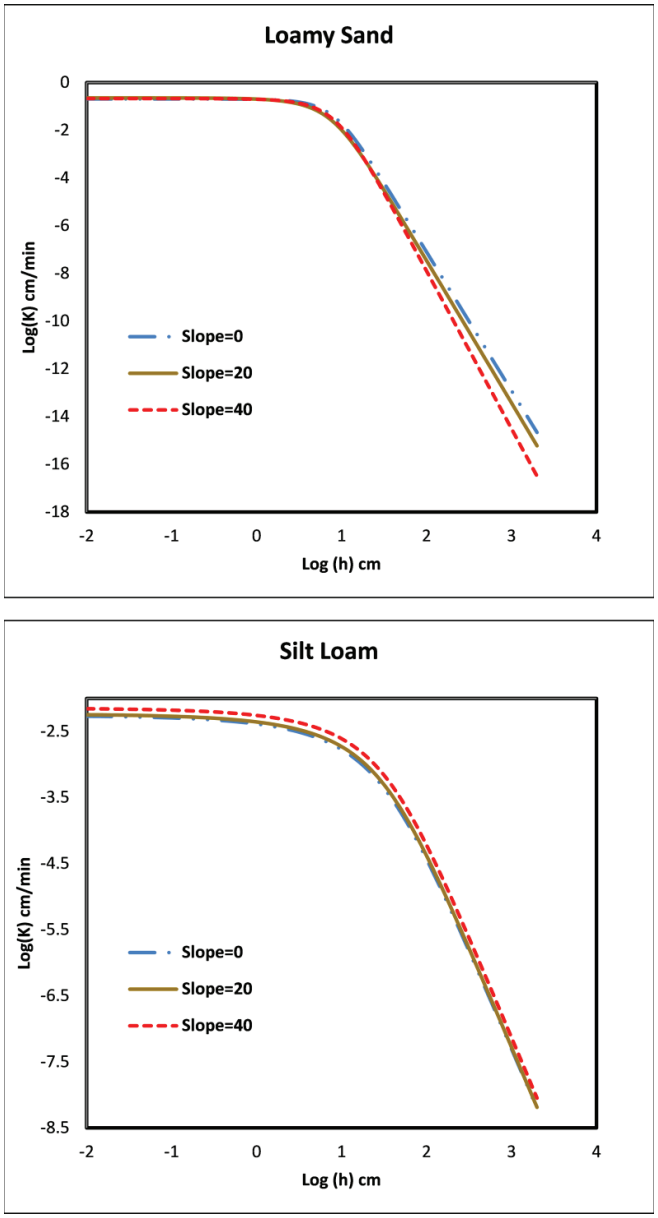

Figure 4.10**:** Estimated hydraulic conductivities of loamy sand and silt loam at different slopes by inversing the simulated infiltrometer data

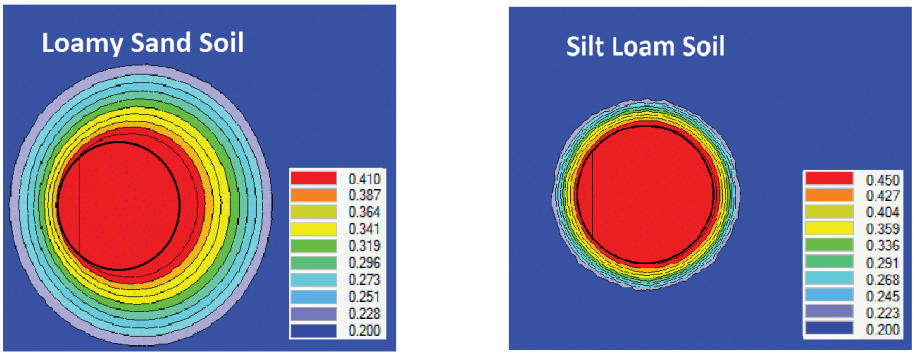

Figure 4.11: Water content under the tension infiltrometer disk at the end of the simulation at a 20-degree slope

Table 4.5: Maximum slope at which accurate hydraulic property can be estimated using 2D approximation for different soil types

Soil Texture	*Infiltration Rate*	*Maximum land slope (degree)*
Sand	Very High	<3
Loamy Sand	High	8
Sandy Loam	Moderate	11
Loam	Moderate	13
Silt Loam	Low	22
Clay	Very Low	25

4.5.3.4 Effect of Initial Water Content

Table 4.6 shows the maximum allowable slope for the application of 2D approximation to estimate hydraulic conductivity from tension infiltrometer data simulated on various soils with different water content to avoid any

significant difference with horizontal estimation. The results showed that the maximum allowable slope decreases with the decrease in water content. As more infiltration occurs in dry soils, these results again confirmed that with increasing infiltration rate, the error of the 2D approximation of 3D problem is more significant.

As the effect of initial water content on the 2D approximation of the 3D problem was significant, its effect on the horizontal surface was further investigated using the simulated infiltrometer data. The estimated hydraulic conductivities using the inverse approach for two soil types (i.e., loamy sand and silt loam soil types as examples) on horizontal surfaces are shown in Figure 4.12 together with the true values input into the forward models. Hydraulic conductivity was better estimated for sandy, loamy sand and sandy loam soil at lower initial water content. In contrast, higher initial water content for silt loam and clay soil gave higher accuracy. In addition, the best estimation of hydraulic conductivity of loamy soil is achieved at a water content of 20%. The results therefore showed that higher and lower initial water content would respectively lead to under-estimation of the hydraulic conductivity in soils with very high and very low infiltration rate.

Overall, low initial water content (e.g. 10%) for soil with high infiltration rate and high initial water content (e.g. 30%) for soil with low infiltration rate gives accurate estimations of hydraulic conductivity from tension infiltrometer

data. Moreover, in soil with moderate infiltration rate such as loamy soil, best estimation would be achieved at an initial water content of around 20%.

4.5.3.5 Summary and Conclusions

Scenarios of tension infiltrometer data at 0-, 10- and 20- degree slope were also carried out at six locations within the Kent Ridge campus of National University of Singapore. In addition, tension infiltrometer data at different land slopes (e.g., 0, 10, 20, 30 and 40 degrees) and with different initial moisture content (10, 20 and 30%) for six soil types at various specified pressures (15,-10,-6,-3 and -1cm) was simulated using HYDRUS 3D. Measured and simulated tension infiltrometer data was then analyzed by HYDRUS 2D to estimate the soil hydraulic properties using inverse modeling. Finally, statistical tests were then performed on the different hydraulic conductivities to see whether they are significantly different from each other.

Table 4.6: Maximum slope at different initial water contents for different soil types at which accurate hydraulic property can be estimated using 2D approximation

Initial Water Content %	Sand (degree)	Loamy Sand (degree)	Sandy Loam (degree)	Loam (degree)	Silt Loam (degree)	Clay (degree)
10	<1	4	7	10	17	20
20	<3	8	11	13	22	25
30	<5	10	13	17	23	26

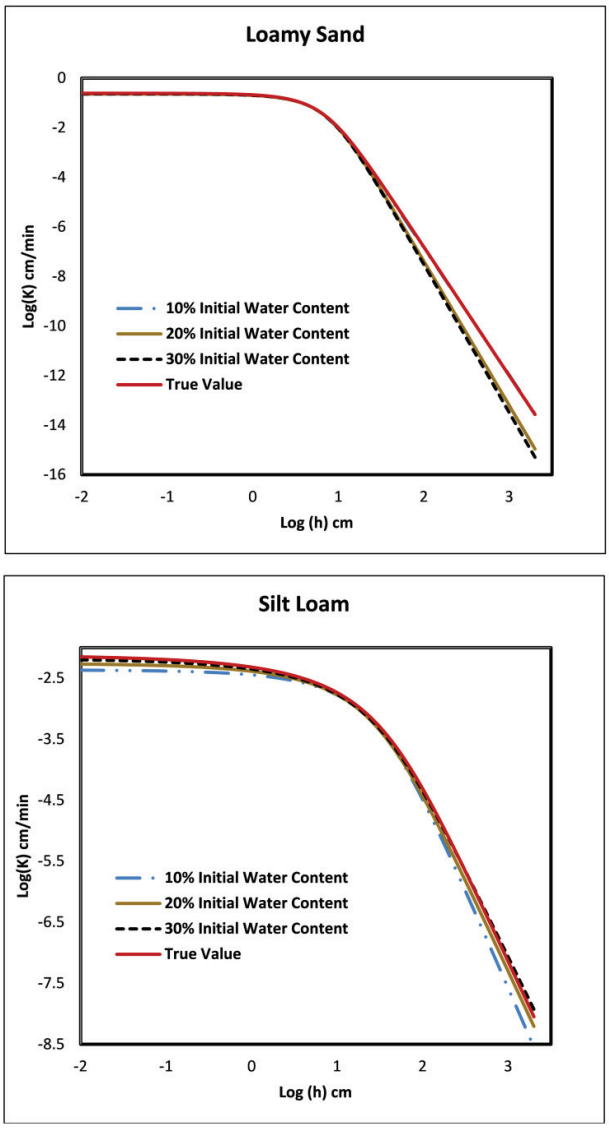

Figure 4.12 **:** Effect of initial water content on estimated hydraulic conductivities on horizontal surface

Both experimental and simulation results showed that the effect of 2D approximation of the 3D problem on soils with higher hydraulic conductivity are more significant. The estimation was accurate for clayey soil at slopes as steep as 25 degrees. However, for accurate estimation of sandy soil, tension infiltrometer measurements should be run on almost horizontal surfaces (i.e., less than 3 degrees). Furthermore, the maximum allowable slope for the application of the 2D approximation to estimate hydraulic conductivity from tension infiltrometer data to avoid any significant difference with horizontal estimation also decreased with decreasing initial water content.

The simulation results also suggested that hydraulic conductivity estimated from tension infiltrometer data can be significantly affected by initial water content. In fact, hydraulic parameters of soils with high infiltration rates can be accurately optimized in low initial water content. In contrast, for soils with low infiltration rates, higher initial water content can enhance the estimation accuracy. Moreover, 20% of initial water content provides the most accurate estimation for soils with moderate infiltration rates.

Overall, the results of this section benefits soil scientists and hydrologists who are interested in applying a tension infiltrometer to estimate soil hydraulic conductivity.

CHAPTER 5 DEVELOPMENT OF AN EMPIRICAL METHOD FOR APPROXIMATING STREAM BASEFLOW TIME SERIES[2]

5.1 Introduction

This thesis used Genetic Programming to establish a modular model consisting of two sub-models: (i) a baseflow module and (ii) a quick flow module to simulate the two hydrograph flow components. In the present chapter, the first modular unit was developed to estimate baseflow time series using GP with minimal data requirements and preservation of physical catchment information. As baseflow time series cannot be obtained from direct field measurements, a validated numerical model was first adopted to simulate baseflow time series for the Kent Ridge Catchment. The simulated baseflow time series were taken as the target parameter variable (i.e. output) in GP to develop an empirical equation predicting a continuous baseflow time series using catchment characteristics and time series of groundwater table elevation in Kent Ridge Catchment collected and processed in Chapter 3 and 4, respectively. The empirical equation was further modified into a generalized

[2] Reprinted from Journal of Hydrology, 519A, Meshgi et al., An empirical method for approximating stream baseflow time series using groundwater table fluctuations,1031-1041, doi:10.1016/j.jhydrol.2014.08.033, Copyright (2014), with permission from Elsevier.

structure for its applicability in other catchments. The generalized baseflow equation was tested in a cross-site, cross-scale application in Beaver River Basin. Finally, its performance was compared to baseflow time series estimates obtained using the RDF method in both study sites.

5.2 Numerical Modeling

Baseflow time series needed for the derivation of the empirical equation in Kent Ridge Catchment, using GP, was obtained by the groundwater flow model HYDRUS-3D. HYDRUS-2D/3D package software is a Windows based modeling environment for water flow and solute transport in variably saturated porous media. One of the main advantages of this software is that instead of coupling different models, HYDRUS-3D is able to model both saturated and unsaturated zones (Kuznetsov et al., 2012) by numerically solving the modified Richards' equation (Šejna, 2007) (See Section 4.5.3.1).

Model setup in HYDRUS-3D involved creating the modeling domain, generating a finite element mesh and defining domain properties, initial conditions and boundary conditions.

- **Modeling Domain**

  Using ArcGIS v10, the surface layer was created based on the available digital elevation model (DEM) with 1×1 meter grid resolution provided by Public Utilities Board (PUB), and the bedrock layer was

generated using information 27 existing boreholes reported by Ryobi Geotechnique PTE LTD (2005) based on the Natural Neighbor method. Surface and bedrock layers were then imported in the HYDRUS-3D. As HYDRUS solves the Richards equation which is a local (point) equation, the HYDRUS thus requires a fine spatial discretization however, fine grid size will computationally expensive. Therefore, we reduced the size of our domain (Figure 5.1) in order to decrease the number of finite elements nodes. The identified land use categories in this sub-catchment include grasses on mild and steep slopes, mixed grasses and trees and relatively natural vegetation which are representative for the entire catchment. In addition, measured pressure heads at BH1 and BH2 located at this sub-catchment (Figure 5.1) can be used to accurately optimize the soil hydraulic parameters in HYDRUS-2D (See section 5.7.1).

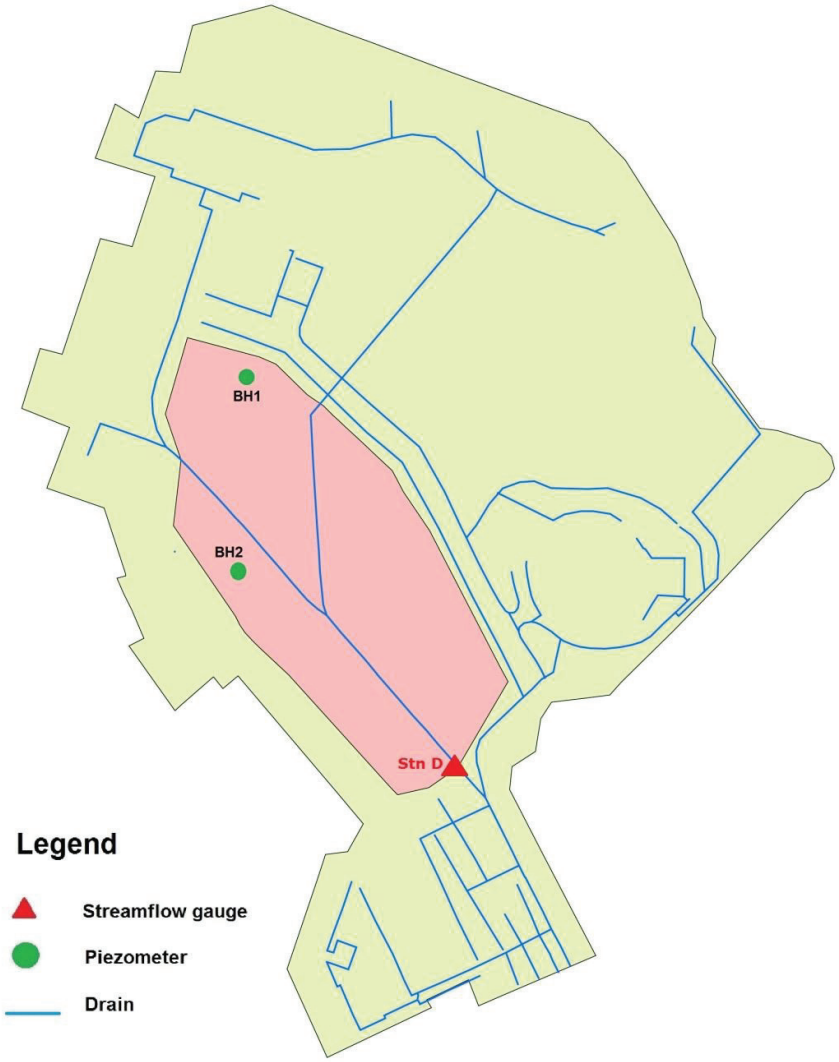

Figure 5.1 : Location of selected sub-catchment for numerical modeling in HYDRUS3D

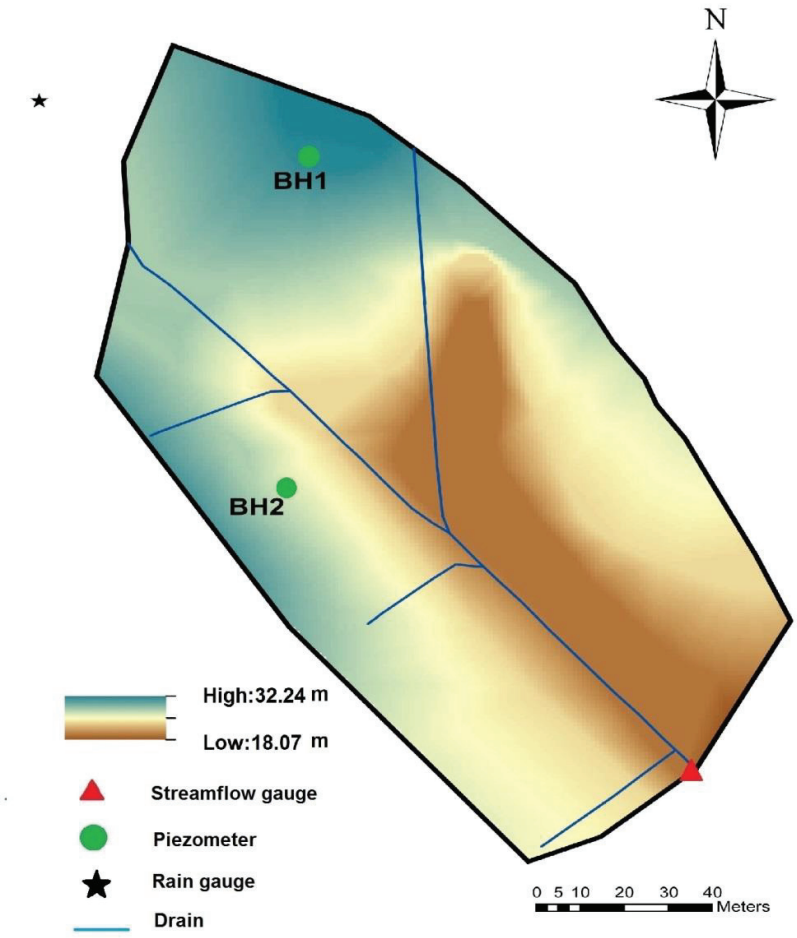

Figure 5.2 : Selected sub-catchment for numerical modeling in HYDRUS3D in Kent Ridge Catchment, Singapore with monitoring stations, drainage network and DEM

- **Finite Element Mesh**

The required size of finite elements is defined according to the three important rules (Šimůnek, 2007):

1. Spatial discretization of the boundary conditions specified for small time intervals requires being finer.
2. Coarse-textured soils generally need a finer discretization.
3. The finite element mesh can be several times coarser in the horizontal direction than in the vertical direction.

Accordingly, 1 meter and 20 centimeter resolutions were applied in horizontal and vertical directions, respectively, resulting in a mesh of 78240 nodes and 141322 finite elements (Figure 5.3).

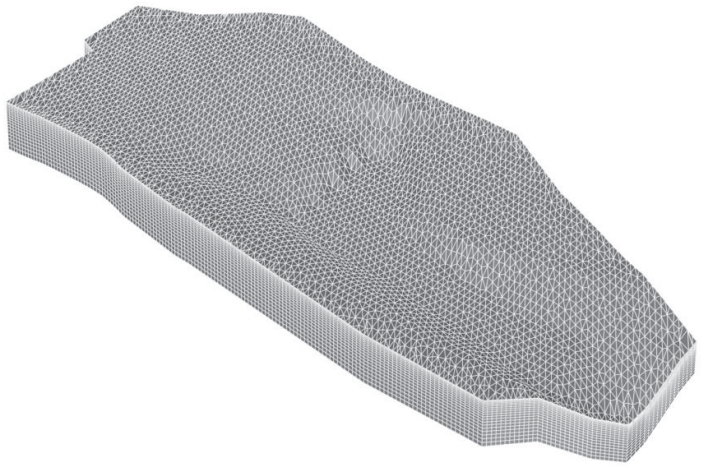

Figure 5.3 : Finite element mesh of Kent Ridge Catchment, Singapore in HYDRUS-3D

- **Soil Hydraulic Properties**

Inverse modeling approach in HYDRUS-2D (See Section 4.5.1) was used to estimate the soil hydraulic properties at different soil layers by matching observed and simulated pressure heads.

In order to estimate the soil hydraulic parameters, a cross section from BH1 to BH2 was defined in HYDRUS-2D. Soil profiles were divided into 4 layers based on the comprehensive study on soil investigation in the Kent Ridge Catchment reported by Ryobi (2005). Soil hydraulic parameters from infiltration measurements (Chapter 3) were used as initial estimates for the surface layer while initial estimates for the soil hydraulic parameters of the three bottom soil layers were chosen according to Carsel and Parrish (1988) (Table 4.3). Afterwards, measured pressure heads at BH1 and BH2 from January until December 2012 were used to optimize the soil hydraulic parameters in HYDRUS-2D, while the data from January until June 2013 were adopted for validation. Afterwards, based on the results of inverse modeling, the soil properties in HYDRUS-3D were specified.

- **Initial and Boundary Conditions**

Four boundary conditions were applied including no flux, specified head, seepage face and atmospheric boundary. No flux boundary was applied to the bottom of domain. Specified head boundary with a distribution versus depth was employed to the vertical boundaries where there should be a groundwater outflow. Seepage face boundary was applied where groundwater table was shallow so that water seeped out of the ground when the groundwater table reached the land surface. The seepage face boundary, however, automatically became an atmospheric boundary condition when the soil was unsaturated (i.e., pressure head is negative). For the unpaved areas including relatively natural vegetation and grasses, atmospheric boundary conditions were implemented to simulate precipitation and evapotranspiration. The physically-based Penman-Monteith equation was applied to estimate reference evapotranspiration using meteorological data from the NUS Geography weather station:

$$ET_0 = \frac{0.408(R_n - G) + \frac{\gamma 9000}{T+273} U_2 (e_s - e_{a)}}{\Delta + \gamma\ (1 + 0.34 U_2)} \qquad 5.1$$

where:

- ET_0 reference evapotranspiration (mm/d)
- R_n net radiation (MJ m^{-2} d^{-1})

- Δ rate of increase with temperature of the saturation vapour pressure of water at air temperature (kPa °C^{-1})
- G soil heat flux(MJ m^{-2} d^{-1})
- T mean daily temperature (°C)
- U_2 wind speed at 2m height (m s^{-1})
- e_s saturation vapour pressure (kPa)
- e_a actual vapour pressure(kPa)
- γ psychrometric constant (kPa °C^{-1})

Estimated reference evapotranspiration was then separated into potential evaporation and transpiration according to the leaf area index (LAI). The actual values of transpiration and evaporation were calculated by HYDRUS based on the potential values and the availability of water in the soil profile (Šimůnek et al., 2006).

HYDRUS-3D was first run for 10 years with constant precipitation and reference evapotranspiration rates of 6.85 and 3.5 mm day^{-1}, respectively. The simulated pressure heads from the 10-year steady state simulation were used as an initial condition for the subsequent unsteady state simulation. The calibrated and validated HYDRUS-3D provided daily simulated groundwater table and baseflow data from January 2011 until June 2013. Baseflow was extracted from the simulation by integrating the

flux across the seepage face boundary. It should be mentioned that the steady state (10 years) and un-steady state (from January 2011 until June 2013) simulations using HYDRUS-3D took more than 72 and 192 hours, respectively, on an Intel Core i7-2600 (quad core) 3.4 GHz CPU PC.

5.3 Genetic Programing

GP, a specialization of Genetic Algorithms (GA), is a powerful tool that uses a tree-structured approach to relate the input information to the output information of a system and develop a data-based model. The following steps summaries the main steps of GP computation (Figure 5.6):

- **Initialization**: GP uses function trees with two different sets defined by a user including 1) a function set which involves mathematical functions and arithmetic operators (e.g. sin, cos, -,*, /, +) and 2) a terminal set which represents external inputs, constants, and zero augment functions. An example of a function tree used in GP is shown in Figure 5.4. These trees can be created randomly in GP using different methods such as full, grow, ramped half-and-half and exact uniform initialization.
- **Selection**: A fitness function is constructed to select the models (trees) which have better performance for reproduction in a probabilistic manner. Models with poorer fitness have less chance to be selected for reproduction than those of better fitness.

- **Reproduction**: In this stage, three genetic operators including crossover, mutation, and reproduction may be applied to create subsequent generations from selected models. Two function trees in the parent models before and after the crossover and mutation operation are shown in Figure 5.5. It should be mentioned that in reproduction operation a model is copied unchanged to the new population.
- **Termination**: GP continues to create new generation from the selected population until satisfying the optimality criteria or the maximum pre-specified number of generations.

In the current research, a GP software called GPKERNEL (Babovic and Keijzer, 2000) was employed to relate baseflow time series with hydrological and physical catchment parameters (Table 5.1). An overview of the evolutionary algorithm setup in this study is presented in Table 5.2. One experiment was set up in GP, to relate baseflow time series simulated by HYDRUS-3D to catchment characteristic and groundwater table elevation time series of Singapore catchment. In this experiment, simulated baseflow time series by HYDRUS-3D was defined as target output.

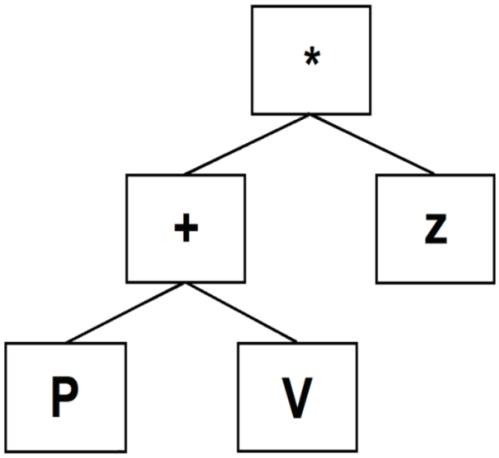

Figure 5.4 : An example of a function tree used in GP representing the expression (p+v)*z where '+' and '*' are inner nodes while p, v, and z represents terminal nodes (Babovic and Keijzer, 2000)

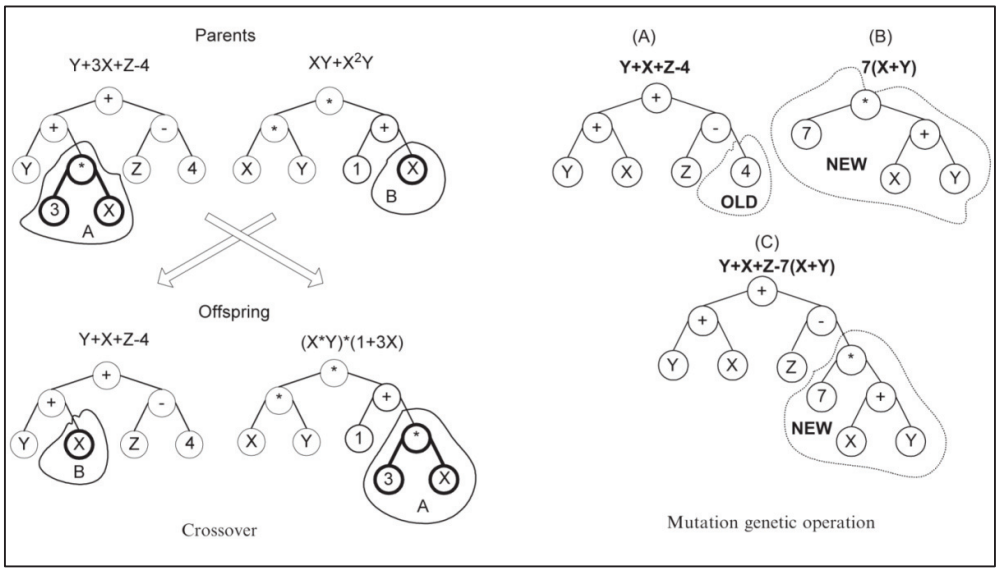

Figure 5.5 : Two function trees in the parent models before and after the crossover and mutation operation (Hong and Bhamidimarri, 2003).

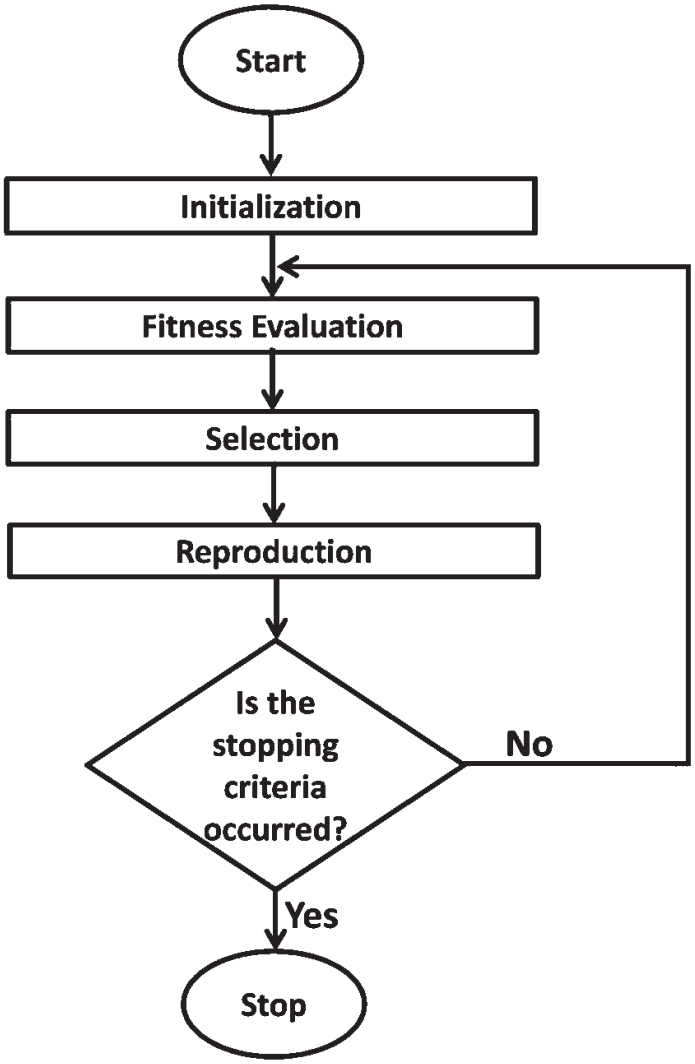

Figure 5.6: The flowchart of the main steps in GP computation

Table 5.1: Definition of terminal set parameters

Parameter name	Parameter definition	Unit	Type
R	Daily precipitation	[L]	Input
ET	Daily evapotranspiration	[L]	Input
Δh_p	Normalized daily average of pressure head	[L]	Input
ET_{av}	Annual daily average of evapotranspiration	[L]	Constant
R_{av}	Annual daily average of precipitation	[L]	Constant
α	Coefficient in the soil water retention function	[L^{-1}]	Constant
n	Exponent in the soil water retention function	[-]	Constant
l	Pore-connectivity parameter	[-]	Constant
K_s	Daily saturated hydraulic conductivity	[L]	Constant
$Q_{B(\min)}$	Minimum daily baseflow volume	[L^3]	Constant
$Q_{B(\max)}$	Maximum daily baseflow volume	[L^3]	Constant
A	Surface area of catchment	[L^2]	Constant

Table 5.2 : An overview of the evolutionary algorithm setup

Parameter	Value
Objective	Find the daily baseflow volume (Q_B)
Population size	250
Number of children to produce	500
Number of generations	500
Tournament size	3
Brood size	2 (culling function on unit error)
Crossover probability	0.4
Mutation probability	0.05
Crossover method	Random subtree crossover
Objective Functions	RMSE and unit error
Function set	*, +,-, %, - x , sqrt, power
Maximum size at initialisation	15
Maximum size	41
Probability of selecting a constant vs. a variable	0.05
Constant mutation probability	0.05
Stopping criteria	500 generations

In addition, normalized pressure head, minimum daily baseflow of the entire period, precipitation and evapotranspiration data from January 2011 until August 2012 were used as input parameters in GP. For this experiment, normalized pressure head was calculated as follows:

$$\Delta h_{p(t)} = h_{(t)} - h_{min} \quad (5.2)$$

in which $\Delta h_{p(t)}$ is normalized pressure head, $h_{(t)}$ is the daily averaged pressure head (m) and h_{min} is the minimum daily averaged pressure head (m) observed over the entire data set.

5.4 Generalization of the Empirical Equation

The groundwater table fluctuation of a borehole with an average depth of 4 m below the surface was used to drive the empirical equation in Kent Ridge catchment. Nevertheless, the groundwater depth or fluctuation may not be at the same range in other catchments. Therefore, the empirical equation should be generalized to estimate baseflow time series from groundwater table at any depth or range of fluctuation. To determine the effect of groundwater table depth on the estimation of baseflow time series, the lag time between the rainfall events and groundwater table responses at fifteen locations within the Kent Ridge Catchment with various groundwater table depth (i.e., from 1-14 m) was extracted from HYDRUS-3D.

5.5 Recursive Digital Filters

The Beaver River Basin was used to test the suitability of the general empirical equation under different conditions. As neither baseflow time series nor a numerical model was available to generate baseflow time series, a recursive filter method was used to evaluate the performance of generalized empirical equation in both study sites. The filter method used in this study has been proposed by Willems (2009) which is a generalization of the original Chapman-filter (1991):

$$f_k = af_{k-1} + b(y_k - \beta y_{k-1}) \quad (5.3)$$

$$b_k = \beta b_{k-1} + c(1-\beta)(f_k + f_{k-1}) \quad (5.4)$$

with:

$$\beta = \exp\left(-\frac{1}{k}\right) \quad (5.5)$$

$$a = \frac{(2+\nu)\alpha - \nu}{2+\nu-\nu\beta} \quad (5.6)$$

$$b = \frac{2}{2+\nu-\nu\beta} \quad (5.7)$$

$$c = 0.5\nu \quad (5.8)$$

with:

$$\nu = \frac{1-w}{w} \quad (5.9)$$

where f_k is the filtered quick response at k^{th} sampling instant ($f_k \geq 0$), y_k is the original streamflow, b_k is the filtered baseflow, β is the filter parameter, w

represents the case-specific average fraction of the quick flow volumes over the total flow volumes. To support the time series processing, Willems (2009) developed a Microsoft Excel-based tool, Water Engineering Time Series Processing tool (WETSPRO) (http://perswww.kuleuven.be/~u0009249/). The tool separates observed discharges into three flow components, i.e. storm water, quick sub-surface flow (interflow) and slow sub-surface flow (baseflow).

Filter parameters for Beaver River Basin were estimated using observed discharge data from January 1990 until December 2002, while the rest of discharge time series data (January 2003- August 2013) was employed for validation. With regards of Kent Ridge Catchment, discharge data from September 2011 until August 2012 was used to calibrate the Chapman-filter parameters proposed by Willems, while the data from January until June 2013 was adopted for validation.

5.6 Statistical Tests

Performance of the established equation in GP was tested using three commonly used error functions: Relative Root Mean Squared Error (RRMSE), Correlation Coefficient (CC) and the Nash–Sutcliffe Efficiency (NSE) statistic (Nash and Sutcliffe, 1970).

RRMSE is calculated by using Equation (5.10):

$$\mathrm{RRMSE} = \sqrt{\frac{1}{n}\sum_{i}^{n}\left(\frac{x_i - y_i}{x_i}\right)^2} \qquad (5.10)$$

where, x_i is observed value, y_i is estimated value, and n is the number of data points.

The correlation coefficient is defined as:

$$\mathrm{CC}(X,Y) = \frac{\mathrm{COV}(X,Y)}{\sigma_x \sigma_y} = \frac{\sum_i^n (x_i - \bar{x})(y_i - \bar{y})}{\sqrt{\sum_i^n (x_i - \bar{x})^2}\sqrt{\sum_i^n (y_i - \bar{y})^2}} \qquad (5.11)$$

in which COV is the covariance between variables x and y; σ_x and σ_y are the standard deviations of x and y, respectively; $\bar{x}$ and $\bar{y}$ are the average values of observed and estimated, respectively. CC ranges within the domain [1,-1] where value of 1 and -1 indicate positive and negative perfect linear correlation while CC of 0 indicates that there is no correlation between the two data series.

The Nash–Sutcliffe efficiency is represented by Equation (5.12):

$$\mathrm{NSE} = 1 - \frac{\sum_i^n (x_i - y_i)^2}{\sum_i^n (x_i - \bar{x})^2} \qquad (5.12)$$

NSE = 1 corresponds to a perfect match of estimated and observed values while an efficiency of 0 indicates that the model estimations are as accurate as the mean of the observed data.

The confidence intervals for the parameters within the equation as well as for the predicted baseflow time series were obtained using the bootstrap method (DiCiccio and Efron, 1996; Efron and Tibshirani, 1993), a resampling

technique suitable for non-normally distributed populations. This method consists of re-sampling the data set independently and with equal probabilities for a specified number of times (Efron and Tibshirani, 1993). The resampling technique was performed using the bootstrap function in MATLAB, using 1000 iterations according to Efron and Tibshirani (1993), computing the corresponding regression coefficients, calculating the standard error and corresponding confidence intervals. Similar procedures were performed for the prediction of baseflow time series.

5.7 Results and Discussion

5.7.1 Simulating Baseflow Time Series in Kent Ridge Catchment Using HYDRUS-3D

Hydraulic parameters estimated from inverse modeling in HYDRUS-2D for all soil layers are given in Table 5.3. Pressure heads from the steady-state simulation in HYDRUS-3D agreed with the average observed groundwater table data. Observed pressure heads at BH1and BH2 were compared with the simulated ones from the unsteady state simulations in Figure 5.7 and the model performance indicators are calculated (Table 5.4). As can be seen, there was excellent agreement between the observed and simulated data, indicating a good calibration of the HYDRUS-3D model. Subsequently, 2.7 years of baseflow and pressure head time series were extracted from HYDRUS-3D.

Table 5.3: Estimated hydraulic parameters based on inverse modeling in HYDRUS-2D

Layer	**Depth (m)**	θ_s (m^3m^{-3})	α (m^{-1})	η $(-)$	K_s $(m\,day^{-1})$	l $(-)$
1	0-0.5	0.30	1.30	1.40	0.18	-0.14
2	0.5-1.5	0.47	0.23	2.96	2.85	0.01
3	1.5-4	0.44	0.11	1.17	2.76	0.03
4	>4	0.38	0.56	2.62	3.58	0.91

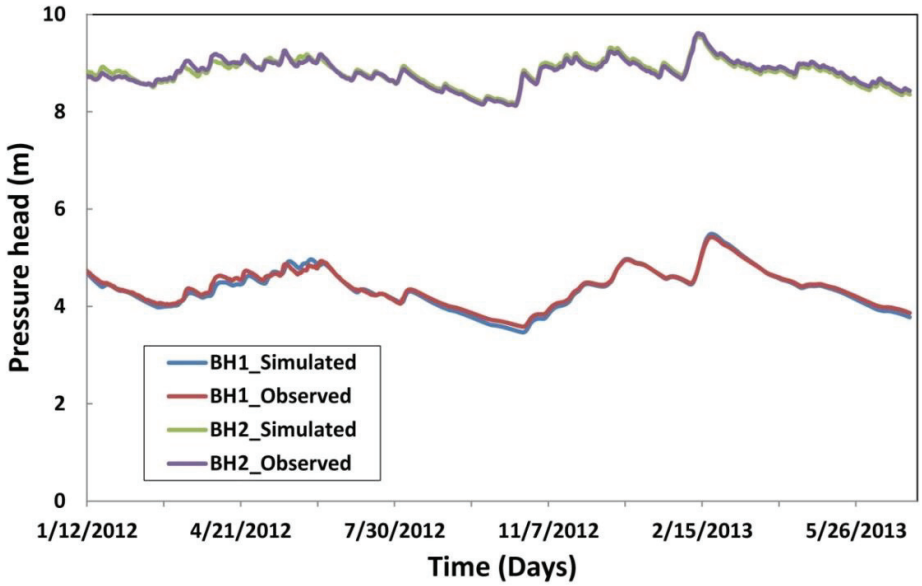

Figure 5.7: Observed and simulated pressure heads at BH1 and BH2 in Kent Ridge Catchment, Singapore which are respectively 180 and 90 m away from the discharge measurement station

Table 5.4: Error functions associated with observed and simulated pressure heads at BH1and BH2

Boreholes	Error criteria		
	RRMSE	NSE	CC
BH1	0.031	0.972	0.995
BH2	0.033	0.957	0.978

5.7.2 Approximating Baseflow Timeseries in Kent Ridge Catchment

Based on the time series baseflow data simulated by HYDRUS-3D, GP was set up to derive the empirical equation. The following equation was obtained:

$$Q_{B(t)} = Q_{B(min)} + \sqrt{0.305A}\,\Delta h_{p(t)}^2 \qquad (5.13)$$

where $Q_{B(t)}$ presents the daily baseflow volume (m^3), $Q_{B(min)}$ is the minimum daily baseflow volume over the entire data set (m^3), A is the total unpaved surface area in the catchment (m^2), $\Delta h_{p(t)}$ is the normalized daily average of pressure head (m) ($\Delta h_{p(t)} = h_{(t)} - h_{min}$ in which $h_{(t)}$ is the daily averaged pressure head and h_{min} is the minimum daily averaged pressure head (m) observed over the entire data set).

Figure 5.8 compares baseflow time series estimated by the empirical equation and those simulated by HYDRUS-3D. Error criteria including NSE, CC and RRMSE between baseflow time series simulated by HYDRUS-3D and the empirical equation are listed in Table 5.5. According to these results, differences between baseflow time series simulated by HYDRUS-3D and

empirical equation were minimal, confirming that the empirical equation can accurately estimate baseflow time series in the absence of discharge measurements. The uncertainty of the parameters using the bootstrapping method showed the significance of both parameters ($Q_{B(min)}$ and $\sqrt{0.305A}$) at $\alpha = 0.05$ with narrow confidence intervals ($\pm 0.77\ m^3$ and ± 1.38, respectively). In addition, the 95% confidence interval for the predicted baseflow time series was $\pm 1.2\ m^3$ resulting in a reasonably small error band around the median.

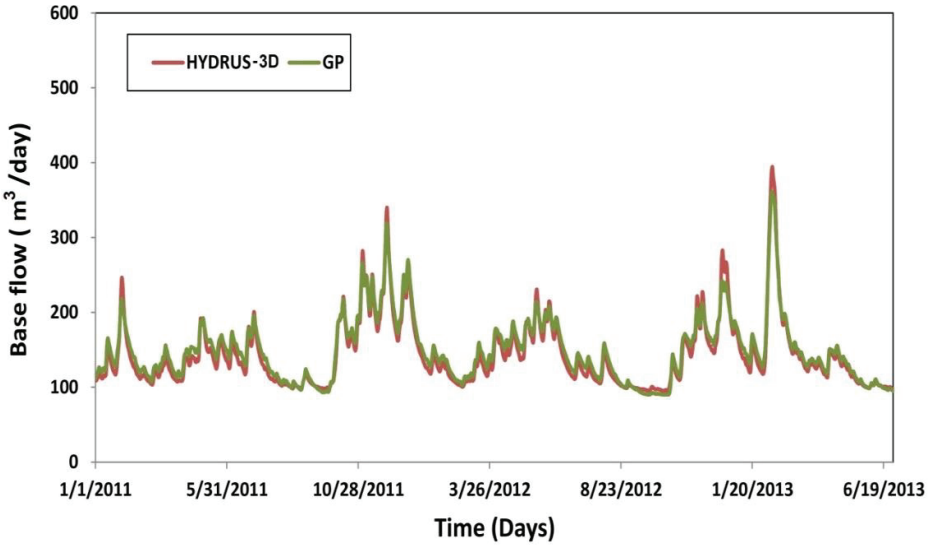

Figure 5.8: Comparison between baseflow estimated by the empirical equation and HYDRUS-3D in Kent Ridge Catchment, Singapore

Table 5.5: Error criteria between baseflow time series simulated by HYDRUS-3D and the empirical equation

Data Set	Error criteria		
	RRMSE	NSE	CC
Train	0.06	0.95	0.98
Test	0.06	0.98	0.99

The first term in the empirical equation is the minimum baseflow corresponding to the deepest groundwater table in the dry period, while the second term approximates the additional baseflow due to the rise in groundwater table. In absence of rainfall, the minimum baseflow is expected to occur during the dry period corresponding to the minimum groundwater table. As it can be assumed that during the dry period groundwater recharge is minimal and relatively constant, the overall minimum discharge observed during these periods can be taken as minimum baseflow.

In this equation, pressure head (h) is the only variable and baseflow is correlated with h^2. This is similar to Darcy's Law ($q = kh(\frac{\partial h}{\partial x})$) that relates discharge through an unconfined aquifer to h^2. It shows that the empirical equation derived by GP for estimating baseflow time series contains physical information. By comparing the empirical equation and Darcy's Law, it also seems that the constant coefficient b (0.305) is related to the saturated hydraulic conductivity (K_s). Therefore, the effect of saturated hydraulic conductivity on the coefficient was further investigated using the simulated

baseflow and pressure head time series for different soil types listed in Table 5.6 using HYDRUS-3D.

Table 5.6 : Soil hydraulic parameters of the van Genuchten functions (van genuchten, 1980) for five soil textural classes of the USDA chosen according to Carsel and Parrish (1988)

Soil Texture	$\theta_r\ (L^3L^{-3})$	$\theta_s\ (L^3L^{-3})$	$\alpha(m^{-1})$	$\eta(-)$	$K_s(m\ day^{-1})$
Loamy Sand	0.057	0.41	12.4	2.28	3.5
Sandy Loam	0.065	0.41	7.5	1.89	1.06
Loam	0.078	0.43	3.6	1.56	0.25
Silt Loam	0.067	0.45	2	1.41	0.11
Clay	0.068	0.38	0.8	1.09	0.05

The following linear relationship between the constant coefficients and saturated hydraulic conductivity with R^2=0.984 was found:

$$b = 0.1\mathrm{K}_s \qquad (5.14)$$

where b is the constant coefficient and K_s is the saturated hydraulic conductivity.

To validate this relationship in Singapore, the average saturated hydraulic conductivity was calculated based on inverse modeling approach in HYDRUS-2D resulting in an average value of 3.09 which yields a value of 0.309 for b according to Equation 5.14. This value is very close to the one in Equation 5.13, showing that $0.1\mathrm{K}_s$ is a good approximation for the coefficient in the empirical equation.

However, soil properties or simulated baseflow time series is also not always available in other catchments to estimate the coefficient in the

empirical equation. Hence, one alternative and general method should be identified for optimization purposes. The proposed method is based on the assumption that before the beginning of the rainfall event, the discharge in the stream is due to baseflow. Therefore, by substituting discharge values in the channel before the beginning and other known parameters (e.g. minimum daily baseflow and area of the catchment) into the empirical equation, the constant coefficient can be easily estimated. However, it is important to identify the amount of data points (i.e., rainfall events) needed to optimize the constant coefficient. Therefore, 17 rainfall events (Table 5.7) at Kent Ridge Catchment covering seasonal variability (monsoon vs. non-monsoon), various dry weather periods prior to the event and groundwater table depth were selected. As can be seen, almost the same average event based constant coefficient estimation was obtained as the one resulting from the empirical equation (Equation 5.13). In addition, this table presents error criteria associated with baseflow estimated by the average event based constant coefficient and the individual event based estimation. As the estimated baseflow time series values did not follow a normal distribution, the nonparametric statistics test namely Kolmogorov–Smirnov (KS) was applied to determine whether estimated baseflow obtained by the average event based constant coefficients were significantly different from those obtained by the individual event based estimation. No significant difference between baseflow obtained by the average event based constant coefficients and the individual

event based estimation was found using the KS test at $\alpha = 0.05$. In other words, the constant coefficient can be optimized based on a single event.

5.7.3 Generalization of the Empirical Equation

This section derives a generalized empirical equation for approximating baseflow time series in other catchments. First, the effect of groundwater table depth on the estimation of baseflow time series was investigated. The lag time between the rainfall events and groundwater table response at 15 locations in HYDRUS-3D are listed in Table 5.8. The results showed that shallower groundwater tables had the shorter lag times with the rainfall events and correspondingly yield higher NSE values. Therefore, if several wells are available, those with shallower groundwater tables yield better and therefore more reliable results.

Table 5.7 : Main characteristics of selected events observed at Kent Ridge Catchment, Singapore

Event	Date	Number of dry days before the beginning of the event	Measured discharge value before the beginning of the event (m^3/day)	Normalized daily average of pressure head (m)	Constant Coefficient (-)	Error criteria		
						RRMSE	NSE	CC
1	10/18/2011	7	167.70	0.84	0.28	0.05	0.96	0.97
2	11/5/2011	3	217.80	1.06	0.30	0.06	0.96	0.97
3	12/14/2011	5	186.60	0.90	0.34	0.07	0.95	0.97
4	1/15/2012	4	136.90	0.63	0.33	0.06	0.95	0.97
5	2/12/2012	6	119.10	0.49	0.35	0.07	0.94	0.97
6	3/1/2012	3	112.60	0.45	0.28	0.05	0.96	0.97
7	4/6/2012	3	163.30	0.83	0.27	0.05	0.96	0.97
8	5/29/2012	3	186.90	0.97	0.25	0.06	0.95	0.97
9	6/27/2012	6	121.60	0.55	0.25	0.06	0.95	0.97
10	7/14/2012	3	125.48	0.55	0.32	0.06	0.96	0.97
11	8/17/2012	13	113.21	0.47	0.26	0.05	0.96	0.97
12	1/8/2013	4	156.00	0.75	0.32	0.06	0.96	0.97
13	2/12/2013	3	297.50	1.37	0.28	0.05	0.96	0.97
14	3/13/2013	3	147.60	0.75	0.24	0.06	0.94	0.97
15	4/21/2013	2	152.50	0.75	0.29	0.06	0.96	0.97
16	5/7/2013	4	135.20	0.66	0.25	0.06	0.95	0.97
17	6/7/2013	3	109.20	0.41	0.30	0.06	0.96	0.97
				Average	0.29	0.06	0.96	0.97

The results additionally revealed that deeper groundwater table corresponds with a longer lag time. Therefore, for locations with the average groundwater table depth exceeding 5 meter, a lag time in the groundwater table should be considered in the derivation of the empirical equation. In addition, soil properties may also affect the lag time. The effect of the soil type over the entire area on the estimation of this parameter was further investigated by generating various baseflow time series with HYDRUS-3D. The results that can be used for estimating this parameter from average groundwater table depth (m) in different soil types are listed in Table 5.8, supporting that due to the low infiltration rates in soils with lower saturated hydraulic conductivity, more lag times need to be taken into account.

As such, a generalization of the empirical equation is as follows:

$$Q_{B(t)} = Q_{B(min)} + \sqrt{bA}\,\Delta h^2_{p(t+k)} \qquad (5.15)$$

where b is the coefficient related to the saturated hydraulic conductivity ($b = 0.1K_s$) and k is the lag time between the rainfall events and groundwater table responses (T).

Assuming the minimum discharge occurring within the dry weather period represents perennial baseflow during extreme seasonal low flow of the catchment. Therefore, the equation reveals the additional baseflow fluctuation

Table 5.8 : Estimation of lag time (k) in empirical equation from average of groundwater table depth (m) in Singapore catchment and different soil types

Soil Type	k (days)								
	0	**1**	**2**	**3**	**4**	**5**	**6**	**7**	**8**
Singapore Catchment	<5	6-7	7-8	8-9	9-10	10-11	11-12	12-13	13-14
Loamy Sand	<5	6-7	7-8	8-9	9-10	10-11	11-12	12-13	13-14
Sandy Loam	<4	5-6	6-7	7-8	8-9	9-10	10-11	11-12	12-13
Loam	<3	4-5	5-6	6-7	7-8	8-9	9-10	10-11	11-12
Silt Loam	<2	3-4	4-5	5-6	6-7	7-8	8-9	9-10	10-11
Clay	<1	2-3	3-4	4-5	5-6	6-7	7-8	8-9	9-10

as function of the lag time dependent normalized water table fluctuations and accounts for the recharge characteristics of the catchment through the average hydraulic conductivity of the unpaved area as well as its contributing drainage area (m^2).

The structure of Equation 5.15 is comparable to the rating carve method proposed by Sellinger (1996) as follows:

$$Q = B_0 h^B \qquad (5.16)$$

where Q (m^3/s) is the discharge at the outlet of the catchment, h (m) is the groundwater level in an observation well, or an average groundwater level all over the catchment, and B_0 (m^3/s), B (1/m) are fitting parameters. The parameters in Equation 5.16 can be related to ones obtained in Equation 5.15 as follows:

- B_0 can be approximated from the saturated hydraulic conductivity (Ks) and the catchment area(A) ($B_0 = \sqrt{0.1 K_s A}$).
- B is equal to 2 and one may not need to determine this parameter separately for each event.
- As groundwater tables vary significantly throughout catchments, the effect of groundwater table fluctuations on baseflow prediction is improved by using a lag time coefficient in the general equation.

5.7.4 Evaluation of the Generalized Equation in Beaver River Basin

The performance of the general equation was evaluated using an independent dataset from a larger vegetation-dominated basin located in the US. (i.e. Beaver River Basin). As no baseflow time series were available in Beaver River Basin, the RDF method was used to obtain baseflow time series in both study sites and results were compared with the ones obtained from the empirical equation. By visually inspecting the plots of filtered results in WETSPRO, the filtering parameters 'k' and 'w' for baseflow separation were found to be 4 days and 0.7 for Kent Ridge Catchment, respectively. Filtering parameters 'k' and 'w' in the RDF were optimized as 40 days and 0.3 for Beaver River Basin, respectively. Figure 5.9 shows baseflow filter results based on daily river flow of Beaver River from 1/1/1990 until 31/08/2013. The slant dotted lines in the figure, representing the slope recession constant baseflow, follow the recession trends, implying that the filter parameters were well estimated according to the criteria reported by Willems (2009).

The $Q_{B(min)}$, b, and k parameters in Equation 5.15 for the Beaver Basin were 55 m^3, 0.123 and 0 respectively. Based on these results and the proposed relationship between b and Ks (Equation 5.14), the average of saturated hydraulic conductivity was estimated as 1.23 m/day which represents sandy loam soils for this basin and was confirmed by the soil report available for this basin (Rhode Island Digital Atlas, 2014).

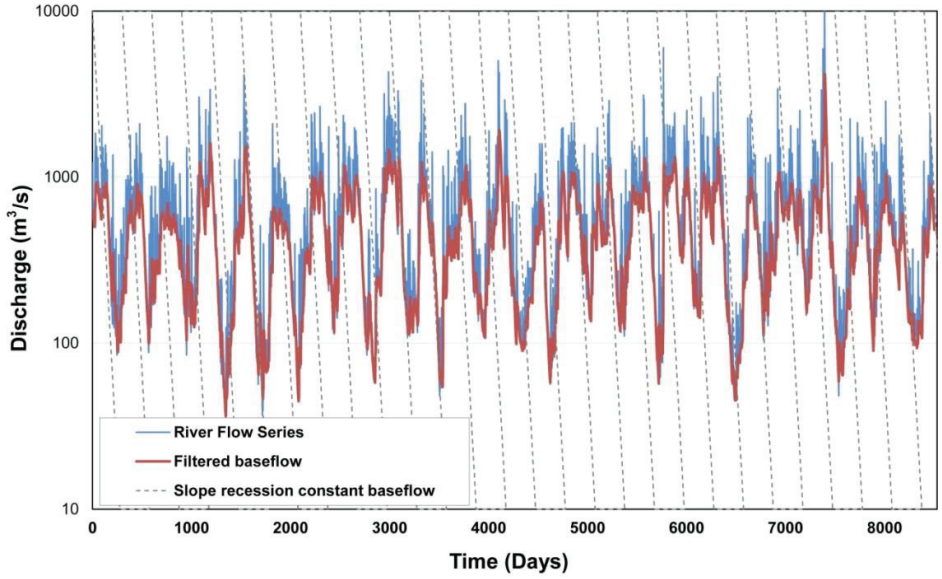

Figure 5.9 : Baseflow filter results based on daily river flow series of Beaver River, US from 1/1/1990 until 31/08/2013

Figure 5.10a compares the baseflow estimated by the empirical equation and with the filtered results from WETSPRO in Kent Ridge catchment. It should be noted that no discharge data from September 2012 to December 2012 was available. Error criteria including NSE, CC and RRMSE between baseflow time series estimated by WETSPRO and the generalized empirical equation were 0.959, 0.972 and 0.065, respectively. According to these results, differences between the baseflow obtained by WETSPRO and empirical equation were minimal. In addition, a comparison between baseflow time series estimated by WETSPRO and the generalized empirical equation in

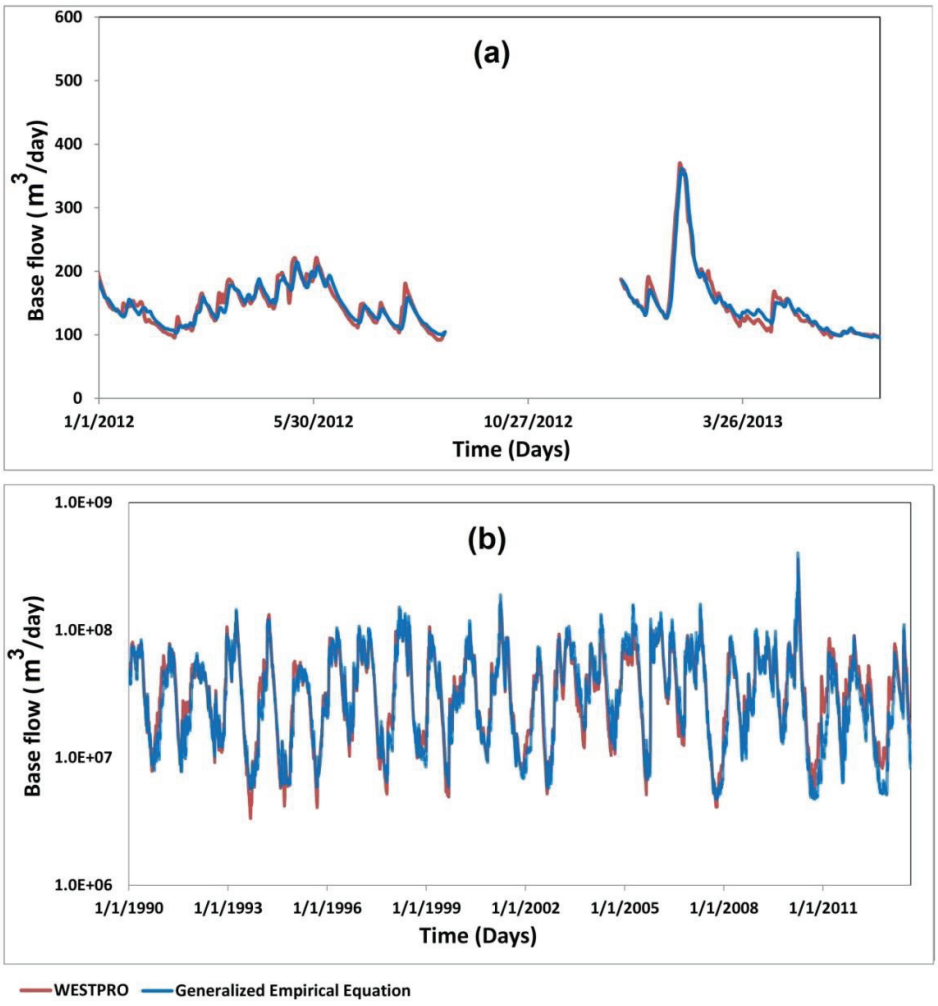

Figure 5.10 : Comparison between baseflow estimated by WETSPRO and the generalized empirical equation in a) Kent Ridge Catchment, Singapore and b) Beaver River Basin, US

Beaver River Basin are shown in Figure 5.10b. Error criteria including NSE, CC and RRMSE between baseflow time series estimated by WETSPRO and the generalized empirical equation were 0.901, 0.957 and 0.21,

respectively. These results demonstrate the successful prediction of baseflow time series using the generalized empirical equation derived in this study.

5.8 Summary and Conclusion

This study used GP to derive an empirical equation for estimating baseflow time series using groundwater table fluctuations. First, a groundwater model was adopted to simulate baseflow time series for a small semi-urban catchment in Singapore. GP was then used to derive an empirical equation predicting a continuous baseflow time series based on minimum perennial baseflow, catchment area, and a time series of groundwater table elevation. Baseflow time series estimated by the empirical equation matched very well with those from the HYDRUS-3D in both the training and the testing of data sets, giving NSEs of 0.95 and 0.98 respectively. The empirical equation was further modified into a generalized structure for application in other catchments. This method proved successful in a cross-site, cross-scale application in a northeastern US watershed. Overall, this study proposes a new approach to predict baseflow time series with only three parameters. It serves as an alternative approach for baseflow estimation in un-gauged systems when only groundwater table and soil information is available, and is thus complementary to other methods that require discharge measurements (e.g., digital filter method). This method also contributes to multi-proxy estimations

of baseflow where both streamflow and groundwater water table measurements are available. The simple equation can also be implemented in a modular model to simulate streamflow time series with little computational time and data requirement (See CHAPTER 6).

CHAPTER 6 DEVELOPMENT OF A MODULAR MODEL FOR THE SIMULATION OF STREAMFLOW TIME SERIES

6.1 Introduction

As stated in Chapter 1, streamflow is commonly conceptualized to include baseflow and quickflow (also called quickflow) components. One way of retaining as much information as possible is to build separate models for each of the different physically interpretable flow components leading to a modular approach. Therefore, this thesis used Genetic Programming to establish a modular model consisting of two sub-models: (i) a baseflow module and (ii) a quickflow module to simulate the two hydrograph flow components. In the previous chapter, the first modular unit was developed to estimate baseflow time series using GP. In the present chapter, the second modular unit was developed to simulate quickflow using hydrological parameters (e.g. precipitation), catchment initial conditions prior to the event (e.g. groundwater table) and area of the Kent Ridge Catchment collected and processed in Chapter 3 and 4, respectively. The model developed on Singapore catchment was further generalized to approximate streamflow in other catchments and validated in a cross-site, cross-scale application on a large vegetation dominated basin in the US. The modular model has then been applied in

Chapter 7 to estimate the effect of various land use types (i.e. impervious, steep grassland, grassland on mild slope, mixed grasses and trees and relatively natural vegetation) towards hydrograph flow components in tropical urban systems.

6.2 Approximating Quickflow Time Series Using Genetic Programming

A modular model for simulating streamflow can be defined as:

$$Q_{Total(t)} = Q_{Baseflow(t)} + Q_{Quickflow(t)}$$

where, $Q_{Total(t)}$ is streamflow (L/T), $Q_{Baseflow(t)}$ is baseflow (L/T), $Q_{Quickflow(t)}$ is quickflow (L/T).

As total streamflow includes baseflow as well as quickflow, baseflow was calculated first based on the function established in CHAPTER 5. Subtracting the predicted baseflow from the measured discharge resulted in the quickflow which was taken as target parameter (i.e. output) in GP. For a detailed description of the GP, readers are referred to Section 5.3. The GP software called GPKERNEL (Babovic and Keijzer, 2000) was employed to relate quickflow with hydrological parameters (e.g. precipitation), catchment antecedent conditions (e.g. groundwater table elevation prior to the rainfall event) and area of the catchment. In this experiment, five-minute average precipitation and discharge at the catchment outlet (i.e., Station 5), daily

evapotranspiration data, and simulated pressure head by HYDRUS-3D (See CHAPTER 5), were used as input parameters in GP. Data from September 2011 until August 2012 was used for model development, while the data from January to June 2013 was used for model validation. Moreover, to evaluate the performance of the model in rainfall events with different characteristics such as seasonal variability (monsoon vs. non-monsoon), various antecedent conditions such as duration of dry period and groundwater table depth prior to the event, total rainfall, duration and shape of hydrograph (single peak versus multiple peaks), six rainfall events within the period September 2011to June 2013 were selected and are listed in Table 6.1.

An overview of the evolutionary algorithm setup in GPKERNEL is presented in Table 5.2.

Table 6.1 : Main characteristics of selected events observed at Kent Ridge Catchment, Singapore

Event	Date	Number of dry hours before the beginning of the event	Normalized daily average of pressure head (m)	Total Rainfall (mm)	Rainfall duration (hour)	Maximum 30-minutes rainfall intensity (mm/hour)	Shape of hydrograph
1	21/11/2011	15.8	0.94	39.8	2.3	69.2	Single
2	09/03/2012	87.2	0.59	32.6	3.6	46.1	Single
3	25/03/2012	74.7	0.65	64.2	4.8	89.5	Multiple
4	08/02/2013	16.7	1.18	82.2	2.7	104.1	Single
5	09/03/2013	165.4	0.81	34.0	3.6	58.7	Multiple
6	27/04/2013	25.5	0.78	12.0	2.7	22.5	Single

6.3 Generalization of Modular Model

As the local modular model developed, described in the previous section, was derived for a small semi-urban catchment with a short time of concentration (about half an hour), only total rainfall of the event may affect the runoff component. However, for a large catchment with a gentle slope and a long time of concentration, the total rainfall which occurred in the previous days may also need to be taken into account. Therefore, a local modular model needs to be generalized for simulating streamflow in other catchments. A generalized equation for simulating baseflow in other catchment was developed in CHAPTER 5. Therefore, this study first derived a generalized equation for approximating quickflow in other catchments and combined with the general module for baseflow approximation in CHAPTER 5 which resulted in a generalized two-unit modular model.

To estimate model parameters in the baseflow component, an appropriate method was identified in CHAPTER 5. A proper optimization technique should also be adopted to choose suitable parameter values for the quickflow component.

6.3.1.1 Optimization Technique (Hybrid Genetic Algorithm)

Genetic algorithm (GA), one of the most popular stochastic global search methods, is an evolutionary algorithm which finds the optimal solution of a problem using the evolutionary ideas of natural selection and genetics. GA evolves four main steps including initialization, selection, reproduction and termination in order to optimize the parameters for a specific problem (Reeves and Rowe, 2002). GA first randomly generates a population of individuals within the constraints of the decision variables to be optimized. After initialization, a fitness function of each individual is then calculated to select the individuals which have better performance. In fact, individuals with the better objective values are selected for reproduction. In the next stage, GA uses three genetic operators including crossover, mutation and reproduction to create subsequent generations from selected individuals. GA then continues creating new generation from the selected population. The evolution is usually terminated by a pre-specified number of generations.

On the other hand, Interior Point Algorithm (IPA) is a popular local search method and has been widely used successfully in many optimization problems including linear and nonlinear, convex and non-convex (Abadie and Carpentier, 1969; Mousavi et al., 2004; Vanderbei and Shanno, 1999). This method applies a direct step (e.g. Newton step or a conjugate gradient step) at each iteration to solve a system of Karush-Kuhn-Tucker (KKT) equations (Byrd et al., 1999) until it reaches an optimal solution.

A hybrid Genetic Algorithm which is the combination of GA with a local search method (e.g. IPA) has been widely applied successfully in many optimization problems with good results (Grosan and Abraham, 2007). Therefore, in the current study, hybridization of GA with IPA is proposed to choose suitable parameter values in the quickflow component (Equation 8). In this optimization procedure, the GA is first used for global optimization which provides the global optimal solution. The global optimal solution is subsequently fed into IPA for local search to achieve the improved results. The flow chart of the proposed GA-IPA algorithm is shown in Figure 6.1. Model parameters in the quickflow component were determined based on the hybrid GA using the Optimization Tool in MATLAB. The parameter settings for the implementation of these algorithms are given in Table 6.2.

6.4 Statistical Tests of Accuracy

Performance of the established equation in GP was tested using three commonly used error functions: Relative Root Mean Squared Error (RRMSE), Correlation Coefficient (CC) and the Nash–Sutcliffe Efficiency (NSE) statistic (Nash and Sutcliffe, 1970) (See Section 5.6).

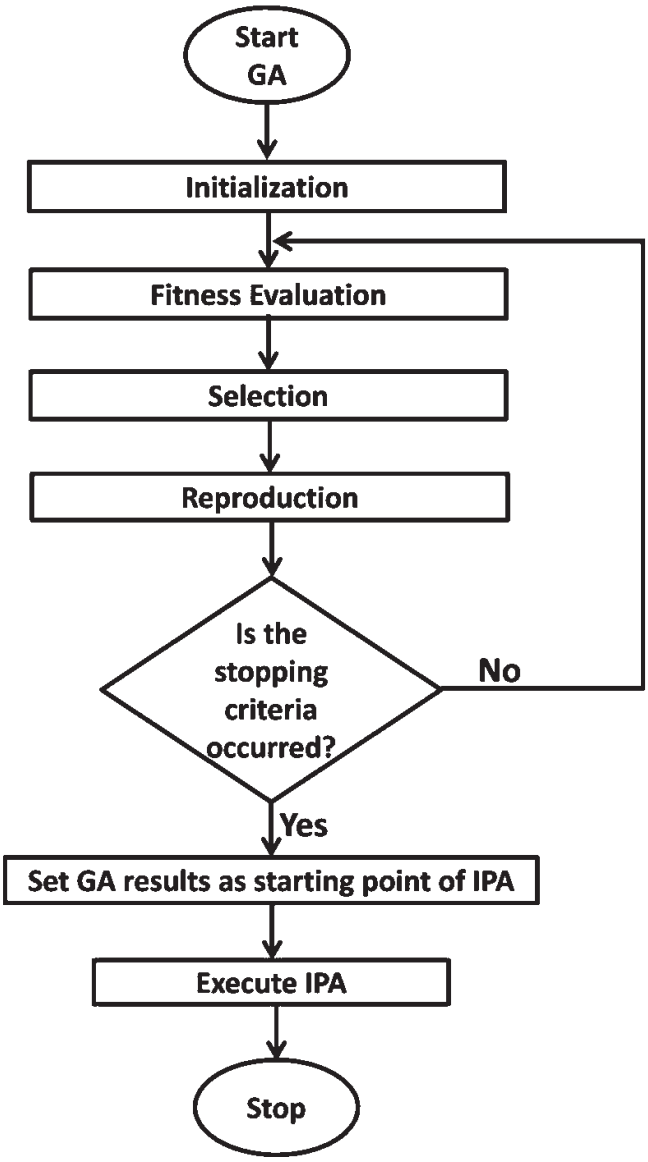

Figure 6.1: The flow chart of the proposed hybrid GA (GA-IPA algorithm)

Table 6.2: Parameter settings of algorithms

GA		IPA	
Parameters	**Settings**	**Parameters**	**Settings**
Population size	50	Start point	Optimal values from GA
Selection function	Stochastic uniform	Maximum iterations	1000
Mutation function	Adaptive feasible	Maximum function evaluations	3000
Crossover function	Scattered	Function tolerance	1e-10
Hybridization	IPA	Nonlinear constraint tolerance	1e-10
Number of generations	100	X tolerance	1e-10
Function tolerance	1e-10	Hessian	BFGS
Nonlinear constraint tolerance	1e-10	Derivative type	Central differences

6.5 Results and Discussion

6.5.1 Approximating Quickflow Time Series Using Genetic Programming

Based on the quickflow time series filtered from the observed streamflow data using Equation (5.15), GP was set up to derive the empirical equation. The equation that has a physically realistic set of variables and minimum RMSE was selected as follows:

$$\begin{aligned} Q_{Quickflow(t)} &= 10^{-3}\mathrm{Aa}\left(\Delta h_p \times P_T\right)^r \left[b_1 P_{(t-5)} + b_2 P_{(t-10)}\right] \\ &\quad + 10^{-3}\mathrm{Ac}\left(\Delta h_p \times P_T\right)^r \left[\begin{matrix} d_1 P_{(t-15)} + d_2 P_{(t-20)} + d_3 P_{(t-25)} \\ + d_4 P_{(t-30)} + d_5 P_{(t-35)} \end{matrix}\right]^{0.5} \end{aligned} \tag{6.1}$$

where $Q_{Quickflow(t)}$ presents the quickflow (L/s), $P_{(t-L)}$ is the rainfall intensity (mm/min) with L being minutes of lag time, P_T is the total rainfall depth during the event (mm), Δh_p is the normalized daily averaged pressure head

prior to the event and A is the total area of the catchment (m^2), "a" , "c" , "b" and "d" are the dimensionless coefficient.

Based on the error criteria, differences between the filtered quickflow from observed discharge data and those obtained by the empirical equation, at Station-E, were minimal in both training and testing periods (Table 6.3).

Table 6.3 : Error criteria between observed quickflow time series and those estimated by the empirical equation in Kent Ridge catchment, Singapore

Station	Data Set	Error criteria		
		RRMSE	NSE	CC
MD04	Train	0.54	0.97	0.99
	Test	0.65	0.96	0.98

The first term of the empirical equation is the quick runoff component corresponding to quickflow, while the second term approximates the delayed runoff component as the lag time increases. Both terms include the total catchment area (A), rainfall (e.g. $b_1 P_{(t-5)} + b_2 P_{(t-10)}$) and antecedent catchment condition (Δh_p). In this equation, the term of $\Delta h_{p(t)}. P_T$ allows variability in the percentage of rainfall that appears as runoff component for different events; higher $\Delta h_{p(t)}$ and P_T yield higher runoff volume.

As such, a modular model for simulating streamflow in Singapore catchment is:

$$Q_{Total(t)} = Q_{Baseflow(t)} + Q_{Quickflow(t)}$$

and:

$$\begin{cases} Q_{Baseflow(t)} = Q_{Bmin} + \sqrt{b\,A}\,\Delta h^2_{p(t+k)} \\ Q_{Quickflow(t)} = 10^{-3} Aa \left(\Delta h_p \times P_T\right)^r \left[b_1 P_{(t-5)} + b_2 P_{(t-10)}\right] \\ \qquad + 10^{-3} Ac \left(\Delta h_p \times P_T\right)^r \left[\begin{matrix} d_1 P_{(t-15)} + d_2 P_{(t-20)} + d_3 P_{(t-25)} \\ + d_4 P_{(t-30)} + d_5 P_{(t-35)} \end{matrix}\right]^{0.5} \end{cases} \quad (6.2)$$

A comparison between observed streamflow and those estimated by the modular model are shown in Figure 6.2. In addition, according to the results of previous chapter , differences between baseflow time series simulated by a groundwater numerical model (i.e. HYDRUS-3D) and the baseflow module were minimal, indicating that the baseflow module can accurately estimate baseflow time series. Moreover, error criteria including NSE, CC and RRMSE between filtered quickflow from observed discharge data and those obtained by the runoff module are listed in Table 6.3, confirming that the runoff module can successfully estimate quickflow. These results demonstrate the successful prediction of streamflow as well as hydrograph flow components using the modular model derived in this study.

Figure 6.3 presents the different hydrograph components including quick runoff, delayed runoff and baseflow estimated by Equation 6.2 for several selected events with different characteristics (Table 6.1). The estimated total streamflow hydrograph shows a good correspondence with observed streamflow hydrograph confirming that the modular model can successfully estimate streamflow in rainfall events with different characteristics.

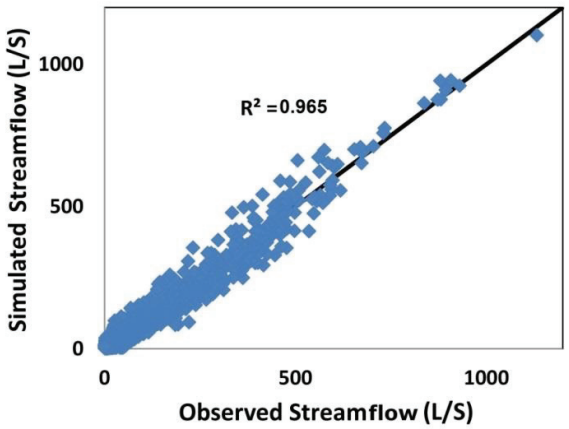

Figure 6.2 : Scatter plot between observed streamflow and those estimated by modular model at Station E which situates at catchment outlet in Kent Ridge Catchment, Singapore

From these hydrographs, it can also be seen that the time of concentration is very short and the quick runoff component has a steep rising and falling limb, dominating the total runoff hydrograph during a rainfall event (66%). The contribution of the delayed runoff and baseflow components were 26% and 8%, respectively. These phenomena reflect the hydrological characteristics of the basin: slopes are steep, infiltration is low through which the rainfall results in a rapid quick flow component, being unable to recharge the groundwater in such a short-time period.

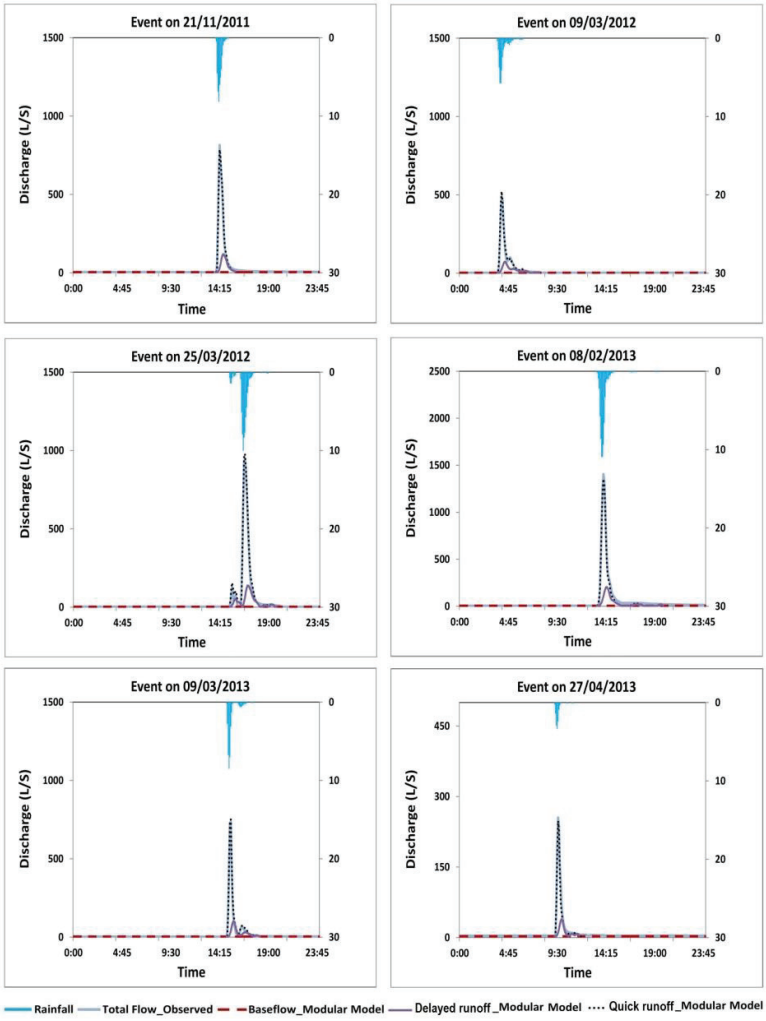

Figure 6.3 : Separation of observed streamflow data into its respective flow components using modular model for six selected rainfall events as listed in Table 6.1 Kent Ridge Catchment, Singapore

To evaluate the influence of dependent variables including $\Delta h_{p(t)}$ and P_T on the estimated quickflow, sensitivity analysis was carried out on the empirical equation. First, normalized pressure heads were kept constant at the average of the entire data series, whereas the total rainfall events varied from 10 to 80 mm. For the second part of the sensitivity analysis, total rainfall was kept constant at the average of the entire data series, whereas the normalized pressure heads varied from 0.1 to 2.5 m. Two sets of rainfall intensities with low (8 mm/hr.) and high (88 mm/hr.) rainfall intensities were assessed (Figure 6.4). Estimated runoff with 2.5 m pressure head is about 50% larger than one obtained by 0.1m pressure head in both low and high rainfall intensities (Figure 6.4a). Similar trends regarding the dependence of estimated quickflow on the total rainfall was observed (Figure 6.4b). These results indicate that the empirical equation is almost equally sensitive to both total rainfall and the normalized pressure head.

6.5.2 Generalization of Modular Model

As explained in Section 6.3, the local modular model was derived for simulating streamflow in catchment outlet (i.e., Station-E). However, this local modular model should be generalized for simulating hydrograph flow components in other sub-catchments/catchments.

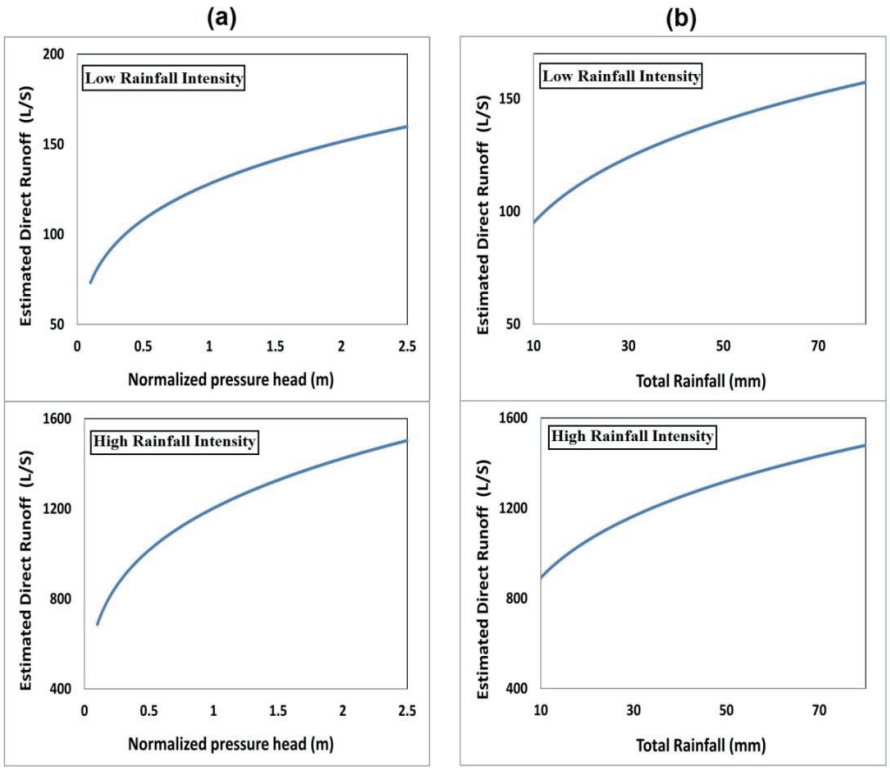

Figure 6.4 : Sensitivity analysis of a) normalized pressure head and b) total rainfall, on estimated quickflow for low (8 mm/h) and high (88 mm/h) rainfall intensities

As such, a generalized equation for approximating quickflow in other catchments is proposed as follows:

$$\begin{aligned} Q_{Quickflow(t)} &= 10^{-3} A\, a \left(\Delta h_{p(t+k)}\left(e_1 P_{T(t)} + \cdots + e_n P_{T(t-n)}\right)\right)^r \left[b_1 P_{(t)} + \cdots + b_n P_{(t-n)}\right] \\ &\quad + 10^{-3} A\, c \left(\Delta h_{p(t+k)}\left(g_1 P_{T(t)} + \cdots + g_n P_{T(t-n)}\right)\right)^r \left[d_1 P_{(t)} + \cdots + d_n P_{(t-n)}\right]^{0.5} \end{aligned} \quad (6.3)$$

where "a" , "c", "b_n", and "d_n" are the dimensionless coefficients.

As such, a generalization of the modular model is as follows:

$$\begin{cases} Q_{Baseflow(t)} = Q_{Bmin} + \sqrt{b\,A}\,\Delta h^{2}_{p(t+k)} \\ Q_{Quickflow(t)} = 10^{-3}A\left[\begin{array}{l} a\left(\Delta h_{p(t+k)}\sum_{i=1}^{n} e_i P_{T(t-i+1)}\right)^{r}\left[\sum_{i=1}^{n} b_i P_{(t-i+1)}\right] \\ +c\left(\Delta h_{p(t+k)}\sum_{i=1}^{n} g_i P_{T(t-i+1)}\right)^{r}\left[\sum_{i=1}^{n} d_i P_{(t-i+1)}\right]^{0.5} \end{array}\right] \end{cases} \quad (6.4)$$

and $Q_{Total(t)} = Q_{Baseflow(t)} + Q_{Quickflow(t)}$.

Details regarding the estimation of model parameters in baseflow component can be found in CHAPTER 5. With regards of parameter "n" in quickflow component, the time differences between the beginning of a rainfall event and the start of the rising limb or the end of a rainfall event and the end of recession limb can be used to approximate this parameter in Equation 6.4; whichever is longer.

In the present study, the suitability of hybrid GA for estimating model parameters in quickflow component was first tested in Singapore catchment outlet (i.e. Station E, Figure 3.1). In order to prevent parameters from taking unrealistic values and ensure that the true parameter values will be reached, the following constraints were set based on the physical meaning of the model's parameters:

$\sum_{i=1}^{n} e_i = \sum_{i=1}^{n} b_i = \sum_{i=1}^{n} g_i = \sum_{i=1}^{n} d_i = 1$,

$a, c, e_i, b_i, g_i, d_i \geq 0$.

The model parameters $(a, c, \mathrm{e}_i, \mathrm{b}_i, \mathrm{g}_i, \mathrm{d}_i)$ optimized with hybrid GA were same as those obtained in GP model, confirming that the proposed hybrid GA is an appropriate method for estimating model parameters in quickflow component.

The performance of the generalized modular model was evaluated using an independent dataset from a larger vegetation-dominated basin located in the US (i.e. Beaver River Basin). A comparison between observed streamflow and those estimated by the generalized modular model are shown in Figure 6.5. Moreover, error criteria including NSE, CC and RRMSE between observed streamflow and those estimated by the generalized modular model are listed in Table 6.4. These results demonstrate the successful prediction of streamflow using the generalized modular model derived in this study. The results also show that baseflow is a significant contribution to streamflow during a flood period (75%) which reflects stable flow regimes due to groundwater inflow. In addition, the contributions of quick and delayed runoff components were 14% and 11% of the total runoff during a flood period, respectively.

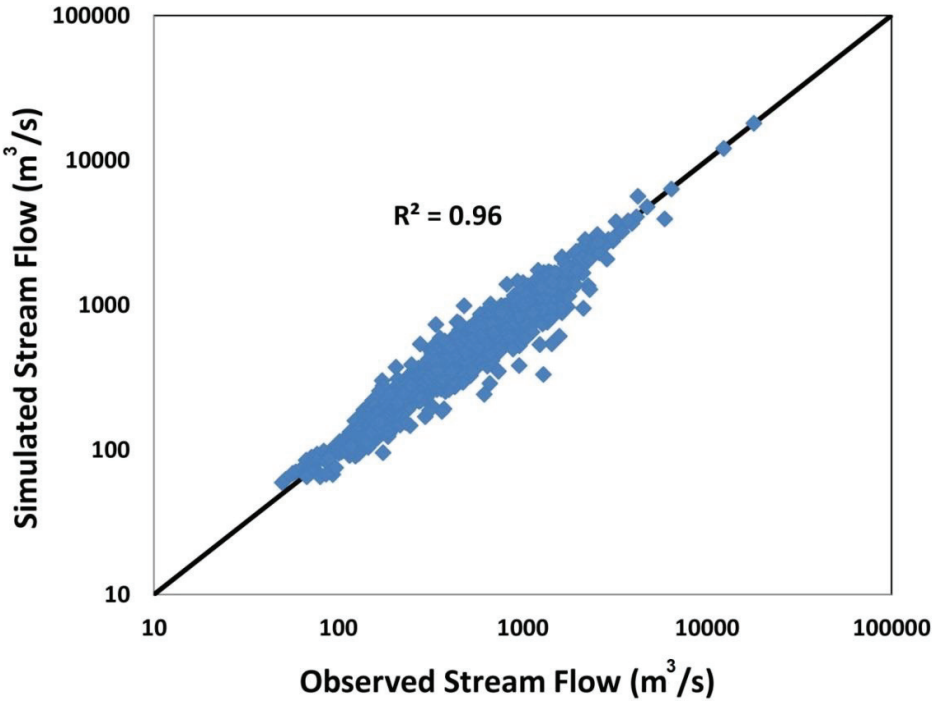

Figure 6.5 : Scatter plot between observed streamflow and those estimated by the modular model in Beaver River Basin, US

Table 6.4 : Error criteria between observed streamflow time series and those estimated by the modular model in Beaver River Basin, US

Data Set	Error criteria		
	RRMSE	NSE	CC
Train	0.18	0.955	0.98
Test	0.32	0.945	0.97

These phenomena reflect the gentle slopes and generally drained soils according to the soil report and DEM available for this basin (Rhode Island Digital Atlas, 2014). Therefore, the storms mainly infiltrate into the soils and recharge the groundwater.

6.6 Summary and Conclusion

This chapter used GP to derive a physically interpretable modular model for estimating streamflow. First, a baseflow separation technique developed in CHAPTER 5 was adopted to separate baseflow from observed streamflow for a small semi-urban catchment located in Singapore. An empirical equation was then derived using GP to relate the filtered quickflow with characteristics of rainfall events, catchment initial condition and area of the catchment. The quickflow estimated by the empirical equation matched very well with observed data in both the training and the testing of data sets, giving NSEs of 0.97 and 0.96 respectively. A modular model was then developed for simulating streamflow time series, which included two local models associated with baseflow and quickflow. The modular model was further modified into a generalized structure and was validated in a cross-site, cross-scale application on a large vegetation-dominated basin located in the US. Overall, this study proposes a physically interpretable model with understandable structure to simulate streamflow with the following features:

a. The model consists of two modules, one for baseflow and the other for quickflow.
b. The baseflow module represents the relatively steady contribution to streamflow from groundwater flow.
c. The quickflow module contains a rapid and delayed streamflow generation component which corresponds to the overland flow and shallow sub-surface flow, respectively.
d. The relationship between the input variables in the model (i.e. meteorological data and catchment initial conditions) and its overall structure can be explained in terms of catchment hydrological processes. The model allows visualization of information about catchment hydrological processes and therefore is a partial greying of what is often a black-box approach in catchment modelling.

This method can be applied in other catchments and can simulate and separate hydrograph flow components on both event as well as time series bases. It can also be used to estimate the effect of various land use types (i.e. impervious, steep grassland, grassland on mild slope, mixed grasses and trees and relatively natural vegetation) towards hydrograph flow components (See CHAPTER 7).

CHAPTER 7 QUANTIFICATION OF LAND-USE CONTRIBUTIONS TOWARDS HYDROGRAPH FLOW COMPONENTS [3]

7.1 Introduction

Increasing global urbanization has severely altered the hydrological cycle resulting in the decrease of pervious areas, infiltration and therefore the sub-surface component during rainfall events, and consequently in the increase of peak discharges in urban drainage infrastructure. On the other hand, the behaviour of rainfall-runoff process in urban systems experiences a high degree of non-linearity and heterogeneity. This call for a better understanding of rainfall-runoff processes in urbanized areas especially with regards to contributions from specific land uses towards surface and sub-surface flow. However, this knowledge in tropical urban environments is still limited. Therefore, this chapter used the physically interpretable modular model developed in CHAPTER 6 to simulate the hydrograph flow components (i.e.

[3] Reprinted from Journal of Hydrology, Meshgi et al., Development of a modular streamflow model to quantify runoff contributions from different land use types in tropical urban environments using Genetic Programming, 525: 711-723, doi:10.1016/j.jhydrol.2015.04.032 , Copyright (2015), with permission from Elsevier.

baseflow and quickflow). Furthermore it used the events as well as time series predictions of both flow components from the modular model and optimization techniques to estimate the effect of various land use types (i.e. impervious, steep grassland, grassland on mild slope, mixed grasses and trees and relatively natural vegetation) towards hydrograph flow components in tropical urban systems.

7.2 Quantification of Quickflow Contributions from Specific Land Uses

7.2.1 Clustering Analysis

In a tropical area, catchment responses to the rainfall events are expected to vary significantly from event to event due to different types of rainfall events and antecedent catchment conditions (Peng and Wang, 2012). Therefore, rainfall events were divided into clusters and sub-clusters based on types of rainfall events and antecedent catchment conditions using a statistical hierarchical clustering technique proposed by Ward (1963).

The following variables were used: total precipitation in the event, maximum 30-min intensity and duration. This resulted in a total of 150 events grouped into four clusters (Table 7.1). Rainfall Cluster I represents rainfall events which are less intensive than other clusters. Rainfall Cluster II includes rainfall events with moderate rainfall depth, intensity and duration while

Rainfall Cluster III consists of storms that have high rainfall depth, intensity and duration. Rainfall Cluster IV represents extreme rainfall storms with very high rainfall depth and intensity. Most rainfall events were categorized into Rainfall Cluster I with 102 events while Rainfall Cluster IV only contained 10 events. In addition, events in Rainfall Cluster III and II occurred 21 and 17 times, respectively.

The sub-clusters contained the various antecedent catchment conditions. As the spatio-temporal variations of the antecedent soil moisture data are often not available, the antecedent baseflow derived using the baseflow module (Equation 6.4) was used to present the catchment state prior to the event for the entire period, resulting in three sub-clusters (Table 7.1). Sub-cluster one contained events with low antecedent baseflow between 0.98 and 2.4 L/s, events with moderate antecedent baseflow between 2.41 and 3.83 L/s were grouped in Sub-Cluster-2 while events with high antecedent baseflow between 3.84 and 5.26 L/s were classified in Sub-Cluster-3.

Table 7.1: Statistical feature of the rainfall events

Rainfall Event	Parameter	Mean	StDev	Number of occurrences		
				Sub-Cluster 1	Sub-Cluster 2	Sub-Cluster 3
Cluster I	P	3.8	2.6	35	24	43
	I_{30}	5.5	4.6			
	R_D	1.5	0.4			
Cluster II	P	16.2	3.9	4	10	3
	I_{30}	22.6	4.6			
	R_D	2.7	0.6			
Cluster III	P	31.2	4.3	4	7	10
	I_{30}	42.5	9.2			
	R_D	3.5	0.3			
Cluster IV	P	59.7	10.9	3	4	3
	I_{30}	67.6	20.0			
	R_D	5.0	1.0			

P: Rainfall depth (mm)
I_{30}: Maximum 30-min intensity (mm/hr.)
R_D: Rainfall duration (hr.)

7.2.2 Land use specific runoff coefficient

This section derived an approach to estimate land use specific runoff coefficients (i.e. the portion of rainfall contributing to quickflow) during an event. For each station, the relation between the weighted average runoff coefficient and runoff coefficient of each particular land use was derived for a given event:

$$\begin{bmatrix} C_{T_{St1\,i}}.A_{T_{Stn\,1}} \\ C_{T_{St2\,i}}.A_{T_{Stn\,2}} \\ C_{T_{St3\,i}}.A_{T_{Stn\,3}} \\ C_{T_{St4\,i}}.A_{T_{Stn\,4}} \\ C_{T_{St5\,i}}.A_{T_{Stn\,5}} \end{bmatrix} =$$

$$[C_{IMPi}\ C_{GMi}\ C_{GSi}\ C_{MGTi}\ C_{RNVi}] \begin{bmatrix} A_{IMP_{Stn\,1}} & A_{IMP_{Stn\,2}} & A_{IMP_{Stn\,3}} & A_{IMP_{Stn\,4}} & A_{IMP_{Stn\,5}} \\ A_{GM_{Stn\,1}} & A_{GM_{Stn\,2}} & A_{GM_{Stn\,3}} & A_{GM_{Stn\,4}} & A_{GM_{Stn\,5}} \\ A_{GS_{Stn\,1}} & A_{GS_{Stn\,2}} & A_{GS_{Stn\,3}} & A_{GS_{Stn\,4}} & A_{GS_{Stn\,5}} \\ A_{MGT_{Stn\,1}} & A_{MGT_{Stn\,2}} & A_{MGT_{Stn\,3}} & A_{MGT_{Stn\,4}} & A_{MGT_{Stn\,5}} \\ A_{RNV_{Stn\,1}} & A_{RNV_{Stn\,2}} & A_{RNV_{Stn\,3}} & A_{RNV_{Stn\,4}} & A_{RNV_{Stn\,5}} \end{bmatrix} \quad 7.1$$

where, i is an event, C_T is the weighted average runoff coefficient (-), C_{IMP}, C_{GM}, C_{GS}, C_{MGT}, C_{RNV} are the runoff coefficients of total impervious, grass on mild slope, grass on steep slope, mixed grasses and trees and relatively natural vegetation areas, A_T is the total area (m^2), A_{IMP}, A_{GM}, A_{GS}, A_{MGT}, A_{RNV} are the areas of impervious, grass on mild slope, grass on steep slope, mixed grasses and trees and relatively natural vegetation (m^2), respectively.

The weighted average runoff coefficient in Equation 7.1 can be calculated as follows at each station:

$$C_{T_i} = \frac{Q_R}{P.A} \quad 7.2$$

where C_{T_i} presents the weighted average runoff coefficient for event i, Q_R and P are total runoff volume (m^3) and total precipitation depth (m) of a given event, respectively, and A is the area of a catchment/sub-catchment (m^2).

Total runoff volume in Equation 7.2 was calculated from the quickflow component of the modular model developed in CHAPTER 6.

Hybrid GA was used to optimize the parameter values for land use specific runoff coefficients (C_{IMP}, C_{GM}, C_{GS}, C_{MGT}, C_{RNV}) in Equation 7.1 using the Optimization Tool in MATLAB. The objective function of the optimization processes was defined as reducing the Root Mean Squared Error (RMSE), a commonly used error function namely. The parameter settings for the implementation of GA and IPA are given in Table 6.2. The following constraints were set based on the physical meaning of runoff coefficient:

$0 \leq C_{GM}, C_{GS}, C_{MGT}, C_{RNV} \leq C_{IMP} \leq 1.$

7.2.3 Estimating total contribution of different land use types towards the quickflow component

To evaluate the contribution of various land uses towards the quickflow component, the runoff volume generated by each land use was calculated at catchment level. Total contributions of each land use were normalized as follows:

$$C_{N_j} = \frac{\frac{C_{T_j}}{A_j}}{S}, \; j = IMP, GS, GM, MGT, RNV \qquad 7.3$$

and,

$$S = \frac{C_{T_{IMP}}}{A_{IMP}} + \frac{C_{T_{GS}}}{A_{GS}} + \frac{C_{T_{GM}}}{A_{GM}} + \frac{C_{T_{MGT}}}{A_{MGT}} + \frac{C_{T_{RNV}}}{A_{RNV}} \qquad 7.4$$

where, C_N, is the normalized contribution and C_T is the total contribution of each land use type, IMP, GS, GM, RNV, and MGT represent impervious,

grass on steep slope, grass on mild slope, relatively natural vegetation, mixed grasses and trees, respectively.

7.3 Results and Discussion

7.3.1 Quantifying Quickflow Contributions from Different Land Uses

7.3.1.1 Approximating quickflow time series in discharge monitoring stations

Runoff module of modular model developed in CHAPTER 6 was first used to approximate quickflow time series in discharge monitoring stations. Total runoff volume in Equation 7.2 (See Section 7.3.1.2) was then calculated from the quickflow component of the modular model. Error criteria including NSE, CC and RRMSE between observed quickflow in Station-A to -E and those estimated by runoff module of modular model developed in CHAPTER 6 are listed in Table 7.2. These results again demonstrate the successful prediction of quickflow using the model derived in CHAPTER 6.

Table 7.2: Error criteria between observed quickflow time series and those estimated by runoff module of modular model

Station	Data Set	Error criteria		
		RRMSE	NSE	CC
A	Train	0.69	0.94	0.96
	Test	0.73	0.95	0.97
B	Train	0.67	0.95	0.96
	Test	0.71	0.94	0.97
C	Train	0.65	0.95	0.97
	Test	0.66	0.95	0.97
D	Train	0.51	0.97	0.99
	Test	0.60	0.96	0.98
E	Train	0.54	0.97	0.99
	Test	0.65	0.96	0.98

7.3.1.2 Event-based land use specific runoff coefficient

The average runoff coefficients of different land uses towards the predicted quickflow for each cluster and sub-cluster were obtained with hybrid GA using the runoff module (Table 7.3). Comparison of the average runoff coefficient for all events belonging to one sub-cluster using Equation (7.1) and those estimated by Equation (7.2) (Table 7.3), demonstrates the successful estimation of land-use specific runoff coefficients.

Table 7.3: Average quickflow contribution and error criteria of each land use within clusters and sub-clusters

Rainfall Event	Sub-Cluster	Surface Runoff Coefficient (-)					Relative absolute error (%)[1]	
		Impervious surfaces	Grass on steep slope	Grass on mild slope	Mixed grasses and trees	Relatively natural vegetation	Mean	Std.dev
Cluster I	1	0.66	0.30	0.25	0.20	0.04	4.6	0.7
	2	0.67	0.31	0.27	0.21	0.05	3.9	1.7
	3	0.69	0.38	0.34	0.29	0.06	4.4	1.0
Cluster II	1	0.73	0.52	0.43	0.36	0.07	3.8	1.6
	2	0.75	0.53	0.45	0.38	0.07	3.6	1.2
	3	0.75	0.55	0.45	0.38	0.10	4.2	1.9
Cluster III	1	0.82	0.57	0.46	0.39	0.11	3.9	0.6
	2	0.83	0.63	0.47	0.40	0.12	3.2	0.9
	3	0.84	0.66	0.55	0.52	0.17	3.7	0.3
Cluster IV	1	0.94	0.71	0.63	0.55	0.17	3.4	1.4
	2	0.95	0.75	0.68	0.61	0.18	4.0	0.4
	3	0.96	0.81	0.77	0.73	0.24	3.8	2.0

[1] The relative absolute error was calculated according to the absolute error of Equation 4 estimates relative to values obtained from Equation 3

The small standard deviation of relative absolute errors (Equation 7.1 estimates relative to Equation 7.2 values) suggests that the average runoff coefficients were estimated with low uncertainty.

Results indicated that land uses exert a major influence on runoff coefficients of an urban tropical environment. Similar results have been also reported for urban temperate systems, indicating that there is a strong positive correlation between the amount of quickflow and the level of urbanization (e.g.Sun et al., 2013). The average runoff coefficient of different land uses decreased from impervious surface (0.8), grass on steep slope (0.56), grass on mild slope (0.48), mixed grasses and trees (0.42) and to relatively natural vegetation (0.12). As expected, impervious surfaces contributed the most to the rapid and delayed runoff among all land uses. In contrast, the lowest runoff coefficient was found for relatively natural vegetation ranging from 0.04 to 0.24 due to canopy interception and evapotranspiration (Sriwongsitanon and Taesombat, 2011). In addition, larger infiltration in relatively natural vegetation area occurs as a result of extensive root zone development which increases the porosity. Human activities, resulting in soil compaction and subsequently reducing soil porosity and infiltration capacity, in recreational grass areas, play an important role in generating surface runoff (Dadkhah and Gifford, 1980). Additionally, runoff increases with increasing slope gradients,

due to decreased infiltration rates (Huang et al., 2013). As such, higher runoff coefficients were observed for the grass areas with steep slopes than those areas with mild slopes that included trees.

With regards to the effect of antecedent catchment conditions, the antecedent soil moisture content had a larger effect on the pervious land uses. Normalized variation in runoff coefficients (with respect to their minimum value within each land use) of different land uses from Cluster-I/Sub-Cluster-1 to Cluster-IV/Sub-Cluster-3 listed in Table 7.3 are shown in Figure 7.1. Table 7.3 shows the increasing trend of runoff coefficients from Cluster-I/Sub-Cluster-1 to Cluster-IV/Sub-Cluster-3 for all the land uses. In addition, Figure 6 shows the largest variation for the runoff coefficients associated with the relatively natural vegetation followed by grass based land uses and impervious surfaces. As the types of rainfall events had the largest effect on relatively natural vegetation areas compared to other land uses, runoff coefficients for relatively natural vegetation fluctuated about 2 to 4 times more compared to those for grass based and impervious surfaces, respectively (Figure 7.1). This is because rainfall loss due to evapotranspiration, canopy interception and infiltration, especially during small rainfall events, is typically higher for natural vegetation areas than for non- natural vegetation areas (Sriwongsitanon and Taesombat, 2011). In addition, canopy interception may reduce with increasing rainfall intensity due to splashing of larger raindrops from vegetation (Calder, 2005).

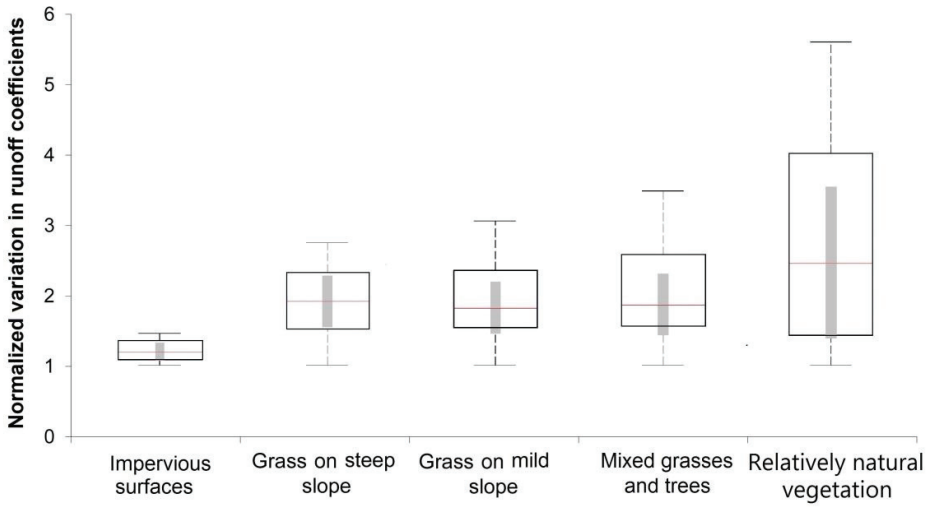

Figure 7.1: Normalized variation in runoff coefficients (with respect to their minimum value within each land use) of different land uses from Cluster-I/Sub-Cluster-1 to Cluster-IV/Sub-Cluster-3 (grey bars represents the expected range of variability of the median)

This could cause a large variation in runoff coefficient for relatively natural vegetation area from Cluster-I/Sub-Cluster-1 to Cluster-IV/Sub-Cluster-3. On average, the runoff coefficients of all the land uses increased gradually from sub-cluster-1 (relatively un-saturated condition) to sub-cluster-3 (relatively saturated condition) by 17% (Table 7.3). With regards to the pervious surfaces, this can be explained by the catchment initial conditions. In fact, higher levels of groundwater table and initial soil moisture would reduce the soil water suction and potential (Hawke et al., 2006) which reduces infiltration rate (Philip, 1957) and consequently increases the runoff volume. However, with regards to the impervious surfaces, the runoff coefficients

increased slightly probably due to the antecedent precipitation which could increase the initial storage and subsequently lead to the greater runoff coefficient.

The suitability of land use specific runoff coefficients derived in this section for the assessment of runoff generated by an extreme rainfall event (e.g., 10 year ARI) was investigated. According to the Rainfall Intensity-Duration-Frequency (IDF) (Figure 7.2) established for Singapore by Public Utilities Board (PUB) (Code of Practice-Drainage Design and Considerations, 2011), an event with 10 year ARI (128 mm) was monitored during 2010-2011. It should be mentioned that this event was not used during the optimization procedure for quantifying land use contributions towards rapid and delayed runoff component. Assessment of the runoff generated by this event which would be categorized in Cluster-IV/Sub-Cluster-3 showed that with less than 5% error, the runoff coefficient of Cluster-IV/Sub-Cluster-3 can be used to estimate the total runoff for an extreme rainfall event. This indicated that even for such a rainfall event, the contribution of relatively natural vegetation area is about 4 times smaller than that of impervious surfaces. As such, increasing urban pressure and the related conversion of pervious surfaces to impervious areas clearly influences not only hydrological processes at watershed scale but also increases flood risks tremendously.

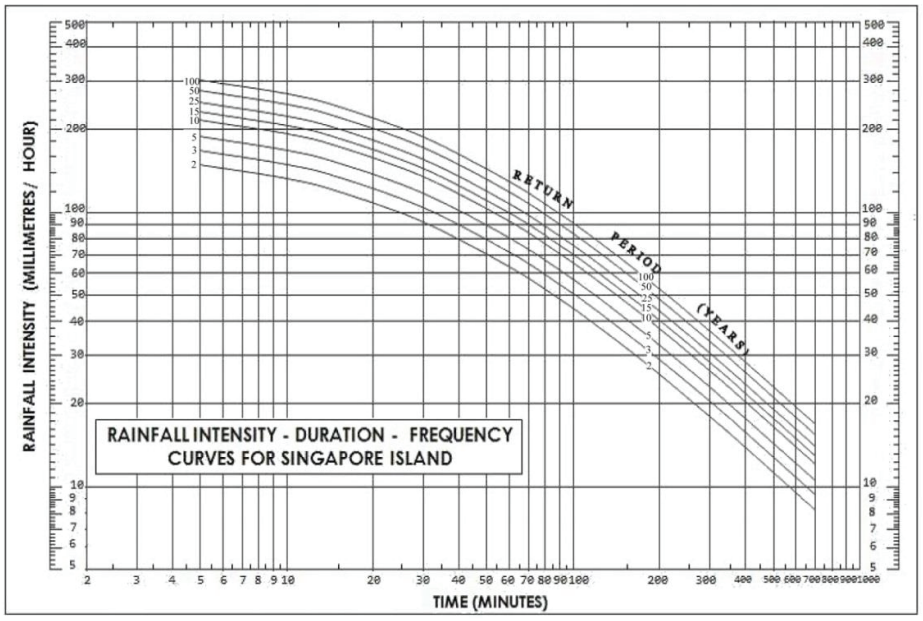

Figure 7.2: The Rainfall Intensity-Duration Frequency curves established for Singapore by Public Utilities Board (PUB) (Code of Practice-Drainage Design and Considerations, 2011)

However, land use conversion due to demographic pressure, frequently inhibits the conservation of forests and natural vegetation. Therefore, it is of uttermost importance to account for water sensitive features in urban cities that have similar properties to natural vegetation in order to restore hydrological processes in tropical urban environments. This could eventually ensure dry season baseflow sustenance as well as modulation of quickflow responses to the extreme rainfall events.

7.3.2 Average runoff coefficients at catchment scale

Average runoff coefficients varied between 0.09 and 0.61 for the various sub-catchments (Figure 7.3). As expected, the average runoff coefficients among the various types of rainfall events differed significantly ($p < 0.001$, $\alpha = 0.05$) and were in decreasing order of Rainfall Cluster IV>III>II>I. These results showed a consistent positive relationship between types of rainfall events and runoff coefficient (i.e. increasing runoff volume with increasing rainfall depth, duration and intensity). Sub-Cluster-3 (relatively saturated condition) contributed the most towards the quickflow during rainfall events. Rainfall events in Sub-clusters 3 had a shorter dry antecedent weather period (0.8 days) when compared to sub-clusters 1 and 2 (2.3 and 1.8 days, respectively). As evapotranspiration losses increases with increasing dry weather period, higher antecedent soil moisture was expected in Sub-Cluster-3 as compared to other sub-classes. Therefore, a reduction in the infiltration and thus the water buffering capacity of the soil results in a larger quickflow fraction.

When analyzing the various sub-catchments, larger average runoff coefficients were found for Station A due to the larger fraction of impervious surface of the sub-catchment (Figure 7.3, Table 3.2). In contrast, the lowest runoff coefficient was observed at Station B where relatively natural

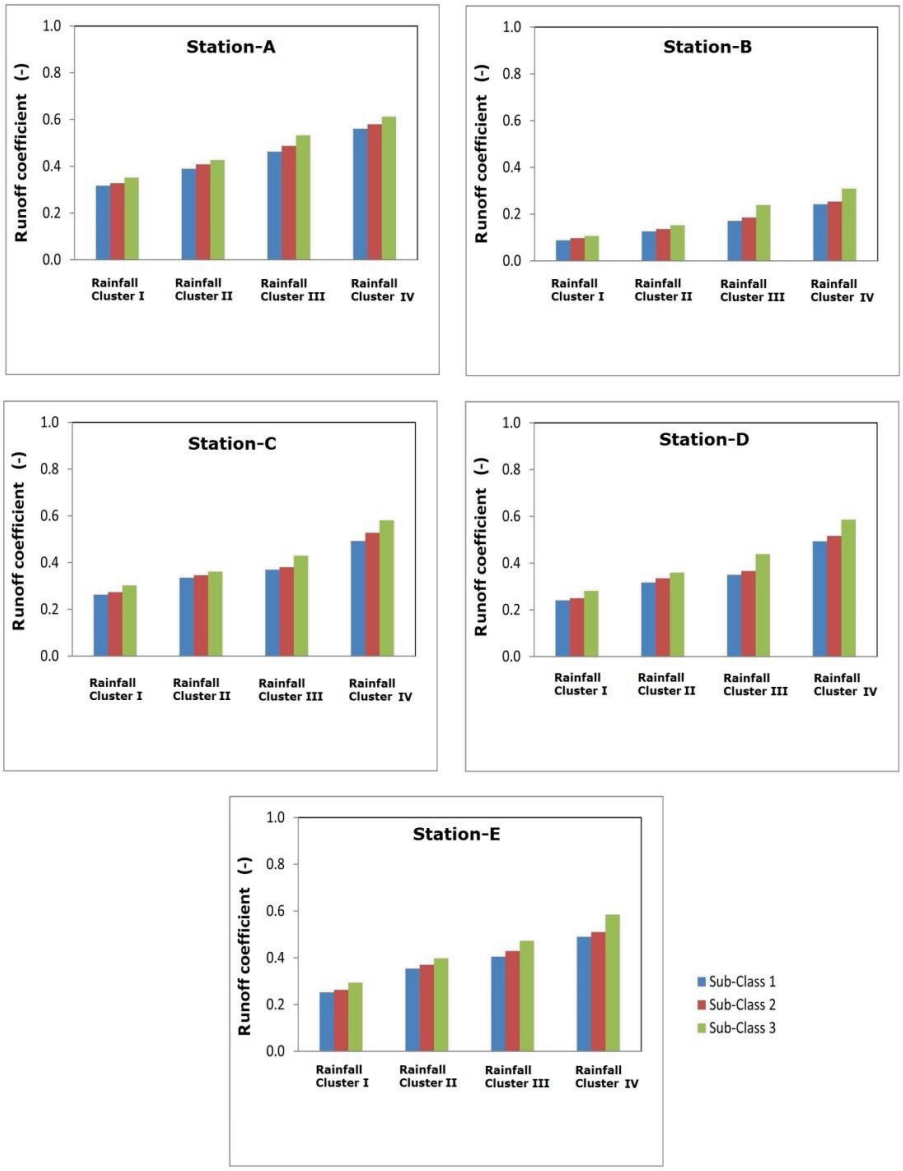

Figure 7.3 : Average runoff coefficient within the clusters and sub-clusters for each discharge monitoring station within Kent Ridge Catchment, Singapore

vegetation areas were the dominating. In fact, quickflow was very small for most rainfall events, and large runoff in this station could only be generated by rainfall storms larger than 55 mm (Cluster-IV/Sub-Cluster-3). No significant differences in the average catchment runoff coefficients were observed among Stations C, D, and E ($p = 0.4$, $\alpha = 0.05$) due to the relative similar land use distributions in those stations (Table 3.2).

7.3.2.1 Contribution of different types of land use towards overall stormwater runoff

The mean total quickflow of five land uses descended in an order of impervious surfaces, grass on mild slope, relatively natural vegetation, mixed grasses and trees, grass on steep slope (Figure 7.4a). Although the percentage of area covered by relatively natural vegetation is about 1.7 times larger than that covered by impervious surfaces, the mean total quickflow from impervious surface is approximately 3.4 times greater than from the relatively natural vegetation. As can be seen in Table 3.2, the areas of different land uses vary largely. Hence, in order to provide a fair comparison, total contributions of land uses on equivalent area basis (i.e. area of each land use is equal) is presented in Figure 7.4b. The amount of total quickflow on equivalent area basis change to: impervious surfaces > grass on steep slope > grass on mild slope > mixed grasses and trees > relatively natural vegetation. These results

showed that impervious surfaces exhibited the greatest quickflow while the average contribution of relatively natural vegetation areas was as low as about 5.4% which was 5.8 times smaller than that of impervious surfaces. The total quickflow on equivalent area basis were similar among the grass based land uses with grass areas on steep slopes being the second largest contributor (23.5%), followed by grass on mild slope (21%) and grass with trees (18.7%). Due to the urbanization effect such as soil compaction, the contribution of impervious surfaces was in average only 1.4 times greater than the grass based land uses (i.e. steep slope, mild slope and underneath trees) contributions. The buffer capacity of the relatively natural vegetation area is large enough to even buffer heavy rainfall events, reducing the quickflow in an urban environment.

The results indicated that land-cover transformation from relatively natural vegetation to impervious surfaces is associated with an increase in the total quickflow by 26% (Figure 7.5). In addition, changes from mixed grasses and trees, grass on mild slope and grass on steep slope to impervious surfaces could increase the total quickflow by 13, 10 and 8 %, respectively. In addition, the conversion of total pervious surfaces to impervious ones increases total quickflow by 57%. These results suggest that the conversion of pervious surfaces (especially relatively natural vegetation) to impervious surfaces may lead to important changes in runoff generation processes in tropical urban environments.

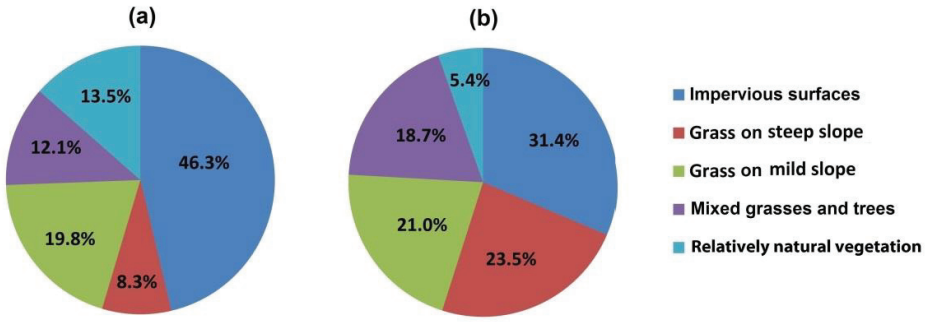

Figure 7.4 : Total land use specific quickflow contributions towards Station E from September 2011 until August 2012 for: a) absolute amount basis and b) equivalent area basis

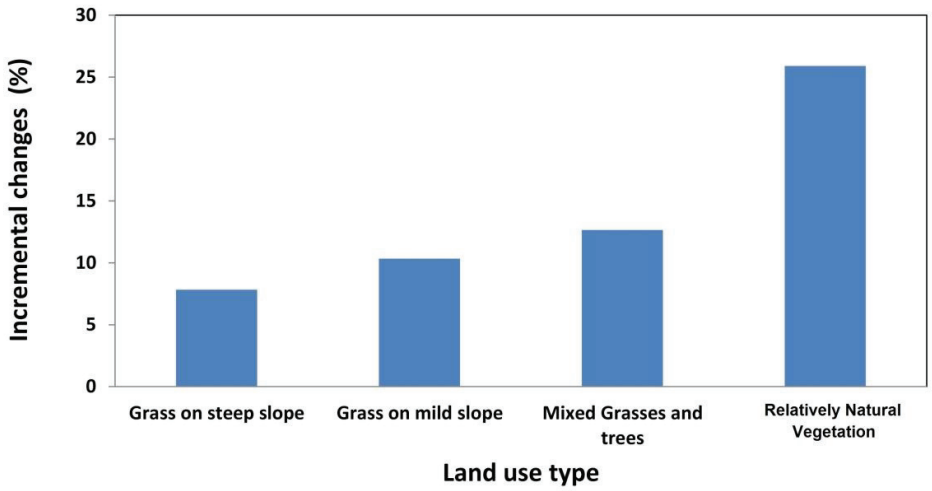

Figure 7.5: The effect of land-cover transformation from pervious surfaces to impervious ones on total quickflow

7.3.3 Baseflow contributions at catchment scale

Comparison was made between the average baseflow contributions towards the overall discharge at the various stations. The lowest baseflow contribution (6.3%) was observed at Station A whose drainage area contained 40% of impervious surfaces (Figure 7.6). In contrast, the highest proportion of baseflow contribution to the streamflow generation (34.9%) was detected at Station B with relatively natural vegetation being the main land use (87% of the total area). As natural vegetation can both increase baseflow and reduce runoff, it plays an important role in catchment water yields, streamflow dynamics and sustainable development of water resources. Similar contributions of baseflow (about 18%) were observed for Stations C, D, and E due to the similar land use composition (Table 3.2). These results showed a negative relationship between the amount of impervious surfaces and baseflow contributions (i.e. decreasing baseflow contributions with increasing impervious surfaces). Similar results have also been found in some studies indicating that increasing urbanization (i.e. impervious surface) might result in significant loss of groundwater flow contribution in streams due to reduced infiltration (Chang, 2007; Leopold and Geological, 1968; Price, 2011; Rose and Peters, 2001; Simmons and Reynolds, 1982).

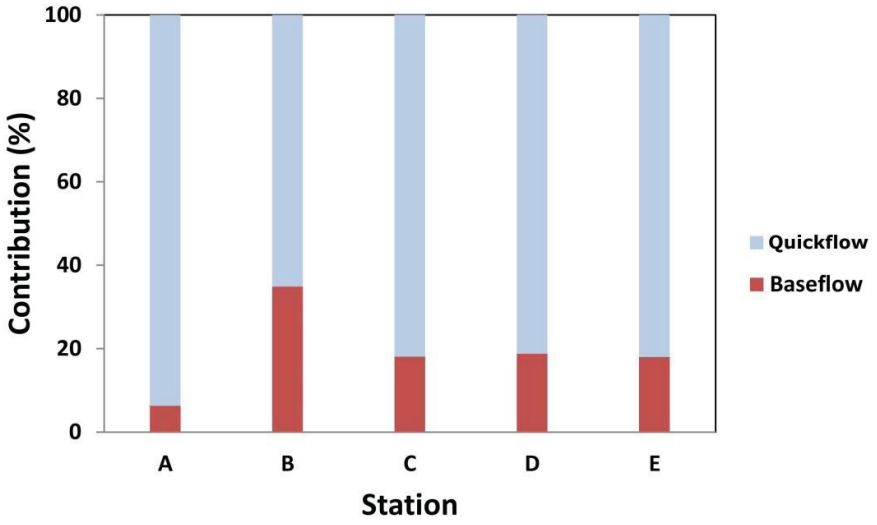

Figure 7.6 : Average contribution (%) of baseflow and quickflow from 150 rainfall events towards the discharge measured at sub-catchment (Stations A-D) and catchment (Station E) level

7.4 Summary and Conclusion

Meteorological, physiographic, hydrologic and land use data was used to derive a physically interpretable modular model consisting of a baseflow module and a quickflow module. The structure of the derived modular model, using GP, was simple and physically interpretable. The quickflow module contained a rapid and delayed streamflow generation component which corresponds to the overland flow and shallow sub-surface flow, respectively.

The modular model was generalized to predict rapid and delayed runoff at sub-catchment and catchment scales, revealing its potential application for other catchments independent from the prevailing meteorological and

catchment condition. In a latter step the model was further validated on its representation of catchment processes through the quantification of land use specific overland flow, shallow sub-surface and baseflow contributions in the tropical urban context. Results from the modular model showed that baseflow contributions decrease with the increase of impervious surfaces, and runoff volume increases with the increase in rainfall depth, duration and intensity. The model results also suggested that both very large and small rainfall events may cause runoff generation processes to be significantly different among different land uses. Even for an extreme rainfall event, the quickflow contribution of relatively natural vegetation areas was about four times less than that of impervious surfaces. As such, the modular model is able to quantify the various hydrograph components in the landscape and could potentially be used in other catchments to simulate the rainfall-runoff processes and also to quantify runoff contributions from different land uses.

CHAPTER 8 CONCLUSIONS AND RECOMMENDATIONS FOR FUTURE RESEARCH WORK

8.1 Conclusions

Knowledge about the land use contributions towards hydrograph flow components (i.e. baseflow and quickflow) in tropical urban environments is sorely lacking in the literature. Moreover, development of an appropriate approach for quantifying these contributions in a tropical urban system plays a vital role. Therefore, this thesis was aimed at providing a better understanding of hydrological rainfall-runoff processes in an urban tropical system through a deeper insight into hydrograph flow components and runoff response of specific land use types. In order to reach this goal, extensive climatic, physiographic, hydrologic and land use data of a small catchment in Singapore was first used to derive a physically interpretable modular model to simulate hydrograph flow components (i.e. baseflow and quickflow) using Genetic Programing (GP). Contributions from different land use types towards hydrograph flow components in a tropical urban context were then quantified using the modular model and optimization techniques. The following are the conclusions drawn from this research.

8.1.1 Development of a modular physically interpretable model for the simulation of streamflow time series, consisting of two sub-models (i.e. baseflow and quickflow)

Most data driven models such as GP are often one unit models with adequate input variables that cover all system processes in one input/output structure. Such models do not contain the knowledge that experts may have about the studied system. One way of incorporating hydrological knowledge into these models is to uncover and build separate models for each of the different physically interpretable sub-processes which is called a modular approach. Modular units in a modular model for the simulation of streamflow time series would be suitable in identifying baseflow and quickflow components. This part of study used GP to develop a modular physically interpretable model consisting of two sub-models (i.e. baseflow and quickflow) to simulate streamflow time series.

(1) Development of baseflow module

As baseflow time series cannot be obtained from direct field measurements, a validated groundwater model was first adopted to simulate baseflow time series for Singapore catchment. The simulated baseflow time series were taken as the target parameter variable (i.e. output) in the GP software called GPKERNEL to develop an empirical equation predicting a continuous baseflow time series based on minimum

perennial baseflow, catchment area, and a time series of groundwater table elevation. This method was further modified into a generalized structure for application in other catchments and proved successful in a cross-site, cross-scale application in a northeastern US watershed. Results showed that:

- Genetic programming is a successful tool for predicting baseflow.
- The proposed equation performs as well as a recursive filter or a numerical model.
- The generalized equation predicts baseflow irrespective of land use or scale.

Overall, this part of study proposed a new approach which serves as an alternative method for baseflow estimation in un-gauged systems when only groundwater table and soil information is available. This method also contributes to multi-proxy estimations of baseflow where both streamflow and groundwater water table measurements are available. The simple equation can also be implemented in a modular model to simulate streamflow time series with little computational time and data requirement. It was proven that the proposed equation performs as well as a recursive filter or a numerical model. Future research could evaluate the performance of these three methods as compared to other techniques such as tracer based approaches in tropical urban environments.

(2) Development of quickflow module

Subtracting the predicted baseflow from the measured discharge for Singapore catchment resulted in the quickflow which was taken as target parameter (i.e. output) in GP to develop the second modular unit based on hydrological parameters (e.g. precipitation), catchment antecedent conditions (e.g. groundwater table elevation prior to the rainfall event) and area of the catchment. The quickflow module was further modified into a generalized structure for application in other catchments. Results showed that:

- Differences between the filtered quickflow from observed discharge data and those obtained by runoff module derived by GP were minimal in both training and testing periods; confirming that quickflow module can accurately estimate quickflow time series.
- The model accounts for hydrological parameters and catchment initial conditions.
- The term of antecedent catchment conditions allows variability in the percentage of rainfall that appears as runoff component for different events.

(3) Development of a modular module

Combining baseflow and quickflow modules resulted in a modular model for the simulation of streamflow time series and hydrograph flow components ($Q_{streamflow} = Q_{baseflow} + Q_{quickflow}$). Results show that:

- GP successfully derived a physically interpretable modular model for simulating streamflow time series, which included two local models associated with baseflow and quickflow.
- The relationship between the input variables in the model (i.e. meteorological data and catchment initial conditions) and its overall structure can be explained in terms of catchment hydrological processes. Therefore, the model is a partial greying of what is often a black-box approach in catchment modelling and has strong extrapolation capability.
- The simulated results in a semi-urban catchment in Singapore matched very well with observed data in both the training and the testing data sets.
- The modular model proved successful in a cross-site, cross-scale application in a northeastern US watershed

Overall, this part of study proposed a physically interpretable model with understandable structure to simulate streamflow. This method can be

applied in other catchments and can simulate and separate hydrograph flow components on both event as well as time series basis. It can also be used to estimate the effect of various land use types towards hydrograph flow components. Moreover, as it requires less computational time as compared to the distributed hydrological models, it can be potentially coupled with a global climate model (GCM) to assess the climate change impacts on streamflow.

8.1.2 Enhancement of our understanding on contributions from different land uses towards hydrograph flow components using the modular model and optimization techniques

An extensive dataset of various climatic, physiographic, hydrologic and land use data combined with a modular model and optimization techniques provided an effective way to better understand the hydrological rainfall-runoff processes in an tropical urban context.

Results showed that:

- Runoff coefficients differ significantly among land uses for all rainfall clusters.
- Rainfall events have greater impact on runoff coefficients of pervious areas.

- Baseflow contributions decrease with the increase of impervious surfaces.

The results also showed that due to the urbanization, the soil hydraulic conductivity for soils covered by grass is significantly lower than the generally reported rate for these soil types. This could consequently reduce infiltration capacity which increases surface runoff during a rainfall event. However the estimated soil hydraulic conductivity for non-urban areas (i.e. relatively natural vegetation) corresponded to the soil hydraulic conductivity related to the soil texture.

Overall this part of study offered a new approach with regards to the quantification of land-use specific contributions to quickflow component. Moreover, it provided enhanced knowledge on the hydrological rainfall-runoff processes in an urban tropical system through a better insight into hydrograph flow component and land use specific runoff response using a modular approach. This knowledge would be essential for integrated water resources management and the sustainable development of water resources particularly in tropical megacities.

8.2 Recommendations for Future Work

A few possible directions for future research are highlighted below.

8.2.1 Modeling of Streamflow under the Effects of Climate Change Using a Hybrid Model

Changes in precipitation patterns are considered to be a significant component of climate change. Changes in precipitation, in combination with increases in temperature, may have important effects on the streamflow of a watershed. Understanding and assessing the potential impacts of climate change on future streamflow, especially in an urban system, is essential for water policy and environmental management, particularly in the context of water quantity, quality, and aquatic ecosystem sustainability.

Climate change can have a variety of impacts on surface and sub-surface flow. However, quantifying these effects remains one of the most challenging issues in hydrology. With the advances in technology and the increasing need for integrated environmental management, the distributed hydrological models, offer an appropriate approach to model the rainfall-runoff relationship and also to quantify the climate change effects on hydrological responses in watershed scale. However these models are computationally expensive and the modeling of streamflow under the effects of climate change then require significant computational time. The modular model developed in CHAPTER 6

on the other hand is based on statistical relationship and hence require less computational time. Therefore one may couple this modular model with global climate models (GCMs) to assess the climate change impacts on streamflow using a hybrid model. In addition, as the model is modular, the impacts of climate change on hydrograph flow components (i.e. baseflow and quickflow) can be assessed separately.

8.2.2 Runoff Generation Mechanism at Different Spatial Scales

To better understand the hydrological rainfall-runoff processes in a tropical urban context, an extensive dataset of various climatic, physiographic, hydrologic and land use data should be available. For this purpose, a small catchment is more economically and technically feasible to install a dense monitoring equipment network. The results of the current study also showed that a small experimental catchment represents a valuable tool for collection of detailed hydro-meteorological data and conceptualization of rainfall runoff processes in tropical urban systems. On the other hand, detailed analyses and monitoring are usually more difficult in a larger catchment. Therefore, an upscaling approach can offer insights about the main rainfall-runoff processes occurring at larger scales.

Therefore, the runoff coefficient estimated in the present study for small catchments might be used as an indicator of the hydrological behavior of larger catchments in Singapore (e.g. Marina catchment). Upscaling the

observations and the knowledge gained over small research catchments to larger watersheds, would be valuable for flood modelling and prediction as well as risk assessment.

8.2.3 Enhancement of water resources management in tropical urban environments

To reduce the impact of surface runoff, water sensitive urban infrastructure (e.g. green roofs, porous pavement, bioretention ponds, swales) retaining rainfall and enhancing infiltration rates in urban cities are being promoted. Water Sensitive Urban Design (WSUD) is an engineering design approach which aims to minimize hydrological and water quality impact of urban development by integrating land use planning with urban water management. The implementation of such technologies requests for a detailed understanding of runoff contributions from each specific land use in order to plan the location of these local source control measures. Therefore, the knowledge of contributions from different land uses towards quickflow as well as baseflow achieved in the present study could be adopted to enhance integrated management and sustainable development of water resources particularly in tropical megacities which are dependent on water sources that are more vulnerable to inter-annual fluctuations in precipitation.

REFERENCES

Abadie, J., Carpentier, J., 1969. Generalization of the Wolfe reduced gradient method to the case of nonlinear constraints. In: R. Fletcher (Ed.), Optimization, Academic press, New York, Chapter 4, USA., pp. 37-47.

Abrahart, R.J., See, L., 1999. Multi-model data fusion for river flow forecasting: an evaluation of six alternative methods based on two contrasting catchments. Hydrology and Earth System Sciences, 6(4): 655-670.

Anctil, F., Lauzon, N., Andréassian, V., Oudin, L., Perrin, C., 2006. Improvement of rainfall-runoff forecasts through mean areal rainfall optimization. Journal of Hydrology, 328(3–4): 717-725.

Ankeny, M.D., Ahmed, M., Kaspar, T.C., Horton, R., 1991. Simple field method for determining unsaturated hydraulic conductivity. *Soil Science Society of America Journal*, **55**: 467-470.

Aquatic Informatics Inc., 2009. Aquarius Hydrologic Workstation Software, Vancouver, Canada.

Arnold, J.G., Allen, P.M., 1999. Automated Methods For Estimating Baseflow And Ground Water Recharge From Streamflow Records1. Journal of the American Water Resources Association, 35(2): 411-424.

Babovic, V., 2005. Data mining in hydrology. Hydrological Processes, 19(7): 1511-1515.

Babovic, V., Keijzer, M., 2000. Genetic programming as a model induction engine. Journal of Hydroinformatics, 2(1): 35-60.

Babovic, V., Keijzer, M., 2002. Rainfall runoff modelling based on genetic programming. Nordic Hydrology, 33(5): 331-346.

Babovic, V., Keijzer, M., 2006. Rainfall-Runoff Modeling Based on Genetic Programming, Encyclopedia of Hydrological Sciences. John Wiley & Sons, Ltd.

Barthold, F.K. et al., 2010. Identification of geographic runoff sources in a data sparse region: hydrological processes and the limitations of tracer-based approaches. Hydrological Processes, 24(16): 2313-2327.

Beven, K.J., 2012. Rainfall-runoff modelling: the primer. Wiley-Blackwell, Chichester, West Sussex; Hoboken, NJ.

Bodhinayake, W., Si, B.C., Noborio, K., 2004. Determination of hydraulic properties in sloping landscapes from tension and double-ring infiltrometers. *Vadose Zone Journal*, 3(3): 964-970.

Bodhinayake, W., Si, B.C., Noborio, K.,, 2004. Comparison of Single- and Double-Ring Infiltrometer Methods on Stony Soils. Vadose Zone Journal, 3(3): 964-970.

Bos, M.G., 1989. Discharge measurement structures, 20. International Institute for Land Reclamation and Improvement, Wageningen, Netherlands.

Bouma, J., Belmans, C., Dekker, L.W., Jeurissen, W.J.M., 1983. Assessing the suitability of soils with macropores for subsurface liquid waste disposal. *Journal of Environmental Quality*, 12(3): 305-311.

Bowden, G.J., Dandy, G.C., Maier, H.R., 2005. Input determination for neural network models in water resources applications. Part 1—background and methodology. Journal of Hydrology, 301(1–4): 75-92.

Brown, A.E., Zhang, L., McMahon, T.A., Western, A.W., Vertessy, R.A., 2005. A review of paired catchment studies for determining changes in water yield resulting from alterations in vegetation. Journal of Hydrology, 310(1–4): 28-61.

Brown, V.A., McDonnell, J.J., Burns, D.A., Kendall, C., 1999. The role of event water, a rapid shallow flow component, and catchment size in summer stormflow. Journal of Hydrology, 217(3–4): 171-190.

Bruce, R.R., Klute, A., 1956. The measurement of soil moisture diffusivity. *Soil Science Society of America Journal*, 20: 458-462.

Burns, D. et al., 2005. Effects of suburban development on runoff generation in the Croton River basin, New York, USA. Journal of Hydrology, 311(1): 266-281.

Burns, M.J., Fletcher, T.D., Walsh, C.J., Ladson, A.R., Hatt, B.E., 2012. Hydrologic shortcomings of conventional urban stormwater management and opportunities for reform. Landscape and Urban Planning, 105(3): 230-240.

Byrd, R.H., Hribar, M.E., Nocedal, J., 1999. An Interior Point Algorithm for Large-Scale Nonlinear Programming. SIAM J. on Optimization, 9(4): 877-900.

Calder, I.R., 2005. Blue revolution: integrated land and water resources management. Earthscan, Sterling, VA.

Carsel, R.F., Parrish, R.S., 1988. Developing joint probability distributions of soil water retention characteristics. Water Resources Research, 24(5): 755-769.

Casanova, M., Messing, I., Joel, A., 2000. Influence of aspect and slope gradient on hydraulic conductivity measured by tension infiltrometer. Hydrological Processes, 14(1): 155-164.

Chang, H., 2007. Comparative streamflow characteristics in urbanizing basins in the Portland Metropolitan Area, Oregon, USA. Hydrological Processes, 21(2): 211-222.

Chang, N.-B., 2010. Hydrological Connections between Low-Impact Development, Watershed Best Management Practices, and Sustainable Development. Journal of Hydrologic Engineering, 15(6): 384-385.

Chapman, T., 1999. A comparison of algorithms for stream flow recession and baseflow separation. Hydrological Processes, 13(5): 701-714.

Chapman, T.G., 1991. Comment on "Evaluation of automated techniques for base flow and recession analyses" by R. J. Nathan and T. A. McMahon. Water Resources Research, 27(7): 1783-1784.

Chapman, T.G., Maxwell, A.I., 1996. Baseflow separation - comparison of numerical methods with tracer experiments, In: Proceedings of the 23rd Hydrology and Water Resources Symposium, Hobart Australia.

Christophersen, N., Hooper, R.P., 1992. Multivariate analysis of stream water chemical data: The use of principal components analysis for the end-member mixing problem. Water Resources Research, 28(1): 99-107.

Christophersen, N., Neal, C., Hooper, R.P., Vogt, R.D., Andersen, S., 1990. Modelling streamwater chemistry as a mixture of soilwater end-members — A step towards second-generation acidification models. Journal of Hydrology, 116(1–4): 307-320.

Chu, H.-J., Lin, Y.-P., Huang, C.-W., Hsu, C.-Y., Chen, H.-Y., 2010. Modelling the hydrologic effects of dynamic land-use change using a distributed hydrologic model and a spatial land-use allocation model. Hydrological Processes, 24(18): 2538-2554.

Code of Practice-Drainage Design and Considerations, 2011. http://www.pub.gov.sg/general/code/Pages/SurfaceDrainagePart2-7.aspx.

Corey, A.T., 2002. Long column. In: *Methods of soil analysis. Part 4. Physical methods,SSSA Book Series*. Soil Science Society of America, Madison, WI, USA.

Corzo, G., Solomatine, D., 2007. Baseflow separation techniques for modular artificial neural network modelling in flow forecasting. Hydrological Sciences Journal, 52(3): 491-507.

Dadkhah, M., Gifford, G.F., 1980. Influence of Vegetation, Rock Cover, and Trampling on Infiltration Rates and Sediment Production. Water Resources Bulletin, 16(6): 979-979.

Dane, J.H., Hopmans, J.W., Romano, N., Nimmo, J., Winfield, K.A., 2002. Soil Water Retention and Storage - Laboratory Methods. In: *Methods of Soil Analysis. Part 4. Physical Methods, SSSA Book Series*. Soil Science Society of America, Madison, WI, USA.

DeFries, R., Eshleman, K.N., 2004. Land-use change and hydrologic processes: a major focus for the future. Hydrological Processes, 18(11): 2183-2186.
Deltares, 2009. SOBEK manual. Deltares, Netherland.
DHI, 2003. MOUSE – Reference Manual, DHI, Hørsholm, Denmark.
Diaz-Palacios-Sisternes, S., Ayuga, F., Garcia, A.I., 2014. A method for detecting and describing land use transformations: An examination of Madrid's southern urban-rural gradient between 1990 and 2006. Cities, 40: 99-110.
DiCiccio, T., Efron, B., 1996. Bootstrap confidence intervals. Statistical Science, 11(3): 189–228.
Dye, P.J., Croke, B.F.W., 2003. Evaluation of streamflow predictions by the IHACRES rainfall-runoff model in two South African catchments. Environmental Modelling & Software, 18(8–9): 705-712.
Eckhardt, K., 2005. How to construct recursive digital filters for baseflow separation. Hydrological Processes, 19(2): 507-515.
Eckhardt, K., 2008. A comparison of baseflow indices, which were calculated with seven different baseflow separation methods. Journal of Hydrology, 352(1–2): 168-173.
Efron, B., Tibshirani, R.J., 1993. An Introduction to the Bootstrap. Chapman and Hall:New York.
Fallah-Mehdipour, E., Bozorg Haddad, O., Mariño, M.A., 2013. Prediction and simulation of monthly groundwater levels by genetic programming. Journal of Hydro-environment Research. doi:http://dx.doi.org/10.1016/j.jher.2013.03.005.
Feldman, A.D., 2000. Hydrologic Modeling System HEC-HMS, Technical Reference Manual, U.S. Army Corps of Engineers report CPD-74B, Davis, California.
Fodor, N., Sandor, R., Orfanus, T., Lichner, L., Rajkai, K., 2011. Evaluation method dependency of measured saturated hydraulic conductivity. *Geoderma*, 165(1): 60-68.
Gilfedder, M., Walker, G.R., Dawes, W.R., Stenson, M.P., 2009. Prioritisation approach for estimating the biophysical impacts of land-use change on stream flow and salt export at a catchment scale. Environmental Modelling & Software, 24(2): 262-269.
Gonzales, A.L., Nonner, J., Heijkers, J., Uhlenbrook, S., 2009. Comparison of different base flow separation methods in a lowland catchment. Hydrology and Earth System Sciences, 13(11): 2055-2068.
Grosan, C., Abraham, A., 2007. Hybrid Evolutionary Algorithms: Methodologies, Architectures, and Reviews. In: Abraham, A., Grosan, C., Ishibuchi, H. (Eds.), Hybrid Evolutionary Algorithms. Studies in Computational Intelligence. Springer Berlin Heidelberg, pp. 1-17.
Haverkamp, S., Fohrer, N., Frede, H.G., 2005. Assessment of the effect of land use patterns on hydrologic landscape functions: a comprehensive GIS-based tool to minimize model uncertainty resulting from spatial aggregation. Hydrological Processes, 19(3): 715-727.
Hawke, R.M., Price, A.G., Bryan, R.B., 2006. The effect of initial soil water content and rainfall intensity on near-surface soil hydrologic conductivity: A laboratory investigation. CATENA, 65(3): 237-246.
Holko, L., Kostka, Z., 2008. Impact of Landuse on Runoff in Mountain Catchments of Different Scales. Soil and Water Research(3): 113-120.
Hong, Y.-S., Bhamidimarri, R., 2003. Evolutionary self-organising modelling of a municipal wastewater treatment plant. Water Research, 37(6): 1199-1212.
Hooper, R.P., 2003. Diagnostic tools for mixing models of stream water chemistry. Water Resources Research, 39(3): 1055.
Hu, T.S., Lam, K.C., Ng, S.T., 2001. River flow time series prediction with a range-dependent neural network. Hydrological Sciences Journal, 46(5): 729-745.

Huang, J., Wu, P., Zhao, X., 2013. Effects of rainfall intensity, underlying surface and slope gradient on soil infiltration under simulated rainfall experiments. CATENA, 104: 93-102.

Huber, W.C., Heaney, J.P., 1981. Storm Water Management Model User's Manual, Version III, US EPA, Cincinnati, Ohio.

Izadifar, Z., Elshorbagy, A., 2010. Prediction of hourly actual evapotranspiration using neural networks, genetic programming, and statistical models. Hydrological Processes, 24(23): 3413-3425.

Jakeman, A.J., Hornberger, G.M., 1993. How much complexity is warranted in a rainfall-runoff model? Water Resources Research, 29(8): 2637-2649.

Jeong, D.-I., Kim, Y.-O., 2005. Rainfall-runoff models using artificial neural networks for ensemble streamflow prediction. Hydrological Processes, 19(19): 3819-3835.

Jones, J.P., Sudicky, E.A., Brookfield, A.E., Park, Y.J., 2006. An assessment of the tracer-based approach to quantifying groundwater contributions to streamflow. Water Resources Research, 42(2): W02407.

Kechavarzi, C., Spongrova, K., Dresser, M., Matula, S., Godwin, R.J., 2009. Laboratory and field testing of an automated tension infiltrometer. *Biosystems Engineering*, 104(2): 266-277.

Kim, S., Kim, H.S., 2008. Neural networks and genetic algorithm approach for nonlinear evaporation and evapotranspiration modeling. Journal of Hydrology, 351(3–4): 299-317.

Kisi, O., Shiri, J., Tombul, M., 2013. Modeling rainfall-runoff process using soft computing techniques. Computers & Geosciences, 51: 108-117.

Kliner, K., Knezek, M., 1974. The underground runoff separation method making use of the observation of ground water table. Hydrology and hydromechanics, XXII(5): 457–466.

Kottegoda, N.T., Natale, L., 1994. Two-component log-normal distribution of irrigation-affected low flows. Journal of Hydrology, 158(1–2): 187-199.

Kuznetsov, M., Yakirevich, A., Pachepsky, Y.A., Sorek, S., Weisbrod, N., 2012. Quasi 3D modeling of water flow in vadose zone and groundwater. Journal of Hydrology, 450–451(0): 140-149.

Leopold, L.B., Geological, S., 1968. Hydrology for urban land planning - a guidebook on the hydrologic effects of urban land use, 554. United States Government Printing Office, Washington.

Li, L., Jiang, D., Hou, X., Li, J., 2013a. Simulated runoff responses to land use in the middle and upstream reaches of Taoerhe River basin, Northeast China, in wet, average and dry years. Hydrological Processes, 27(24): 3484-3494.

Li, L., Maier, H.R., Lambert, M.F., Simmons, C.T., Partington, D., 2013b. Framework for assessing and improving the performance of recursive digital filters for baseflow estimation with application to the Lyne and Hollick filter. Environmental Modelling & Software, 41(0): 163-175.

Li, Q. et al., 2013c. Investigation into the Impacts of Land-Use Change on Runoff Generation Characteristics in the Upper Huaihe River Basin, China. Journal of Hydrologic Engineering, 18(11): 1464-1470.

Linsley, R.K., Kohler, M.A., Paulhus, J.L.H., 1982. Hydrology for engineers. McGraw Hill Book Company, London.

Loperfido, J.V., Noe, G.B., Jarnagin, S.T., Hogan, D.M., 2014. Effects of distributed and centralized stormwater best management practices and land cover on urban stream hydrology at the catchment scale. Journal of Hydrology, 519: 2584-2595.

Malmer, A., 1992. Water-yield changes after clear-felling tropical rainforest and establishment of forest plantation in Sabah, Malaysia. Journal of Hydrology, 134(1–4): 77-94.

Marquardt, D.W., 1963. An algorithm for least-squares estimation of non-linear parameters. *SIAM Journal of Applied Mathematics*, 11: 431–441.

Marshall, E., Shortle, J., 2005. Urban development impacts on ecosystems. In: Goetz, S., Shortle, J., Bergstrom, J. (Eds.), In: *Land Use Problems and Conflicts: Causes, Consequences and Solutions*. Routledge, Taylor and Francis group, New york.

McDonnell, J.J. et al., 2014. Debates—The future of hydrological sciences: A (common) path forward? A call to action aimed at understanding velocities, celerities and residence time distributions of the headwater hydrograph. Water Resources Research, 50(6): 5342-5350.

McDonnell, J.J., Tanaka, T., Mitchell, M.J., Ohte, N., 2001. Hydrology and biogeochemistry of forested catchments. Hydrological Processes, 15(10): 1673-1674.

McGlynn, B.L., McDonnell, J.J., 2003. Quantifying the relative contributions of riparian and hillslope zones to catchment runoff. Water Resources Research, 39(11): 1310.

Meshgi, A., Chui, T.F.M., 2014. Analysing tension infiltrometer data from sloped surface using two-dimensional approximation. Hydrological Processes, 28(3): 744-752.

Meshgi, A., Schmitter, P., Babovic, V., Chui, T.F.M., 2014. An empirical method for approximating stream baseflow time series using groundwater table fluctuations. Journal of Hydrology, 519: 1031-1041.

Meshgi, A., Schmitter, P., Chui, T.F.M., Babovic, V., 2015. Development of a modular streamflow model to quantify runoff contributions from different land uses in tropical urban environments using Genetic Programming. Journal of Hydrology, 525: 711-723.

Miller, J.D. et al., 2014. Assessing the impact of urbanization on storm runoff in a peri-urban catchment using historical change in impervious cover. Journal of Hydrology, 515: 59-70.

Mousavi, S.J., Moghaddam, K.S., Seifi, A., 2004. Application of an Interior-Point Algorithm For Optimization of a Large-Scale Reservoir System. Water Resources Management, 18(6): 519-540.

Muñoz-Villers, L.E., McDonnell, J.J., 2013. Land use change effects on runoff generation in a humid tropical montane cloud forest region. Hydrology and Earth System Sciences, 17(9): 3543.

Nash, J.E., Sutcliffe, J.V., 1970. River flow forecasting through conceptual models part I — A discussion of principles. Journal of Hydrology, 10(3): 282-290.

Nathan, R.J., McMahon, T.A., 1990. Evaluation of automated techniques for base flow and recession analyses. Water Resources Research, 26(7): 1465-1473.

Parasuraman, K., Elshorbagy, A., Si, B.C., 2007. Estimating Saturated Hydraulic Conductivity Using Genetic Programming Soil Science Society of America Journal, 71(6): 1676-1684.

Partington, D. et al., 2011. A hydraulic mixing-cell method to quantify the groundwater component of streamflow within spatially distributed fully integrated surface water–groundwater flow models. Environmental Modelling & Software, 26(7): 886-898.

Peng, T., Wang, S.-j., 2012. Effects of land use, land cover and rainfall regimes on the surface runoff and soil loss on karst slopes in southwest China. CATENA, 90: 53-62.

Perrin, C., Michel, C., Andréassian, V., 2001. Does a large number of parameters enhance model performance? Comparative assessment of common catchment model structures on 429 catchments. Journal of Hydrology, 242(3): 275-301.

Perroux, K.M., White, I., 1988. Design for disc permeameters. *Soil Science Society of America Journal*, 52(5): 1205-1215.

Philip, J.R., 1957. The theory of infiltration: 5. The influence of the initial moisture content. Soil Science, 84(4): 329-340.

Potter, K.W., 1991. Hydrological impacts of changing land management practices in a moderate-sized agricultural catchment. Water Resources Research, 27(5): 845-855.

Price, K., 2011. Effects of watershed topography, soils, land use, and climate on baseflow hydrology in humid regions: A review. Progress in Physical Geography, 35(4): 465-492.

Rajurkar, M.P., Kothyari, U.C., Chaube, U.C., 2002. Artificial neural networks for daily rainfall—runoff modelling. Hydrological Sciences Journal, 47(6): 865-877.

Ramos, T.B., Gonçalves, M.C., Martins, J.C., van Genuchten, M.T., Pires, F.P., 2006. Estimation of soil hydraulic properties from numerical inversion of tension disk infiltrometer data. *Vadose Zone Journal*, 5(2): 684-696.

Ramos, T.B., Gonçalves, M.C., Martins, J.C., van Genuchten, M.T., Pires, F.P., 2006. Estimation of soil hydraulic properties from numerical inversion of tension disk infiltrometer data. Vadose Zone Journal, 5(2): 684-696.

Raoof, M., Pilpayeh, A., 2011. Estimating unsaturated soil hydraulic properties in sloping lands by numerical inversion. Food, Agriculture and Environment, 9(3&4): 1067-1070.

Reed, S. et al., 2004. Overall distributed model intercomparison project results. Journal of Hydrology, 298(1): 27-60.

Reeves, C.R., Rowe, J.E., 2002. Genetic Algorithms--Principles and Perspectives: A Guide to GA Theory, 20. Springer US, Boston, MA.

Refsgaard, J.C., Knudsen, J., 1996. Operational validation and intercomparison of different types of hydrological models. Water Resources Research, 32(7): 2189-2202.

Rhode Island Digital Atlas, 2014. Aerial Photographs (1939), URL: http://www.edc.uri.edu/atlas, University of Rhode Island Environmental Data Center, Kingston, Rhode Island.

Richards, L.A., 1931. Capillary conduction of liquids through porous mediums. *Journal of General and Applied Physics*, 1(1): 318-333.

Roa-García, M.C., Brown, S., Schreier, H., Lavkulich, L.M., 2011. The role of land use and soils in regulating water flow in small headwater catchments of the Andes. Water Resources Research, 47(5): W05510.

Rose, S., Peters, N.E., 2001. Effects of urbanization on streamflow in the Atlanta area (Georgia, USA): a comparative hydrological approach. Hydrological Processes, 15(8): 1441-1457.

Salemi, L.F. et al., 2013. Land-use change in the Atlantic rainforest region: Consequences for the hydrology of small catchments. Journal of Hydrology, 499(0): 100-109.

Sedki, A., Ouazar, D., El Mazoudi, E., 2009. Evolving neural network using real coded genetic algorithm for daily rainfall–runoff forecasting. Expert Systems with Applications, 36(3, Part 1): 4523-4527.

Šejna, M., and Šimůnek, J., 2007. *HYDRUS (2D/3D): Graphical User Interface for the HYDRUS Software Package Simulating Two- and Three-Dimensional Movement of Water, Heat, and Multiple Solutes in Variably-Saturated Media*. PC-Progress, Prague, Czech Republic.

Sellinger, C.E., 1996. Computer program for performing hydrograph separation using the rating curve method, US Department of Commerce, National Oceanic and Atmospheric Administration, Technical Memorandum ERL GLERL-100.

Semenova, O., Beven, K., 2015. Barriers to progress in distributed hydrological modelling. Hydrological Processes, 29(8): 2074-2078.

Simmons, D.L., Reynolds, R.J., 1982. Effects of urbanization on base flow of selected south-shore streams, Long Island, New York. JAWRA Journal of the American Water Resources Association, 18(5): 797-805.

Šimůnek, J., van genuchten, M.T., 1996a. Estimating unsaturated soil hydraulic properties from tension disc infiltrometer data by numerical inversion. *Water Resources Research*, 32(9): 2683-2696.
Šimůnek, J., van Genuchten, M.T., 1996b. Estimating Unsaturated Soil Hydraulic Properties from Tension Disc Infiltrometer Data by Numerical Inversion. Water Resources Research, 32(9): 2683.
Šimůnek, J., van genuchten, M.T., 1997. Estimating unsaturated soil hydraulic properties from multiple tension disc infiltrometer data. *Soil Science*, 162(6): 383-398.
Šimůnek, J., van Genuchten, M.T., Šejna, M., 2006. The HYDRUS Software Package for Simulating Two- and Three-Dimensional Movement of Water, Heat, and Multiple Solutes in Variably-Saturated Media. Technical Manual, Version 1.0, PC Progress, Prague, Czech Republic: 241.
Šimůnek, J., Wendroth, O., van genuchten, M.T., 1999. Estimating unsaturated soil hydraulic properties from laboratory tension disc infiltrometer experiments. *Water Resources Research*, 35(10): 2965-2979.
Singh, G., Kandasamy, J., 2009. Evaluating performance and effectiveness of water sensitive urban design. Desalination and Water Treatment, 11(1-3): 144-150.
Sivapragasam, C., Maheswaran, R., Venkatesh, V., 2008. Genetic programming approach for flood routing in natural channels. Hydrological Processes, 22(5): 623-628.
Smakhtin, V.U., 2001. Low flow hydrology: a review. Journal of Hydrology, 240(3–4): 147-186.
Solomatine, D., Xue, Y., 2004. M5 Model Trees and Neural Networks: Application to Flood Forecasting in the Upper Reach of the Huai River in China. Journal of Hydrologic Engineering, 9(6): 491-501.
Sorooshian, S., Hsu, K., Coppola, E.,Tomassetti, B., Verdecchia, M., Visconti, G., 2008. Hydrological Modelling and the Water Cycle Coupling the Atmospheric and Hydrological Models. In: V.P. Singh (Ed.). Springer, Texas A&M University, College Station, U.S.A.
Sriwongsitanon, N., Taesombat, W., 2011. Effects of land cover on runoff coefficient. Journal of Hydrology, 410(3-4): 226-238.
Stonestrom, D.A., Scanlon, B.R., Zhang, L., 2009. Introduction to special section on Impacts of Land Use Change on Water Resources. Water Resources Research, 45(7): W00A00.
Sudheer, K.P., Gosain, A.K., Ramasastri, K.S., 2002. A data-driven algorithm for constructing artificial neural network rainfall-runoff models. Hydrological Processes, 16(6): 1325-1330.
Sun, Z., Li, X., Fu, W., Li, Y., Tang, D., 2013. Long-term effects of land use/land cover change on surface runoff in urban areas of Beijing, China. APPRES, 8(1): 084596-084596.
Talei, A., Chua, L.H.C., 2012. Influence of lag time on event-based rainfall–runoff modeling using the data driven approach. Journal of Hydrology, 438–439: 223-233.
Tarboton, D.G., 2003. Rainfall-Runoff Processes. Utah State University, Logan, United States.
Timlin, D.J., Ahuja, L.R., Ankeny, M.D., 1994. Comparison of three field methods to characterize apparent macropore conductivity. *Soil Science Society of America Journal*, 58(2): 278-284.
Todini, E., 2007. Hydrological catchment modelling: past, present and future. Hydrol. Earth Syst. Sci., 11(1): 468-482.
Tran, L.T., O'Neill, R.V., 2013. Detecting the effects of land use/land cover on mean annual streamflow in the Upper Mississippi River Basin, USA. Journal of Hydrology, 499: 82-90.

Uhlenbrook, S., Hoeg, S., 2003. Quantifying uncertainties in tracer-based hydrograph separations: a case study for two-, three- and five-component hydrograph separations in a mountainous catchment. Hydrological Processes, 17(2): 431-453.

Vachaud, G., Dane, J.H., 2002. Instantaneous profile. In: *Methods of soil analysis. Part 4. Physical methods, SSSA Book Series*. Soil Science Society of America, Madison, WI, USA.

van genuchten, M.T., 1980. A closed form equation for predicting the hydraulic conductivity of unsaturated soils. *Soil Science Society of America Journal*, 44(5): 892-898.

van Tol, J.J., Le Roux, P.A.L., Hensley, M., 2012. Pedotransfer functions to determine water conducting macroporosity in South African soils. Water Sci. Technol., 65(3): 550-557.

Vanderbei, R., Shanno, D., 1999. An Interior-Point Algorithm for Nonconvex Nonlinear Programming. Computational Optimization and Applications, 13(1-3): 231-252.

Vandervaere, J.P., Vauclin, M., Elrick, D.E., 2000. Transient flow from tension infiltrometers: I. The two-parameter equation. *Soil Science Society of America Journal*, 64(4): 1263-1272.

VanShaar, J.R., Haddeland, I., Lettenmaier, D.P., 2002. Effects of land-cover changes on the hydrological response of interior Columbia River basin forested catchments. Hydrological Processes, 16(13): 2499-2520.

Ventrella, D., Losavio, N., Vonella, A., Leij, F.J., 2005. Estimating hydraulic conductivity of a fine-textured soil using tension infiltrometry. *Geoderma*, 124(3-4): 267-277.

Ward, J.H., 1963. Hierarchical Grouping to Optimize an Objective Function. Journal of the American Statistical Association, 58(301): 236-244.

Whigham, P.A., Crapper, P.F., 2001. Modelling rainfall-runoff using genetic programming. Mathematical and Computer Modelling, 33(6–7): 707-721.

Willems, P., 2009. A time series tool to support the multi-criteria performance evaluation of rainfall-runoff models. Environmental Modelling & Software, 24(3): 311-321.

Wooding, R.A., 1968. Steady infiltration from large shallow circular pond. *Water Resources Research*, 4: 1259–1273.

Wu, C.L., Chau, K.W., 2013. Prediction of rainfall time series using modular soft computing methods. Engineering Applications of Artificial Intelligence, 26(3): 997-1007.

Yang, C., Yu, Z., Hao, Z., Lin, Z., Wang, H., 2013. Effects of Vegetation Cover on Hydrological Processes in a Large Region: Huaihe River Basin, China. Journal of Hydrologic Engineering, 18(11): 1477-1483.

Yeh, T.-C.J., Šimůnek, J., 2002. Stochastic Fusion of Information for Characterizing and Monitoring the Vadose Zone. *Vadose Zone Journal*, 1(2): 207-221.

Zhang, B., Govindaraju, R.S., 2000. Prediction of watershed runoff using Bayesian concepts and modular neural networks. Water Resources Research, 36(3): 753-762.

LIST OF PUBLICATIONS

I- Journal Papers:

- **Meshgi, A.**, Chui, T. M., 2014. Analyzing Tension Infiltrometer Data from Sloped Surface Using Two-Dimensional Approximation. *Hydrological Processes*, 28(3): 744–752.

- **Meshgi, A.,** Schmitter P., Babovic, V., Chui, T. M., 2014. An Empirical Method for Approximating Stream Baseflow Time Series Using Groundwater Table Fluctuations. *Journal of Hydrology*, 519:1031-1041.

- **Meshgi, A.,** Schmitter P., Chui, T. M., Babovic, V., 2015. Development of a Modular Streamflow Model to Quantify Runoff Contributions from Different Land Use Types in Tropical Urban Environments Using Genetic Programming. Journal of Hydrology, 525: 711-723

II- Conference Papers:

- **Meshgi, A.,** Babovic, V., Chui, T. M., Schmitter P., Application of Genetic Programing to Develop a Modular Model for the Simulation of Streamflow Time Series. AGU Fall Meeting, San Francisco, California, 15-19 December 2014.

- **Meshgi, A.,** Schmitter P., Babovic, V., Chui, T. M., Predicting Baseflow Using Genetic Programing. Proceedings of the 11th International Conference on Hydroinformatics – HIC 2014, New York, USA, 17-21 August 2014.

- Schmitter P., **Meshgi A**., Bui D., Ooi S.K., Deciphering rainfall-runoff land-cover contributions using computational hydrograph separation techniques in a tropical urban megacity. Proceedings of the 2nd Water Research Conference, Singapore, 20-23 January 2013

- **Meshgi, A**., Chui, T. M., Investigating the Impact of Land Slopes on Tension Infiltrometer Data through Inverse Modeling. Proceedings of the 10th International Conference on Hydroinformatics – HIC 2012, Hamburg, 14-18 July 2012.